

COMPUTERISED

SYNTHESIS AND CHARACTERIZATION OF LARGE PORE ZEOLITES

A THESIS
SUBMITTED TO THE
UNIVERSITY OF POONA
FOR THE DEGREE OF
DOCTOR OF PHILOSOPHY
(IN CHEMISTRY)

COMPUTERISED



BY

RAMANATH NARAYAN BHAT
M. Sc.

661.183.6(043)

BHA

INORGANIC CHEMISTRY DIVISION
NATIONAL CHEMICAL LABORATORY
PUNE-411 008 (INDIA)

MAY 1991

COMPUTERISED

DEDICATED TO MY BELOVED SISTER *REVATI*
AND LOVING FRIEND *AGNEL D'COSTA*

ACKNOWLEDGEMENT

I am deeply indebted to Dr. Paul Ratnasamy, Deputy Director, National Chemical Laboratory, Pune; who provided me an opportunity to work under his fruitful guidance. His specific thoughtful tutorage, through understanding and kindness made my stay at NCL highly memorable. I have learnt a great deal about chemistry in particular and life in general, from him and I am quite confident that this will help me in future endeavours.

I am also grateful to Dr. S.G. Hegde, who always did a superb job in assisting my research work. To be frank I had a friendly relation with him than a student teacher relationship. I shall always remember the stimulating discussions I had, professional and personal help, constant encouragement and above all great sense of humor. I am also thankful to Dr. R. Kumar for his assistance and helpful discussions during this course of investigation. I am also grateful to Dr. S. Shankar and Dr. S.B. Kulkarni for their helpful suggestions and discussions. Grateful acknowledgement goes to Dr. P.P. Moghe and Mrs. A.V. Pol for their enthusiastic help. My thanks are also due to Dr. V.G. Gunjkar and Dr. M.V. Kuber (SIL) and all my colleagues of catalysis group for their whole hearted help and co-operation. The help rendered by Mr. T.A.B. Mulla, Mrs. J.A. Pathak and Mr. A.K. Gangopadhyay, are highly acknowledged.

My special thanks are due to Mr. K. Ramakrishna and Mr. S.B. Pardeshi, for their technical assistance. The immense and valuable services of Library, Instrumentation Section, Liquid Nitrogen Section and Glass Blowing Section of this laboratory are gratefully acknowledged. Finally, I am specially indebted to my Parents for their encouragement and supporting me through their prayers.

(2)

I shall remise in my duty if I do not thank Director, NCL, Pune for permitting me to present this work in the form of a thesis.

MOST OF ALL, I AM THANKFUL TO THE LORD, IN WHOM ALL THINGS ARE POSSIBLE.

Ramanath

(R.N. BHAT)

C E R T I F I C A T E

Certified that the work incorporated in the thesis entitled "*SYNTHESIS AND CHARACTERIZATION OF LARGE PORE ZEOLITES*" submitted by Shri. Ramanath Narayan Bhat for the degree of Doctor of Philosophy was carried out by the candidate under my supervision in the National Chemical Laboratory, Pune. Such material as has been obtained from other sources has been duly acknowledged in the thesis.



Dr. P. Ratnasamy

(Supervisor)

CONTENTS

	Page No
CHAPTER-1 GENERAL INTRODUCTION	1
<i>1-1 INTRODUCTION</i>	1
1-1.1 Historical background	1
1-1.2 Classification of Zeolites	1
1-1.3 Nomenclature of Zeolites	2
1-1.4 Structure of Zeolites	2
1-1.5 Synthesis of Zeolites	2
<i>1-2 PHYSICOCHEMICAL CHARACTERIZATION</i>	9
1-2.1 X-ray Diffraction	9
1-2.2 Infrared Spectroscopy (IR)	11
1-2.3 Adsorption and Diffusion	13
1-2.4 Thermal Analysis	15
1-2.5 Temperature Programmed Desorption of Ammonia (TPD of NH ₃)	15
<i>1-3 SOME PROPERTIES OF ZEOLITES</i>	16
1-3.1 Ion-Exchange	16
1-3.2 Adsorption and Diffusion	16
1-3.3 Thermal Stability	17
1-3.4 Acidic Nature	17

1-3.5	Isomorphous Substitution	18
1.4	<i>APPLICATIONS OF ZEOLITES</i>	20
1-4.1	Zeolites in Petroleum Refinery	20
1-4.2	Zeolites in Organic Chemistry	23
1-4.3	Zeolites in Separation Process	23
1-5	<i>SCOPE OF THE WORK</i>	26
1-6	<i>STRUCTURAL FEATURES OF ZEOLITE BETA</i>	27
CHAPTER – 2 SYNTHESIS OF ZEOLITE BETA		
2-1	<i>INTRODUCTION</i>	29
2-2	<i>EXPERIMENTAL :</i>	29
2-2.1	Synthesis of [Al]-Beta using Silica Get	29
2-2.11	Synthesis of [Al]-Beta using TEOS	31
2-2.2	Synthesis of [Fe]-Beta using TEOS	33
2-2.3	Chemical Analysis	33
2-2.4	X-ray Powder Diffraction	34
2-2.5	Scanning Electron Microscopy	34
2-2.6	Preparation of the Protonic form of Beta Zeolite	34
2-3	<i>RESULTS AND DISCUSSION :</i>	36
2-3.1	X-Ray Powder Diffraction	36
2-3.2	The influence of Synthesis Parameters	43

2-3.21	The Influence of the Reactivity of the Silica Source	43
2-3.22	The Effect of Template Concentration	43
2-3.23	The Effect of Alkalinity	47
2-3.24	The Influence of Na/SiO ₂	47
2-3.25	The Influence of the Water Content	47
2-3.26	The Influence of SiO ₂ /Al ₂ O ₃ , ratio in the Gel	51
2-3.27	The Influence of Temperature on the Synthesis	55
2-4	<i>CONCLUSIONS</i>	55
CHAPTER – 3 PHYSICOCHEMICAL CHARACTERIZATION OF BETA ZEOLITES		
3-1	<i>EXPERIMENTAL</i>	58
3-1.1	Thermal Analysis	58
3-1.2	Sorption Properties	58
3-1.3	Temperature Programmed Desorption of Ammonia (TPD OF NH ₃)	60
3-1.4	Infrared (IR) Spectroscopy	60
3-1.5	Solid State MAS/MNMR Spectroscopy	62
3-1.6	ESR Spectroscopy	64
3-1.7	Magnetic Susceptibility	64
3-1.8	Mossbauer Spectroscopy	64

3-2	<i>RESULTS AND DISCUSSION</i>	64
3-2.1	Thermal Analysis	64
3-2.2	Adsorption of Water and Hydrocarbons	66
3-2.3	Temperature Programmed Desorption of Ammonia (TPD OF NH ₃)	69
3-2.4	Infrared Spectroscopy	75
3-2.5	Solid Stage MASNMR Spectroscopy	92
3-2.6	ESR Spectroscopy	92
3-2.7	Magnetic Susceptibility	92
3-2.8	Mossbaure Spectroscopy	95
3-3	<i>CONCLUSIONS</i>	98
CHAPTER – 4 CATALYSIS		
4-1	<i>INTRODUCTION</i>	99
4-2	<i>EXPERIMENTAL</i>	100
4-2.1	Atmospheric Pressure Reactor	100
4-2.2	Regeneration of the Catalyst	100
4-2.3	High Pressure Reactor	102
4-2.4	Regeneration of the Catalyst	102
4-3	<i>RESULTS AND DISCUSSION</i>	106
4-3.1	Conversion of meta-xylene	106

4-3.11	para-Xylene/ortho-Xylene(p-X/o-X) ratio	106
4-3.12	Isomerization/Disproportionation (I/D) ratio	106
4-3.13	1,3,5-/1,2,4 TMB ratio	112
4-3.2	H-[Fe]-Beta-37	119
4-4	<i>TOLUENE DISPROPORTIONATION</i>	119
4-5	<i>ALKYLATION OF BENZENE TO LINEAR ALKYL BENZENES (LAB)</i>	121
4-5.1	Experimental	121
4-5.2	Results and Discussion	124
4-6	<i>CONCLUSIONS</i>	128
	<i>SUMMARY</i>	130
	<i>REFERENCES</i>	133

LIST OF ILLUSTRATIONS

		Page No.
1.1	Primary, Secondary and Tertiary Building Units [PBU, SBU and TBU] leading to three dimensional zeolite framework.	8
1.2	Projection along [100] of polytype A and of polytype B, of zeolite beta (Fig. B & A respectively).	28
2.1	Stainless steel (316) autoclave with teflon gasket for hydrothermal synthesis.	30
2.2	X-Ray diffraction patterns of beta zeolites. Synthesis time $t = 0, 4, 5, 6$ and 8 days. [Curves A-E respectively].	37
2.3A	X-Ray diffraction patterns of [Al] Beta zeolites. $\text{SiO}_2/\text{Al}_2\text{O}_3 = 28, 45$ and 60 [Curves A,B and C respectively].	38
2.4A	X-Ray diffraction patterns of [Fe] Beta zeolites. $\text{SiO}_2/\text{Fe}_2\text{O}_3 = 25, 37$ and 59 [Curves A,B and C respectively].	39
2.3B	SEM photographs of [Al] Beta -28, 45 and 60 [A, B and C respectively].	40
2.4B	SEM photographs of [Fe] Beta -25, 37 and 59 [A,B and C respectively].	41
2.5	X-Ray diffraction patterns of Na-and H- Beta of Al and Fe zeolites [Curves a to d respectively].	44
2.6	The influence of $\text{TEA}^+/\text{SiO}_2$ ratio on crystallization of beta : Curves 1 to 3 correspond to values of 0.5, 0.25 and 0.165 respectively. [$\text{SiO}_2/\text{Al}_2\text{O}_3 = 60$, $\text{OH}/\text{SiO}_2 = 0.1$, $\text{H}_2\text{O}/\text{SiO}_2 = 25$].	46
2.7	The influence of OH/SiO_2 ratio on crystallization of beta : Curves 1 to 3 correspond to values of 0.2, 0.1 and 0.067 respectively. [$\text{SiO}_2/\text{Al}_2\text{O}_3 = 60$, $\text{TEA}^+/\text{SiO}_2 = 0.165$, $\text{H}_2\text{O}/\text{SiO}_2 = 25$].	48

2.8	The influence of Na^+/SiO_2 ratio on crystallization of beta : Curves 1 and 2 correspond to values 0.1 and 0.2 respectively. [$\text{SiO}_2/\text{Al}_2\text{O}_3 = 60$, $\text{TEA}^+/\text{SiO}_2 = 0.165$, $\text{OH}/\text{SiO}_2 = 0.1$, $\text{H}_2\text{O}/\text{SiO}_2 = 25$].	49
2.9	The influence of $\text{H}_2\text{O}/\text{SiO}_2$ ratio on the crystallization of beta : Curves 1 to 3 correspond to values 15, 25 and 35 respectively. [$\text{SiO}_2/\text{Al}_2\text{O}_3 = 60$, $\text{TEA}^+/\text{SiO}_2 = 0.165$, $\text{OH}/\text{SiO}_2 = 0.1$].	50
2.10	SEM photographs of the zeolite beta samples obtained from three different concentrations of water: $\text{H}_2\text{O}/\text{SiO}_2 = 15, 25$ and 35 [A, B and C respectively].	52
2.11	The influence of $\text{SiO}_2/\text{Al}_2\text{O}_3$ ratio in the gel on the crystallization of beta : Curves 1 to 3 correspond to $\text{SiO}_2/\text{Al}_2\text{O}_3 = 30, 60$ and 90 respectively. [$\text{TEA}^+/\text{SiO}_2 = 0.25$, $\text{OH}/\text{SiO}_2 = 0.1$, $\text{H}_2\text{O}/\text{SiO}_2 = 25$].	53
2.12	Relationship between the yield of crystalline beta and the $\text{SiO}_2/\text{Al}_2\text{O}_3$ ratio in the gel and final zeolite. Data from Ref. (94) are also included (see text).	54
3.1	Automatic recording electromicrobalance [Cahn-2000 G].	59
3.2	Temperature Programmed Desorption (TPD) apparatus.	61
3.3	FT-IR Transmittance Cell.	63
3.4	TG, DTG and DTA curves for TEA [Al] Beta -45 (a) and TEA[Fe] Beta -37 (b).	65
3.5	The thermograms of [Al] Beta -45 samples obtained in 0, 2, 4, 6, 7 and 8 days. [Curves a to f respectively].	67
3.6	Correlation between XRD crystallinity and relative crystallinity estimated from IR spectroscopy (- Δ -), thermal analysis (-0-) and adsorption of n-hexane (- Δ -) respectively.	72
3.7	TPD spectra of NH_3 from H[Al] Beta -28, 45 and 60 [Curves A,B and C], H[Fe] Beta -25, 37 and 59 [Curves d, e and f] respectively.	73

3.8	FT-IR spectra of TEA[Al]Beta-45 having 0, 20, 30, 60 and 100% XRD crystallinity [Curves a to e] respectively.	76
3.9	FT-IR spectra of TEA[Al]Beta-28 (a) and TEA[Fe]Beta-25 (b).	79
3.10	FT-IR difference spectra [TEA ⁺ - Na ⁺] of zeolite [Al]Beta-28, 45 and 60. [Curves a, b and c respectively].	81
3.11	FT-IR spectra of TEA[Fe]Beta-37 treated at 450, 575, 653 and 673 K [Curves a to d respectively].	83
3.12	FT-IR spectra of NH ₄ [Al]Beta-45 decomposed at 473, 573 and 773 K [Curves a, b and c] and of NH ₃ -H[Al]Beta-45 desorbed at 423, 573, 723 and 823 K [Curves d to g] respectively.	84
3.13	FT-IR spectra of NH ₄ [Fe]Beta-37 decomposed at 423, 573 and 773 K [Curves a, b and c] and NH ₃ -H[Fe]Beta-37 desorbed at 423, 573, 623 and 723 K [Curves d to g] respectively.	86
3.14	FT-IR spectra of H[Al]Beta-45 (a) and H[Fe]Beta-37 (b) with adsorbed D ₂ O.	88
3.15	FT-IR difference spectra of [sample with benzene - sample] H[Al]Beta-45 (a) and H[Fe]Beta-37 (b).	89
3.16	FT-IR spectra of pyridine chemisorbed on H[Al]Beta-45, Na[Al]Beta-45, H[Fe]Beta-37 and Na[Fe]Beta-37 [Curves a to d respectively].	91
3.17	MASNMR of [Al]Beta-45 and [Fe]Beta-37 [A and B shown respectively]. *spinning side bands.	93
3.18	ESR spectra of [Fe]Beta-37 at 297 and 94 K [Curves A and B respectively].	94

3.19	Mossbauer spectra of TEA[Fe]Beta-37 at 300 K	96
	(A) Normal scale	
	(B) Expanded scale	
3.20	Mossbauer spectra of TEA[Fe]Beta-37 at	97
	(A) 4.2 K and (B) 4.2 K with an externally applied magnetic field of 4.57 T.	
4.1	Fixed bed down flow on-line silica reactor used for catalytic reactions.	101
4.2	High pressure reactor used in studies.	103
4.3	Reaction paths for the m-xylene isomerization over zeolite beta and other medium pore zeolites leading to equilibrium point.	110
4.4	PX/OX ratio against m-xylene conversion obtained by changing temperature (●,○), WHSV (▲, △) and time on stream, TOS (■ □), filled and empty symbols represent medium and large pore zeolites respectively. Numbers followed by "-" represent zeolite ZSM-.	111
4.5	Log (I/D) against m-xylene conversion obtained by changing temperature (●,○), WHSV (▲, △) and time on stream, TOS (■ □), filled and empty symbols represent medium and large pore zeolites respectively. Numbers followed by "-" represent zeolite ZSM-.	114
4.6	1,3,5-/1,2,4 TMB ratio against m-xylene conversion obtained by changing temperature (●,○), WHSV (▲, △) and time on stream, TOS (■ □), filled and empty symbols represent medium and large pore zeolites respectively. Numbers followed by "-" represent zeolite ZSM-.	115
4.7	Effect of temperature on the disproportionation of toluene over H[Al]Beta-28 and 45 [A and B respectively].	122

- 4.8 Effect of space velocity (WHSV) on the disproportionation of toluene over H[Al]Beta-28 and 45 [A and B respectively]. 123

LIST OF TABLES

1.1	Classification based on chemical composition.	3
1.2	Classification based on dimensionality of the pore system.	4
1.3	Classification based on framework topology.	5
1.4	Zeolites classification on the basis of pore size.	6
1.5	Type and species of zeolites as per IUPAC nomenclature.	7
1.6	Organic cations - zeolite structure relationship.	10
1.7	Zeolite infrared assignments.	12
1.8	Synthetic large pore zeolites and some of their properties.	14
1.9	Industrial process based on zeolite catalysts.	19
1.10	Major commercial zeolite processes.	21
1.11	Some organic reactions catalyzed by zeolites.	24
1.12	Purification processes with zeolite absorbents.	25
2.1	Reagents used for the synthesis of zeolite beta and their specifications.	32
2.2	Chemical composition of zeolite beta samples	35
2.3	The "d" values of [Al] Beta -28 and [Fe] Beta -25 as synthesized samples.	42
2.4	The influence of the silica source on the synthesis of zeolite beta .	45
2.5	The influence of the temperature on the synthesis of beta zeolite.	56
3.1	Thermogravimetric data of different crystallinity samples of TEA[Al] Beta -45.	68
3.2	Adsorption properties of H[Al] Beta -45 and H[Fe] Beta -37.	70
3.3	Adsorption properties of Na[Al] Beta having different crystallinity.	71

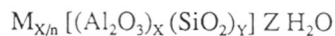
3.4	TPD results for [Al] - and [Fe]- Beta zeolites	74
3.5	Framework vibration frequencies of beta zeolites ($\nu \text{ cm}^{-1}$).	77
4.1	Details of the zeolites used in this study.	104
4.2	Reactant feed (s), their source and purity.	105
4.3	Influence of $\text{SiO}_2/\text{Al}_2\text{O}_3$ ratio in the m-xylene conversion reaction.	107
4.4	Influence of reaction temperature on m-xylene conversion reaction.	108
4.5	Influence of WHSV on the m-xylene conversion reaction.	109
4.6	Influence of pore geometry of zeolites shape selectivity in the isomerization of m-xylene	113
4.7	Effect of temperature on the methylation of toluene over H-[Al] Beta -45	117
4.8	The xylene isomerization process. Comparison of H[Al] Beta -45 with H[Al] ZSM-5 (50).	118
4.9	Isomerization of m-xylene over H[Fe] Beta -37 and H[Al] Beta -45	120
4.10	Influence of $\text{SiO}_2/\text{Al}_2\text{O}_3$ ratio on product distribution in alkylation reaction.	125
4.11	Influence of temperature on alkylation reaction. Zeolite beta R = 28, Benzene: olefin = 1:1.	127
4.12	Effect of change in benzene: Olefin ratio. Zeolite [Al] Beta -45; Temperature = 373 K.	129

CHAPTER - 1
GENERAL INTRODUCTION

GENERAL INTRODUCTION

1-1 INTRODUCTION

Zeolites are crystalline, microporous hydrated aluminosilicates containing cavities and channels. Structurally, they possess a framework based on an infinitely extending three dimensional network of SiO₄ and AlO₄ tetrahedra linked through oxygen atoms forming a rigid three dimensional structure. The negative charge on the AlO₄ tetrahedra is compensated by cations resulting in an electrically neutral framework. Thus an empirical formula for zeolites can be given as



where M is the cation of valence n, Z is the number of water molecules and Y/X is the structure characteristic ratio the summation X + Y represent the total number of tetrahedra in unit cell of zeolite.

1-1.1 Historical background

The term ZEOLITE was proposed by Cronstedt in 1756, from the Greek word, for minerals which expelled water when heated and appeared to boil¹. The discovery of these materials in mineral deposits of relatively high purity in various parts of the world led to the commercial use of natural zeolites². In 1962, the commercialization of these natural zeolites namely chabazite, erionite, mordenite and clinoptilolite commenced for various applications³. It was McBain, who proposed the term "Molecular Sieves" to describe a class of materials that exhibited selective adsorption properties⁴. Molecular sieves separate components of a mixture on the basis of molecular size and shape differences. However, Barrer⁵ was the first to show the molecular sieve behavior of zeolites and their potential in molecular sieving separations.

1-1.2 Classification of Zeolites⁶

As of today about 40 natural zeolites and about 150 synthetic zeolites are known⁸. Classification of these zeolites has been made on the basis of their morphological characteristics,

chemical composition (Table 1.1), effective pore diameter (Table 1.2) and natural occurrence. Several different structural classifications of zeolites have been proposed by various workers^{8,9}. However, the most important classification was proposed by W. Meier⁷ (Table 1.3 & 1.4) who classified them into seven groups based on differences in their secondary building units (SBU). Later Barrer¹⁰ extended the number of groups to ten by adding new synthetic and natural zeolites.

1-1.3 Nomenclature of Zeolites

The IUPAC commission on zeolite nomenclature¹² has put certain guidelines for the nomenclature of zeolites. This is based on their framework density (FD) and number of T-atoms per 1000A³. This classification does not depend on composition, distribution of T-atoms, cell dimensions or symmetry parameters. This does not include numbers and characters other than capital Roman letters. Some of the zeolite types and their important members are given in Table-1.5.

1-1.4 Structure of Zeolites

The Primary Building Unit (PBU) of the Zeolite structure is a tetrahedron of four Oxygen atoms surrounding a central Si or Al atom. These tetrahedras are connected through their shared oxygen atoms to give rise to wide range of Secondary Building Units (SBU). In turn, these SBUs interconnect to give polyhedra which combine in various combinations to form various three dimensional structures of Zeolites, which is shown in Fig.(1.1).

1-1.5 Synthesis of Zeolites

Zeolites are synthesized in hydrothermal conditions by the combination of certain basic oxides like K₂O and Na₂O with Al₂O₃ and SiO₂. These zeolites can be synthesized in many varieties of structure, composition, and properties.

Generally, zeolite crystallization is a nucleation controlled process, occurring from molecularly inhomogeneous¹³, alkaline, aqueous gels, in the temperature range of 348 K to 523 K. Different silica and alumina source materials can be used in formulating a gel, and the

Table - 1.1

Classification Based on Chemical Composition

The zeolites are also classified on the basis of their silica to Alumina ratios⁹

Group	SiO ₂ /Al ₂ O ₃ :(R)	Examples
1. Low silica	2 to 3	A,X, Sodalite
2. Intermediate Silica	4 to 10	Mordenite, Omega, L
3. High Silica	10 to several thousands	ZSM-5, -11, EU-1
4. Silicalite	∞(No Alumina)	Silicalite-1, -2

Table - 1.2

Classification Based on Dimensionality of the Pore System

Unidimensional	eg. Mordenite, Zeolite L, ZSM-12, SAPO-5 VPI-5
Two dimensional	eg. ZSM-5
Three dimensional	eg. Zeolite Y ZSM-20 Zeolite Beta Zeolite BC ₆ SAPO-37

Table - 1.3

Classification Based on Framework Topology^{7,8}

Group and Group Name	Typical Unit Cell composition	Type of Channel	Free aperture of main channel in $\left(\frac{a}{A}\right)$
Group 1 (S4R) eg. Analcime	$\text{Na}_{16}[(\text{Al}_2)_{16} (\text{SiO}_2)_{32}]_{16} \text{H}_2\text{O}$	One	2.6
Group 2 (S6R) eg. Omega	$\text{Na}_{6,8} \text{TMA}_{1,6} [(\text{AlO}_2)_8 (\text{SiO}_2)_{28}] 21\text{H}_2\text{O}$	One	7.5
Group 3 (D4R) eg. Zeolite A	$\text{Na}_{12} [(\text{AlO}_2)_{12} (\text{SiO}_2)_{12}] 27\text{H}_2\text{O}$	Three	4.2
Group 4 (D6R) eg. Natrolite	$\text{Na}_2, \text{K}_2, \text{Ca}, \text{Mg}_{29,5} [(\text{AlO}_2)_{59} (\text{SiO}_2)_{133}] 235\text{H}_2\text{O}$	Three	7.4
Group 5 (T_5O_{10}) ⁱ eg. Natrolite	$\text{Na}_{16} [(\text{AlO}_2)_{16} (\text{SiO}_2)_{24}] 16\text{H}_2\text{O}$	Two	2.6 x 3.9
Group 6 (T_8O_{16}) ⁱ eg. Mordenite	$\text{Na}_8 [(\text{AlO}_2)_8 (\text{SiO}_2)_{40}] 28\text{H}_2\text{O}$	Two	6.7 x 7.0
Group 7 ($\text{T}_{10}\text{O}_{20}$) ^k eg. Stilbite	$\text{Ca}_4 [(\text{AlO}_2)_8 (\text{SiO}_2)_{28}] 28\text{H}_2\text{O}$	Two	2.7 x 5.7

Table - 1.4

Zeolites Classification on the Basis of Pore Size:

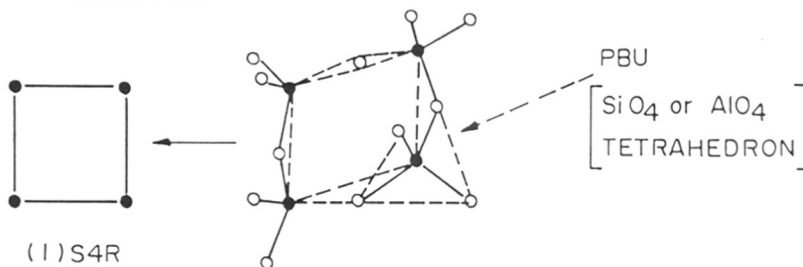
Pore size	No. of tetrahedras	Max. free diameter
Small	6 and 8	4.3 $\overset{\circ}{\text{A}}$ eg. Erionite
Medium	10	6.3 $\overset{\circ}{\text{A}}$ eg. ZSM-5 Stilbite
Large	12	7.5 $\overset{\circ}{\text{A}}$ eg. Zeolite Beta Linde-X, Y Mordenite
Extra large pore	18	~ 12 $\overset{\circ}{\text{A}}$ eg. VPI-5 ¹¹

TABLE - 1.5

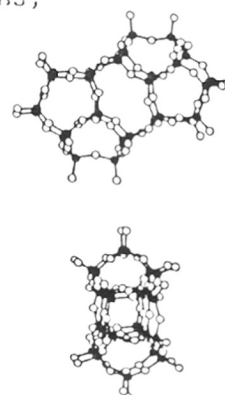
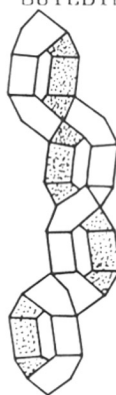
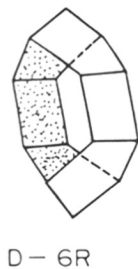
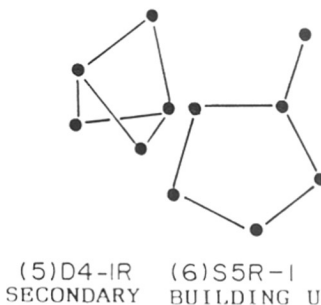
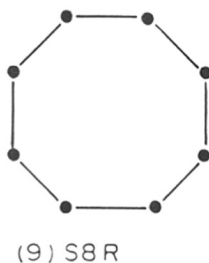
Type and Species of Zeolites as per IUPAC Nomenclature

Type	Species	Type	Species
AEL	ALPO ⁺	FAU	Faujasite
AFI	ALPO ₄ -5	MTW	ZSM-12
ERI	ALPO ₄ -17	MFI	ZSM-5
ATT	ALPO ₄ -33	ERI	Erionite
FAU	ALPO ₄ -37	EUO	EU-1
LTA	ALPO ₄ -42	MTT	EU-13
ANA	Analcime	FER	Ferrierite
MEL	Boralite-D	MOR	Mordenite
CAN	Cancrinite	MFI	NU-4
CHA	Chabazite	TON	NU-10
MTW	NU-13	FER	NU-23
MAZ	Omega	RHO	RhO
LEV	SAPO-35	MEL	ZSM-11
SOD	Sodalite	LTL	Zeolite-L
TON	ZSM-22	EUO	ZSM-50
Novel	Zeolite Beta		

FIG.1.1 : PRIMARY, SECONDARY AND TERTIARY BUILDING UNITS (PBU, SBU AND TBU) LEADING TO THREE DIMENSIONAL ZEOLITE FRAMEWORK



PRIMARY BUILDING UNITS (PBU)



TERTIARY BUILDING UNITS (TBU)

final product obtained is often dependent on the sources chosen and their pre-history. The starting materials normally used are Na_2SiO_3 , Silica gel, silica sol, NaAlO_2 , $\text{Al}_2(\text{SO}_4)_3$, Al metal or Al_2O_3 . The $\text{SiO}_2/\text{Al}_2\text{O}_3$ ratio in reaction mixture imposes constraint on the framework composition of the zeolite.

Organic cations are also used in zeolite synthesis. They are known to 'template' particular framework structures. The specific function of these organics is highly dependent on the details of the experiment¹⁴. Normally, addition of organics to a reaction mixture can lead to four variations: (i) A different zeolite structure is obtained, (ii) Crystallization rate is enhanced (or inhibited), (iii) Same framework but a change in chemical composition is obtained, or (iv) a change in texture is observed¹⁵. A list of templates used and the zeolites obtained are given in Table-1.6. It should be noted that template-zeolite structure relationship is not simple.

1-2 PHYSICOCHEMICAL CHARACTERIZATION

1-2.1 X-ray Diffraction

This technique gives the most significant information about the solid material^{17,18} like phase purity, uniqueness of structure, incorporation of other elements into the framework and degree of crystallinity. When isomorphous substitution occurs, the extent of incorporation of the isomorphous element is correlated with the unit cell expansion/contraction¹⁹⁻²². The most important use of this technique is in the elucidation of the structure of materials, especially single crystals^{23,24}. This technique is also useful when the material is in powder form. When all the peaks in the XRD pattern are sharp and well resolved they can be indexed and the unit cell parameters calculated. Modern methods have used ab initio calculations and Rietveld analyses to solve the zeolite structures using powder X-ray patterns²³⁻²⁵.

TABLE - 1.6

Organic cations - Zeolite Structure Relationship^{14,16}

Organic Cation	Zeolite
Tetraethyl (TEA) ⁺	Beta
	ZSM-8
	ZSM-12
	ZSM-20
	ZSM-25
Tetrapropyl ammonium (TPA) ⁺	ZSM-5
Triethylbutyl ammonium (TEBA) ⁺	ZSM-5
n-propylamine	ZSM-5
Tripropylamine (TPA) ⁺	ZSM-5
TMA + TEA	ZSM-35
Neopentylamine	ZSM-5
Dihexamethylene triamine	ZSM-30
Hexamethonium Bromide (HMBr)	EU-1
	EU-2
Pentaerythritol (PTE)	NU-5

1-2.2 Infrared Spectroscopy (ir):

This is a very important technique to obtain structural information and is complementary to X-ray structural analysis. Flanigen²⁶ et al. carried out investigations in mid-infrared region for structural analysis. The absorption in this region can be classified into two groups:

- i) Internal vibrations of the TO_4 unit
(insensitive to structural vibrations) and,
- ii) Vibrations due to external linkages of the TO_4 units
(sensitive to structural vibrations)

Types of absorptions and corresponding IR values are tabulated in Table-1.7.

Systematic investigation of the framework vibrations of Zeolites namely Mordenite and Omega has been reported²⁶. The bands around 550 cm^{-1} are assigned to double-five [5-5] membered rings whereas the band around 560 cm^{-1} is assigned to [5-3] another type of five membered ring. The infrared spectrum of zeolite **beta** shows the presence and dominance of 5-ring units. The frequencies of certain bands in the IR spectra also shift in a consistent fashion with successive dealumination of zeolite **beta**. Kinetics of zeolite crystallization has been studied by monitoring the changes in the framework vibrations²⁷. Successive incorporation of organic cations into the zeolite lattice is also observed by changes in the C-H vibrations.

The isomorphous substitution of Fe, Ga, B, and P into the zeolite framework has been found to shift the peak positions. On introduction of Fe in the lattice, most of the bands are shifted to lower wavenumbers due to the heavier mass of Fe. Whereas substitution of Boron shifts the peak positions to higher wave numbers due to the lighter mass of B unit²⁸. IR spectroscopy has been extensively used to differentiate various types of -OH groups. The -OH groups are characterized by the absorption bands in the region $3500\text{-}3750 \text{ cm}^{-1}$.²⁹ This technique is also used to

TABLE-1.7

Zeolite Infrared Assignments

Internal tetrahedra	$\nu \text{ cm}^{-1}$
Asymmetric stretch	1250-950
Symmetric stretch	720-650
T-O bend	420-500
External linkages	
Double ring	650-500
Pore opening	300-420
Symmetric stretch	750-820
Asymmetric stretch	1050-1150

estimate the acid sites by adsorption of various bases. Various bases like ammonia, pyridine, benzene are used as probe molecules to measure the acidity. D₂O can also be used to probe the nature of hydroxyl groups.

1-2.3 Adsorption and Diffusion

Zeolites are crystalline, porous materials with good sorption and diffusion properties. Sorption studies give information about³⁰:

- * Void volume of the zeolite (O₂, N₂, n-hexane adsorption)
- * Size of the pore opening (6-, 8-, 10-, 12-membered rings)
- * Degree of crystallinity
- * Hydrophobicity/Hydrophilicity
- * Acidity
- * Diffusion limitations (pore blockage etc. if any)

Important large pore synthetic zeolite and sum of their properties are summarized in Table 1.8.

Barrer and co-workers^{31,32} have extensively studied the sorption of various gases on both natural and synthetic zeolites. They estimated^{33,34} various thermodynamic parameters such as entropy, heat and free energy of sorption.

Sorption studies also help in determining specific interactions between sorbate and sorbents. The nature and strength of interactions³⁵ such as the sorbate-sorbent, and sorbate-sorbate can also be determined.

In heterogeneous catalysis diffusion and adsorption processes affect the overall rate of the chemical transformation. Three types of diffusion, namely, Configurational diffusion, Knudsen diffusion and bulk diffusion are known in zeolite catalysis. In configurational diffusion the molecule takes the proper shape and size to diffuse into the zeolite pore. When the mean free path

Table - 1.8

Synthetic large pore zeolites and some of their properties

Zeolites	U.C. Composition	U.C. Vol. A ^{°3}	P.O. A [°]	P.V. ml/g
X (1-1.5)	Na ₈₆ [Al ₈₆ SiO ₁₀₆ O ₃₈₄]. nH ₂ O	15600	7.4	0.38
Y (3.0 - 6.0)	Na ₅₆ [Al ₅₆ Si ₁₃₆ O ₃₈₄]. 260 H ₂ O	15000	7.4	0.28
Mordenite (9-30)	Na ₈ [Al ₈ Si ₄₀ O ₉₆]. 24 H ₂ O	2974	6.7 x 7.0	0.165
L-type (5.7 - 7.0)	K ₆ Na ₃ [Al ₉ Si ₂₇ O ₇₂]. 21 H ₂ O	2205	7.1	0.24
Ω (5-12)	Na ₄ K ₆ [Al ₁₀ Si ₂₆ O ₇₂]. 28 H ₂ O	2150	7.5	0.23
ZSM-20 (8-10)	Na ₁₆ [Al ₁₆ Si ₈₀ O ₁₉₂]. n H ₂ O	4550	7.4	0.31
ZSM-12 (50-300)	Na _{0.5} [Al _{0.5} Si _{27.5} O ₅₆]. 4 H ₂ O	-	5.7 x 6.1	0.15
Beta (20-200)	Na ₄ [Al ₄ Si ₆₀ O ₁₂₈]. 193 H ₂ O	4094	7.3 x 6.0	0.21
BC ₆ (8-10)	Na ₁₈ [Al ₁₈ Si ₇₈ O ₁₉₂]. n H ₂ O	10000	7.4 x 0.8	-
SAPO-5	Na _m [Al ₁₀ P ₁₁ Si ₃ O ₄₈]. 8 H ₂ O	-	7.3	0.18
SAPO-37	Na ₂₀ [Al ₇₆ P ₉₂ Si ₂₈ O ₃₈₄]. 240 H ₂ O	-	7.4	0.28
VPI-5	Na ₁₁ [Al ₁₆ P ₁₇ Si ₃ O ₇₂]. n H ₂ O	2533	12.1	0.31

of the molecule is comparable to the pore diameter the diffusion is controlled by the laws of Knudsen diffusion. In bulk diffusion the mean free path of the molecule is smaller than the size of the pore. Rates of bulk diffusion are independent of the pore radius. The movement of molecules in zeolite pores has aspects of both adsorption and diffusion.³⁶

1-2.4 Thermal analysis

Information regarding the thermal behavior of the zeolites is obtained by this technique^{37,38}. Various physicochemical changes like dehydration of adsorbed water, decomposition of occluded organics, dehydroxylation leading to Lewis sites during thermal treatment are seen in thermoanalytical curves^{39,40}. This technique is extensively used in the study of kinetics of dehydration of zeolites and also for studying the oxidative decomposition of occluded organics in zeolites^{41,42}.

1-2.5 Temperature Programmed Desorption of Ammonia (TPD of NH₃)

The estimation of acid strength distribution in zeolites is carried out by this technique. Tanabe and coworkers^{43,44} have reviewed the various techniques used for acidity measurements. They have reported results on Na-ZSM-5, H-ZSM-5 and Silicalite suggesting that acid sites of TPD maxima observed at 780K are the probable sites used in hydrocarbon conversion processes. By this technique, one can characterize weak, medium and strong-acid sites depending on the temperature of desorption of ammonia⁴⁵. The amount of ammonia released above 753K is normally considered to represent very strong acid sites. Topsoe et al.²⁹ have reported acidic properties of fresh and partially deactivated catalysts. They have reported three different (α , β and γ) types of sites depending on the temperature ranges. Borade et al.⁴⁶ have reported three different acid sites in TPD of NH₃ on H-ZSM-5 showing the presence of all three types of sites (strong, medium and weak).

1-3 SOME PROPERTIES OF ZEOLITES

1-3.1 Ion-Exchange

This property is a function of the amount of aluminum present in the framework of the zeolite. Each tetrahedral aluminum carries one negative charge and this charge is neutralized by a cation to stabilize the zeolite framework. Usually alkali or alkaline earth metals are used to neutralize the framework.

These charge compensating cations are loosely held to the framework aluminum. So they are easily exchangeable with different monovalent or multivalent cations^{47,48}. This ion exchange property depends on the cation size, cation charge, normality of the exchanging solution, temperature of ion exchange solvent used, structure of the zeolite, and location of the cation site.

1-3.2 Adsorption and diffusion

In zeolites usually intracrystalline surface area constitutes about 97% of total surface area and values of a few hundred m^2/g are known. The large void volume coupled with the electrostatic fields lead to the extremely high adsorption capacity of zeolites. In addition to molecular size and steric hindrance, other factors like polarizability, polarity of the adsorbate, organophobicity, hydrophobicity of the zeolite host structure, and extent of unsaturation of organic adsorbates also have influence on the adsorption⁴⁹.

Diffusion plays a key role in molecular shape selective catalysis. The rates of diffusions can significantly affect the activity and selectivity of zeolite catalysts^{50,51}.

Barrer⁵² has reviewed the major features of diffusion in zeolites. The diffusion coefficients depend on the nature of the zeolite (ionic, hydrophobic, etc.) and the nature of the adsorbate.

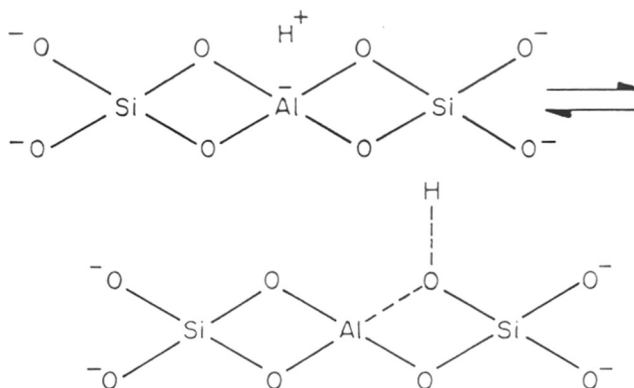
TH-617

1-3.3 Thermal Stability

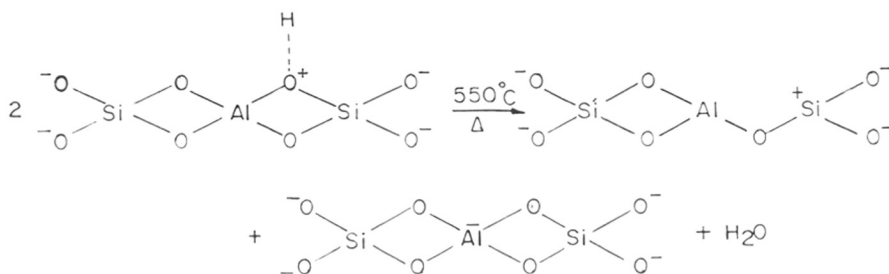
This is a vital information needed before the zeolite is used in any reaction. The structure of zeolites collapse or undergo phase transformation at elevated temperatures^{53,54}. DTA data are normally used in the determination of the thermal stability of zeolites⁵⁵. Thermal stability of zeolites can be improved by increasing the silica to alumina ratios⁵⁶ by acid treatments (dealumination)⁵⁷, or by ion-exchange with polyvalent cations⁵⁶.

1-3.4 Acidic Nature

Substitution of Al for Si in the zeolite framework generates the potential for acidic activity. When the charge compensating cation is hydrogen atom (proton) the zeolite framework exhibits the capacity to act as a proton donor or Brønsted acid.^{56,58,59}



When the zeolite is heated to 550°C, Si-O-Al bonds break giving rise to Lewis acid sites and water.



Here both Lewis and Bronsted acid sites coexist. Dissociation energy calculations⁶⁰ show that between the bridging and terminal hydroxyl groups, the former was found to be more acidic than the latter. This conclusion is supported by the lower vibrational frequency of the bridging hydroxyl group⁶¹.

Acidity in zeolites is a very important parameter. This acidity can be tuned as per the needs by post-modifications of the zeolites. Some of the acid catalyzed reactions are given in Table 1.9.

1-3.5 Isomorphous substitution

Isomorphous substitution of elements other than Si and Al into tetrahedral framework positions is a new area in zeolite research, which is developing very fast. Barrer⁶² has reviewed the synthetic aspects of the problem and presented a theoretical approach to such isomorphous substitutions⁶³. Tielen et al.⁶⁴ reviewed the catalytic implications of T-atom substitutions. Thereafter, a series of Union Carbide patents and papers^{65,66} have described large numbers of new aluminophosphate molecular sieves (AlPO's) and families of related materials obtained by incorporating Si in AlPO framework (SAPO's) or transition metals (MeAPO's). During the same period, Taramoso et al.⁶⁷ reported the synthesis of titanium silicalite (TS-1), a titanium containing silicalite-1 zeolite. TS-1 is known to catalyze oxidation of unsaturated hydrocarbons with aqueous H₂O₂ such as epoxidation of alkenes, the oxidation of alcohols to ketenes, and hydroxylation of aromatics⁶⁸. In the year 1987, Davis et al.⁶⁹ disclosed the synthesis of a new aluminophosphate molecular sieve (VPI-5) containing an 18-member ring pore system. They also reported⁷⁰ the substitution of Si, Mg and Co ions in VPI-5 framework. In fact, the discovery of VPI-5 ushered into a new era in zeolite science and technology, because it opened up new possibilities in the zeolite materials having very large pore size ($> 12\overset{\circ}{\text{A}}$). The important criteria for this isomorphous substitution are:

- * The cation of the substituent element should fit into the space at the center of four oxygen atoms without much strain.

TABLE - 1.9

Industrial Process based on zeolite catalysts⁷⁶

Process	Zeolite	Purpose
Selectoforming	ZSM-5	Octane boosting
M-forming	ZSM-5	Octane boosting
Catalytic cracking	Y-type (USY)	Octane boosting
MDDW	ZSM-5	Distillate dewaxing
M ₂ forming, (Cyclar)	L-type, Ga-ZSM-5	Gas to aromatics
MTG	Modified ZSM-5	Methanol to Gasolene
MTO	Modified ZSM-5	Methanol to Olefins
MCPI	ZSM-5/EU-1	Xylene isomerization
Xylofining	ZSM-5	Xylene isomerization
MEB, ALBENE	ZSM-5	Ethyl benzene manufacture

- * STC (Substitution of Tetrahedral Coordination) will be determined by the size of the T-atom.
- * Elements with ionic radii between $0.61 < r > 0.2$ fit as T atoms in zeolite framework. The isomorphic substitution can be confirmed by many well established techniques.

1-4 APPLICATIONS OF ZEOLITES

1-4.1 Zeolite in Petroleum Refinery

Catalytic processes that use zeolites continue to grow rapidly because of their superiority over conventional silica-alumina catalysts. These zeolites possess some important properties like:

- * Well-defined crystalline structure
- * High internal surface area
- * Uniform pores with one or more discrete sizes
- * Good thermal stability
- * Ability to sorb and concentrate hydrocarbons
- * High acidity when ion exchanged with protons

The very first industrial application of zeolites as catalysts started in the early 1960's with the replacement of conventional silica-alumina cracking catalyst by faujasites^{71,72}. Later zeolite-Y (metal doped) was successfully used in hydrocracking.^{73,74} In 1970's, the discovery of the first member of the pentasil family ZSM-5⁷⁵, made another landmark in zeolite catalysis. The use of high silica zeolites as highly acidic, shape selective and thermally stable materials led to new industrial petrochemical processes. Some of the important industrial processes based on zeolites are summarized in Table 1.10.

TABLE - 1.10

Major Commercial Zeolite Processes⁷⁶

Process	Zeolite	Products
Catalytic cracking	Faujasite	Gasoline, fuel oil
Hydrocracking	Faujasite	Kerosene, jet fuel, benzene, toluene, xylene
Hydroisomerization	Mordenite	i-hexane, heptane
iso/n-paraffin separation	Ca-A	Pure n-paraffins
Dewaxing	ZSM-5	Low pour point
	mordenite	Lubes
Benzene alkylation	ZSM-5	Styrene
Xylene isomerization	Encilite	p-xylene synthesis
MEB, ALBENE		Ethylbenzene synthesis

Shape Selectivity

The zeolite pores are of molecular dimensions. Most of the catalytic sites are confined within these pores. The diffusion of reactant molecules inside the zeolitic pores, formation of product molecules and diffusing out of the product molecules, all depends on relative-dimensions of the pore and reactants^{77,78,79}.

This phenomena of controlling the entry / exit of reactant / products molecules inside the zeolite pores depending on the dimensions is the basis of one aspect of shape selective catalysis. There are four types of shape selectivities discussed in the literature.

1. Reactant Shape Selectivity:

This occurs when only some of the reactant molecules in the reaction mixture are small enough to diffuse into the zeolite pores.

2. Product Shape Selectivity:

This occurs when some of the products that can be formed within the pores are too bulky to diffuse out. They are either converted to less bulky molecules that can diffuse out or eventually deactivate the catalyst by blocking the pores.

3. Restricted Transition State Shape Selectivity:

This is observed in reactions when the transition state requires more space than is available in the cavities of the zeolite. The products which result from less bulky transition states are preferentially produced.

4. Molecular Traffic Control:

The zeolites having more than one type of pore systems exhibit this type of shape selectivity. The reactant molecules may preferentially enter the catalysts through one of the pore systems while the products diffuse out by the other⁸⁰.

1-4.2 Zeolites in Organic Chemistry

The combination of acidity and shape selectivity in zeolites is an important factor for organic synthesis. The tendency to exploit this potential for specific, highly selective synthesis in the area of fine chemicals and intermediates is increasing. The zeolites can be tailor-made as required for added advantage. Some important organic⁸¹⁻⁸³ reactions catalyzed by zeolites are summarized in Table 1.11.

1-4.3 Zeolites in Separation Processes:

Zeolites have been developed for a wide variety of separations^{84,85}. These materials can be employed on regenerative basis and used many times. This regeneration can be done by many methods viz., thermal cycle, pressure cycle, displacement purge cycle, and inert purge cycle. Molecular sieve separations are unique in a number of respects viz., they allow selective removal of one component from a mixture, based on molecular size differences, with the removal of even trace impurities from fluids to give undetectable levels of impurity in the product. These unique adsorptive properties have brought zeolite molecular sieves to the forefront as a major tool of the chemical processing industries.

Commercially they are used for purification and bulk separation. Some examples of zeolite applications in purifications are mentioned in Table 1.12.

TABLE 1.11

SOME ORGANIC REACTIONS CATALYSED BY ZEOLITES

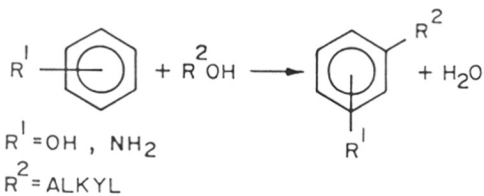
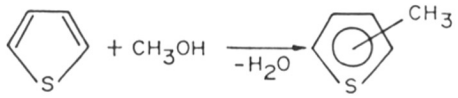
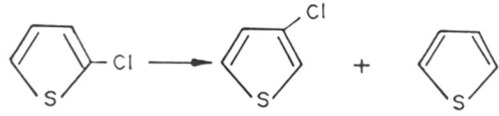

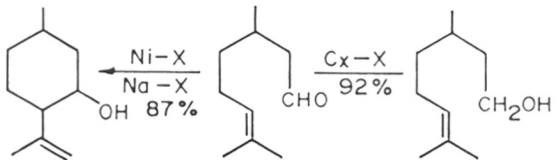
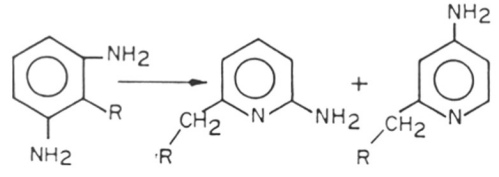
REACTION	ZEOLITE*
<p>ALKYLATION OF AVENOS</p>  <p>$R^1 = \text{OH}, \text{NH}_2$ $R^2 = \text{ALKYL}$</p>	H-ZSM-5 Cs-ZSM-5
<p>ALKYLATION OF HETEROATOMS</p> 	H-ZSM-5 H-Y Li-Y
<p>ISOMERIZATION REACTION</p> 	ZSM-5 Na-ZSM-5
<p>REARRANGEMENT</p>  <p>TETRAHYDRO DICYCLO-PENTA DIENE ADAMANTANE</p>	La-Y Pt/Ce-Y
	Li-X / Cs-X
<p>SYNTHESIS OF AROMATIC N-HETEROCYCLIC COMPOUNDS</p> 	H-ZSM-5 Cd-H-ZSM-5

TABLE - 1.12

Purification Processes with zeolite absorbents⁸⁵

Feed	G/L**	Zeolite
Drying of		
Natural gas	G	4A
Air	G	4A
Refrigerants	G/L	Modified 4A
Cracked gas	G	3A
Organic solvents	L	3A
Acid gases	G	Chabazite
CO ₂ removal		
From air in submarines/ space crafts	G	4A
H ₂ S		
From sour gas	G	CaA or Ca-Chabazite
Kr ⁸⁵ removal		
From air	G	Silicalite/ dealuminated H-mordenite
I ¹²⁹		
From air	G	AgX, Ag-Mordenite

** G: Gas, L: Liquid

1-5 SCOPE OF THE WORK

The foregoing review of the literature reveals that important reactions like cracking and hydrocracking of large hydrocarbon molecules requires the use of large pore zeolites in order to minimize diffusional constraints. Therefore, zeolite-Y is widely used for the catalytic processes. Sometimes it is advantageous to use zeolite-Y with a high framework Si/Al ratios⁸⁶⁻⁸⁸ (Si/Al > 10). But unfortunately it has not been possible till now to directly synthesize zeolite-Y with Si/Al ratio higher than about 3. Hence, it needs dealumination by steam or chemical treatments after the synthesis. This adds additional cost on the process for dealumination. In addition, the extra framework aluminum (EFAL), even if it is catalytically active can create some problems due to nonselective cracking reactions⁸⁹. Another way of solving the problem is the use of other large pore high silica zeolites. One of these is zeolite **beta**, already synthesized in the sixties⁹⁰. Zeolite **beta** has certain unique properties⁹¹. It is the:

- * Only high silica zeolite (Si/Al > 15) to have fully three dimensional 12-ring pore system.
- * It is the only large pore zeolite to have chiral pore intersections.
- * Apart from mordenite it is the only zeolite to have near-random degree of stacking faults and yet maintain full sorption capacity.

In view of these excellent properties and potential applications in hydrocarbon reactions, a detailed and systematic investigation on zeolite **beta** is being carried out. This investigation has been undertaken with the following objectives:

- 1) Study of the kinetics of synthesis of zeolite **beta**.
- 2) Synthesize of iron-analog of zeolite **beta**.
- 3) Characterization of the zeolite **beta** by various physicochemical techniques and.

4) A study of the catalytic properties of **beta** in various hydrocarbon reactions. Chapter 1 provides an introduction to zeolites especially **beta**. The thesis contains four chapters. Chapter 2 describes the synthesis of zeolite **beta** using silica gel as a source of silica and the influence of various parameters on the synthesis. It also describes the synthesis of the iron analogue of zeolite **Beta**.

Chapter 3 describes the various physicochemical characterizations of zeolite **beta** as well as its iron-analog. The isomerization of m-xylene, toluene disproportionation and benzene-alkylation with long chain olefins are described in Chapter 4.

A summary of the investigations is presented at the end.

1-6 STRUCTURAL FEATURES OF ZEOLITE BETA

Zeolite **Beta** is regarded as a highly intergrown hybrid of two distinct but closely related polymorphs A and B (Fig. 1.2). These polymorphs have the space groups $P4_1 22$ and $P4_3 22$ (Right or left handed) respectively. The polymorph A is tetragonal with $a = 1.25$ nm and $c = 2.66$ nm and polymorph B is monoclinic C_2/c , with $a = 1.76$ nm, $b = 1.78$ nm, $c = 1.44$ nm and $\gamma = 114.5^\circ$

The cross-sectional aperture dimensions of the pores in polymorph A is 0.73×0.60 whereas for the polymorph B it is 0.56×0.56 nm. The unit cell volumes calculated for polymorph A and polymorph B are 4.142 and 4.118 nm³, respectively. The framework density (FD = no. of T-atoms per cubic nanometer) is 15.5. The high stacking fault densities give rise to complex X-ray powder diffraction patterns containing both broad and sharp peaks for this zeolite. The 'Low-resolution' model⁹¹ of the pore structure of zeolite **beta** is shown in Fig. 1.2. Here the second channel B is positioned above the first with a little translation in the intralayer direction. This model explains both its high stacking disorder and excellent sorption capacity. Zeolite **beta** contains 5-ring units.

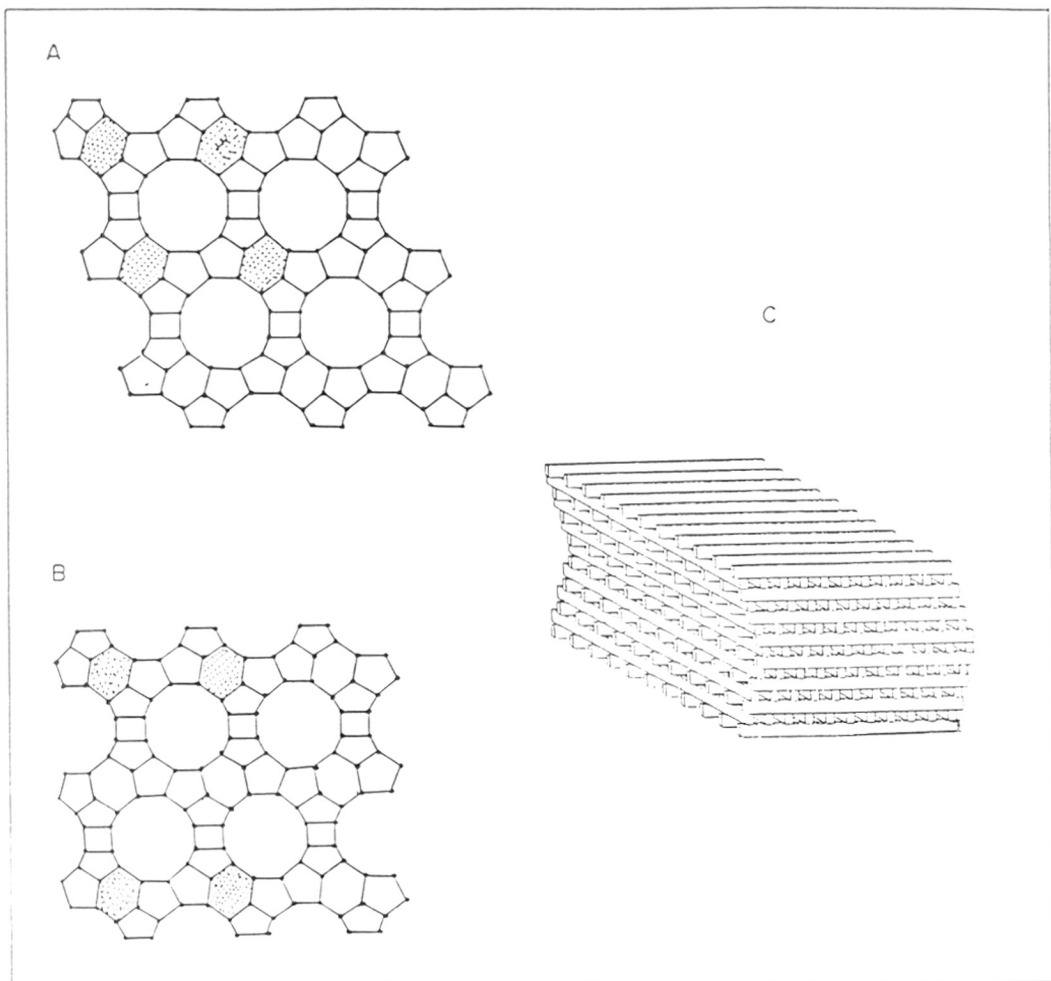


FIG.1.2 : PROJECTION ALONG [100] OF POLYTYPE A AND OF POLYTYPE B OF ZEOLITE BETA.

LOW RESOLUTION MODEL OF THE ZEOLITE BETA PORE STRUCTURE SHOWING AN INTERPENETRATING ARRANGEMENT OF CHANNELS(C).

CHAPTER - 2
SYNTHESIS OF ZEOLITE BETA

2-1 INTRODUCTION

This chapter deals with the crystallization kinetics of zeolite beta. The influence of various reaction parameters such as reactivity of the silica source, template concentration, alkalinity, Na^+/SiO_2 , water content, $\text{SiO}_2/\text{Al}_2\text{O}_3$ ratio, and temperature was studied. In order to optimize the synthesis conditions, the effect of different sources of silica namely pyrogenic silica with different particle size/surface area and tetraethylorthosilicate (TEOS) was studied.

The replacement of T atoms (Al or Si) in the zeolite structure by other elements, generally referred as "isomorphous" substitution modifies its physicochemical characteristics. In this chapter the procedure for synthesizing ferrisilicate analogs of zeolite beta is described. The presence of iron in the framework structure of beta was established by various techniques.

2-2 EXPERIMENTAL

2-2.1 Synthesis of Al-Beta Using Silica Gel

The hydrothermal synthesis was done in stainless steel autoclaves of 150 ml capacity which is shown in Fig. (2.1). Before use, the autoclaves were thoroughly cleaned with hydrofluoric acid and washed with water to minimize seeding effects, if any.

In a general synthesis procedure, the required amount of sodium hydroxide and double distilled water was added to a slurry of pyrogenic silica (A) (Cabosil-S5000). To this was added the required amount of aqueous solution of tetraethyl ammonium hydroxide (40 wt%) (Aldrich). Finally, a solution of sodium aluminate in water was added to the above mixture under stirring in a polythene beaker. The resulting homogeneous gel so obtained was distributed in several autoclaves. The synthesis was carried out at 423 K under static condition. The autoclaves were then taken out from the oven at various time intervals (to study the kinetics of crystallization) and

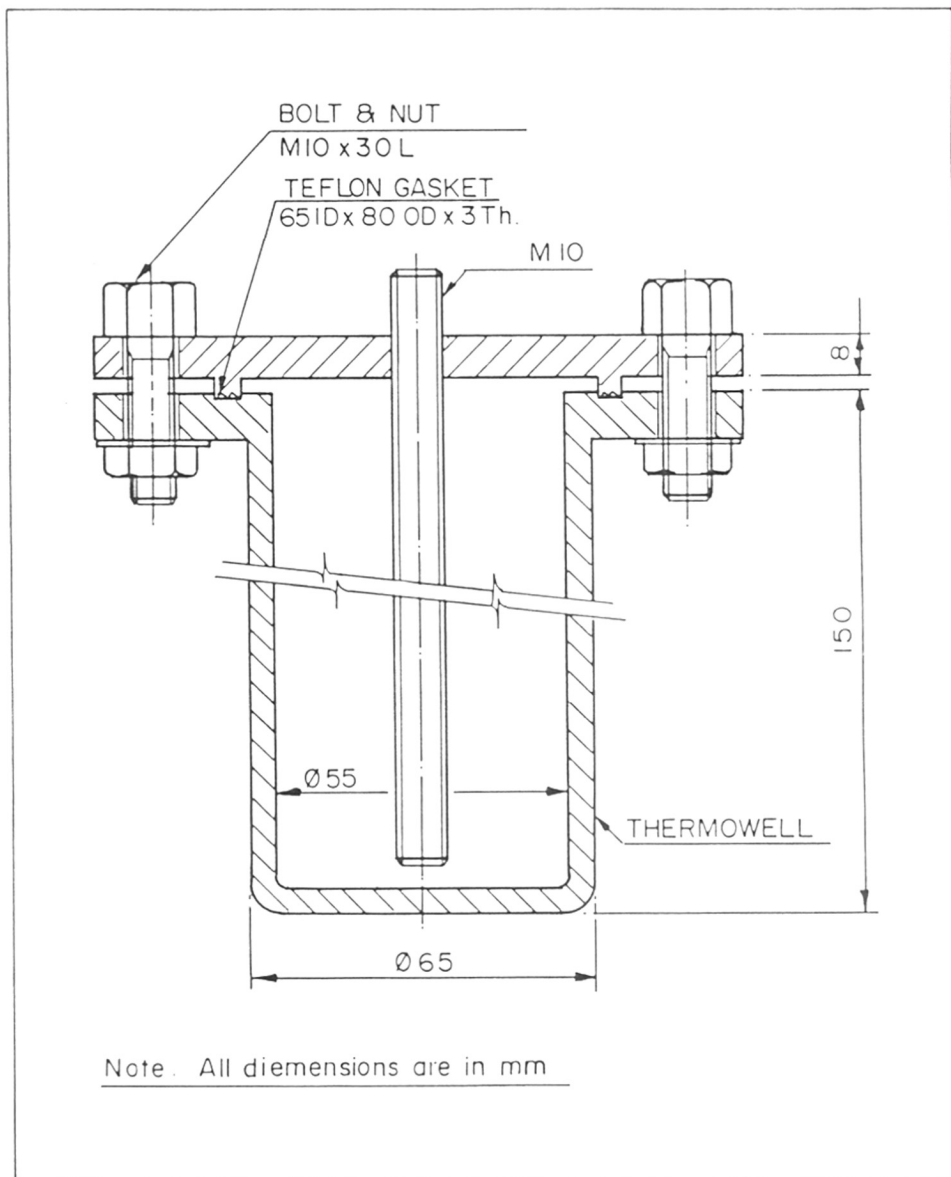


FIG.2.1 : STAINLESS STEEL (316) AUTOCLAVE WITH TEFLON GASKET FOR HYDROTHERMAL SYNTHESIS

quenched with cold water. The solid material was filtered, washed thoroughly with deionized water and dried at 393 K in a static oven. The reagents used with their specifications and purity are mentioned in Table 2.1.

In a typical preparation, 2.46 g of NaOH was mixed with slurry of 72 g SiO₂ (silica gel) in 440 g doubly distilled water. To this was added a mixture of 73.5 g of TEAOH (Tetra Ethyl Ammonium Hydroxide, 40% in water) and a solution of 4.65 g sodium aluminate (NaAlO₂) in 55.9 g of water with stirring in a polythene beaker. The gel so obtained was distributed in several autoclaves.

The molar composition of the aluminosilicate gel was: 3Na₂O : 5(TEA)₂O : Al₂O₃ : 60SiO₂:1500H₂O. The synthesis was carried out at 423K without agitation. The autoclaves were then taken out from the oven after 0,2,4,6,7 and 8 days and quenched with cold water. The solid material was filtered, washed thoroughly with deionized water and dried at 393K in a static air oven. The crystallinity of these samples is determined by the X-ray powder diffraction technique.

2-2.11 Synthesis of [Al]-Beta using TEOS

In a typical procedure, 0.1 g NaOH, 1.55 sodium aluminate and 36.8 g tetraethyl ammonium hydroxide (TEAOH, 40%) were mixed with 48.8 g of deionized water. To this homogeneous mixture, 42.5 g tetraethylorthosilicate was added slowly with continuous stirring at room temperature. In this way the silicic acid ester was slowly hydrolyzed leading to the formation of a gel. The ethanol formed during the hydrolysis was evaporated by stirring the gel for 10-15 hours at room temperature.

The gels were transferred into stainless steel autoclaves, closed tightly and heated at 393 K. After 6-7 days the autoclaves were quenched in cold water. The solids were filtered and washed thoroughly with deionized water and dried at 373K. The gel had the molar composition of:

Table - 2.1

Reactants used for the synthesis of zeolite beta and their specifications

Reagent	Formula & Specifications
A. SILICA GEL	SiO ₂ A. Sigma USA, grade S-5005 Particle size: 0.007 μ Surface area: 400
B. SILICA GEL	SiO ₂ Grade S-5505 Particle size: 0.014 μ Surface area : 200
C. HI-SIL, BOMBAY	SiO ₂ , Surface area: 120
D. TETRA ETHYL AMMONIUM HYDROXIDE (TEAOH)	(C ₂ H ₅) ₄ N-OH 40% in water Alfa, supplied and stored in Polythene bottles
E. TETRA ETHYL ORTHOSILICATE (TEOS)	Aldrich (98%)
F. FERRIC SULPHATE	Fe ₂ (SO ₄) ₃ ·9H ₂ O
G. SODIUM ALUMINATE	NaAlO ₂
H. SODIUM HYDROXIDE	NaOH, (ANALAR)
I. DOUBLE DISTILLED WATER	

$$\frac{TEA^+}{SiO_2} = 0.165, \frac{OH}{SiO_2} = 0.1, \frac{SiO_2}{Al_2O_3} = 60, \frac{H_2O}{SiO_2} = 25.$$

2-2.2 Synthesis of [Fe]-Beta using TEOS

In the preparation of the iron analog of zeolite beta, $Fe_2(SO_4)_3 \cdot 9H_2O$ was used as the source of iron. The synthetic procedure was slightly modified for the iron system.

In a typical preparation, 83.2 g tetraethylorthosilicate (TEOS) was added slowly with stirring to 40 g of tetraethyl ammonium hydroxide to achieve partial hydrolysis of TEOS. The resulting mixture was slowly added to a solution of 2.5 g of ferric sulphate ($Fe_2(SO_4)_3 \cdot 9H_2O$) in 10 g of doubly distilled water with vigorous stirring. To this mixture, a solution of 1.6 g of NaOH in 100 g TEAOH (20% aq solution) was added. The slurry was stirred for 24 hours at 333 K in an open vessel, in order to evaporate the ethanol formed by hydrolysis of TEOS. The resulting gel was of-white in color indicating the absence of brown ferric hydroxide. This gel was then transferred into a stainless steel autoclave and heated in an oven at 393 ± 1 K for 12 days. The autoclave was then taken out and quenched with water. The contents were filtered, washed thoroughly with deionized water and dried at 373 K in air for 8 hrs. The gel had the molar composition of:

$$\frac{SiO_2}{Fe_2O_3} = 60, \frac{SiO_2}{Na_2O} = 20, \frac{H_2O}{SiO_2} = 17, \frac{SiO_2}{R_2O} = 4.2$$

2-2.3 Chemical Analysis

A known weight of the zeolite sample is taken in a platinum crucible with lid. The crucible is heated to ignite the sample. The crucible is then cooled in a desiccator and weighed. The difference in weights gave the loss on ignition. The anhydrous weight of the sample is noted. The residue is digested in water and evaporated to dryness and treated with 20 ml of 1:1 hydrofluoric acid solution in water with few drops of conc. H_2SO_4 . This treatment is repeated three times and the sample was again ignited, cooled in a desiccator and weighed. The difference

in weight gives the percentage SiO₂ present in the sample. The residue is fused with potassium pyrosulphate and dissolved in water. It is then analyzed by atomic absorption spectroscopy for estimating Na and Al.

The results of chemical analysis of [Al] and [Fe] beta are presented in Table 2.2.

2- 2.4 X-Ray Diffraction

The samples synthesized during the course of work under different conditions and different time intervals of crystallization were analyzed for qualitative and quantitative phase identification by using a X-ray powder diffractometer (Rigaku Model No.D/MAX-III VC).

For the quantitative phase identification, the best crystalline sample was taken as the reference sample. The degree of crystallinity was calculated as follows:

$$\%Crystallinity = \frac{\text{Area between } 2\theta = 20^\circ \text{ to } 24^\circ \text{ of the experimental sample}}{\text{Area between } 2\theta = 20^\circ \text{ to } 24^\circ \text{ of ref. sample}} \times 100$$

2-2.5 Scanning Electron Microscopy

We analyzed the zeolites using a JEOL Scanning Electron Microscope (Model JSM-5200). The samples were covered with a thin film of gold. The latter prevents the formation of surface charging. It also saves the zeolite material from thermal damage by the electron beam. In all the analysis an uniform film thickness of about 0.1 mm was maintained.

2- 2.6 Preparation of The Protonic Form of Beta Zeolite

The beta zeolite samples in the as- synthesized form contain occluded templates. The latter which occupy the space in the zeolite channels are removed by calcination.

The samples TEA[Al] **Beta** and TEA[Fe] **Beta** were slowly heated to 703 and 683 K, respectively, in flowing nitrogen (100ml/min) for 8 hrs. Then air is introduced at the same temperature and maintained for 4 hrs. The temperature was subsequently raised to 723 and

TABLE - 2.2

Chemical Composition of Zeolite Beta Samples

Sr. No.	Sample	Percentage Composition (Anhydrous basis)			Unit Cell Formula
		SiO ₂	Al ₂ O ₃	Na ₂ O	
			or Fe ₂ O ₃		
a)	Na[Al]-Beta 28	93.77	5.74	0.49	0.3 Na ₂ O [4.3 AlO ₂ :59.7 SiO ₂]
b)	Na[Al]-Beta 45	95.75	3.60	0.65	0.4 Na ₂ O [2.7 AlO ₂ :61.35 SiO ₂]
c)	Na[Al]-Beta 60	96.22	2.82	0.96	0.6 Na ₂ O [2.1 AlO ₂ :61.9 SiO ₂]
d)	Na[Fe]-Beta 25	89.69	9.60	0.71	0.45 Na ₂ O [4.75 FeO ₂ :59.25 SiO ₂]
e)	Na[Fe]-Beta 37	92.0	6.9	1.10	0.7 Na ₂ O [3.4 FeO ₂ :60.6 SiO ₂]
f)	Na[Fe]-Beta 59	94.89	4.30	0.81	0.5 Na ₂ O [2.1 FeO ₂ :61.9 SiO ₂]

690 K (for the Al- and Fe-analogs, respectively) and maintained at this temperature for 6 hrs to remove the organics. The samples so obtained (Na-Beta) were exchanged with 5 M aqueous ammonium nitrate solution at 368 K under reflux conditions for about 4 hrs with a liquid to solid ratio of 10. The mixture was then filtered, washed with hot deionized water and dried at 393 K. The same procedure was repeated twice to enhance the degree of exchange. After every exchange the sample was calcined at 703 K to get the [H] beta zeolite.

2-3 RESULTS AND DISCUSSION

2-3.1 X-Ray Diffraction

The X-ray diffraction patterns of the products obtained from a synthesis gel after 0,2,4,6,7 and 8 days are shown in Fig.(2.2). The pattern of the fully crystallized sample is identical with those reported in the literature. Newsam and coworkers⁹¹ have suggested that the structure of zeolite beta consists of an intergrowth of two polymorphs 'A' having P4₁,22 symmetry and 'B' having C2/c symmetry. Both contain similar layer structures from the same tertiary building units (TBU) as shown in the Fig.(1.2).

The X-ray powder diffraction pattern of as-synthesized forms of [Al] Beta (Si/Al = 14,22,30) and [Fe] Beta (Si/Fe = 12,19,30) are presented in Figs.(2.3 A and 2.4 A). The corresponding SEM photographs are also given in Figs. (2.3 B and 2.4 B) respectively. The combination of sharp and broad reflections are observed in the pattern. The sharp reflections are attributed to normal Bragg intensity maxima with $h = 3n$, $k = 3n$, and broad reflections result from non-Bragg scattering related to structural disorder. It is observed along the [001] plane. The sharp reflections observed are indexed on the tetragonal unit cell (A polytype). Their d spacing, 2θ and intensity values are given in Table 2.3. A systematic displacement of all sharp lines towards lower 2θ values (higher d -spacings) is observed on isomorphous replacement of Fe³⁺ for Al³⁺ in the zeolite (Table 2.3). This suggests that the unit cell dimensions of zeolite beta slightly increases on isomorphous replacement of Fe³⁺ for Al³⁺, due to the longer Fe-O bond length compared to Al-O.

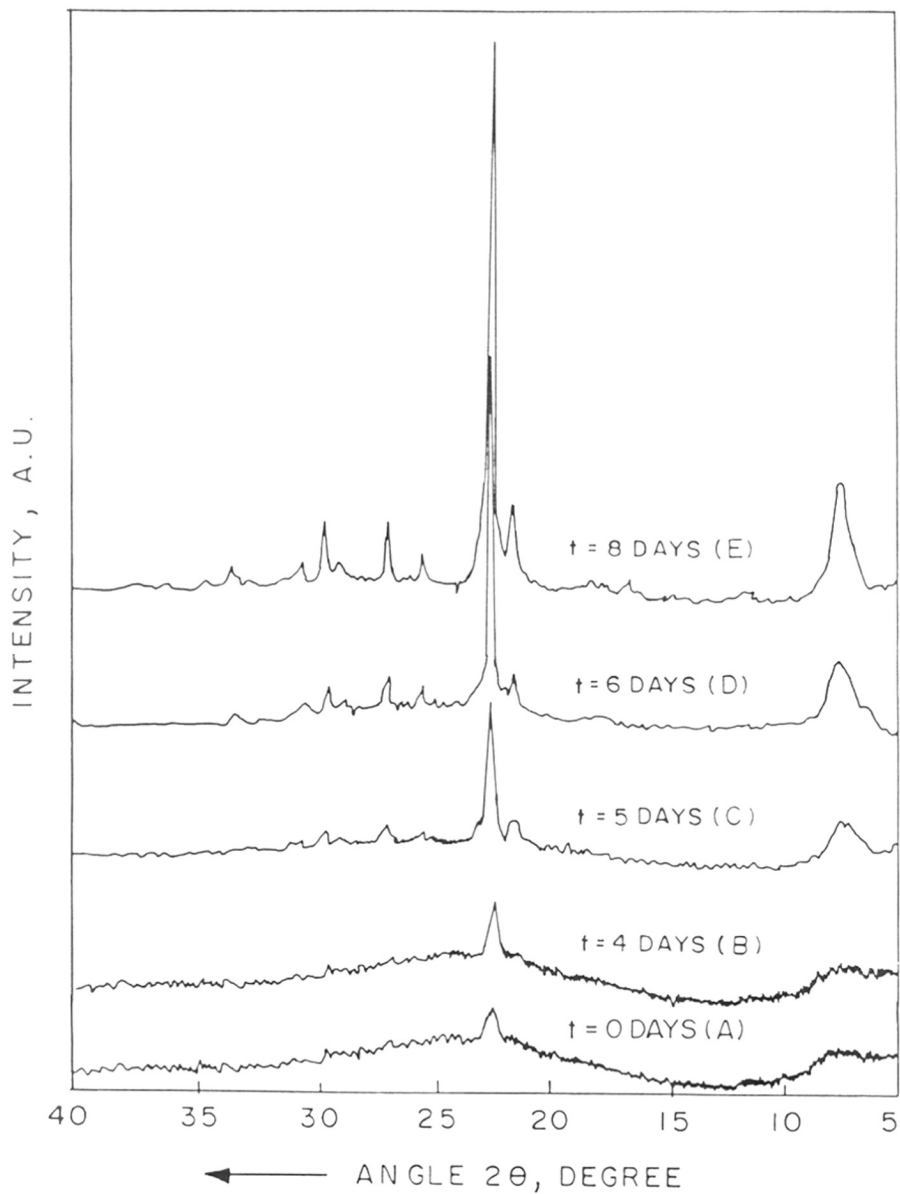


FIG.2.2 : X-RAY DIFFRACTION PATTERNS OF (A) BETA ZEOLITES. SYNTHESIS TIME $t=0,4,5,6$ AND 8 DAYS. [CURVES A-E RESPECTIVELY].

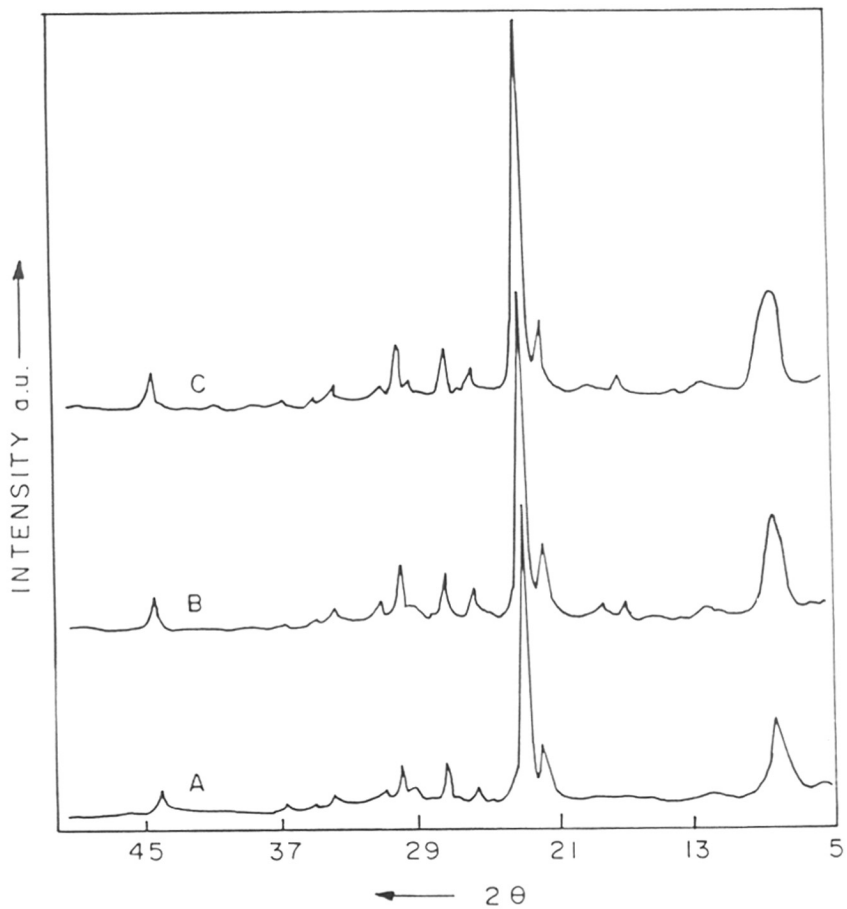


FIG.2.3A: X-RAY DIFFRACTION PATTERNS OF [Al] BETA ZEOLITES. $\text{SiO}_2 / \text{Al}_2\text{O}_3 = 28, 45$ and 60 [CURVES A, B AND C RESPECTIVELY]

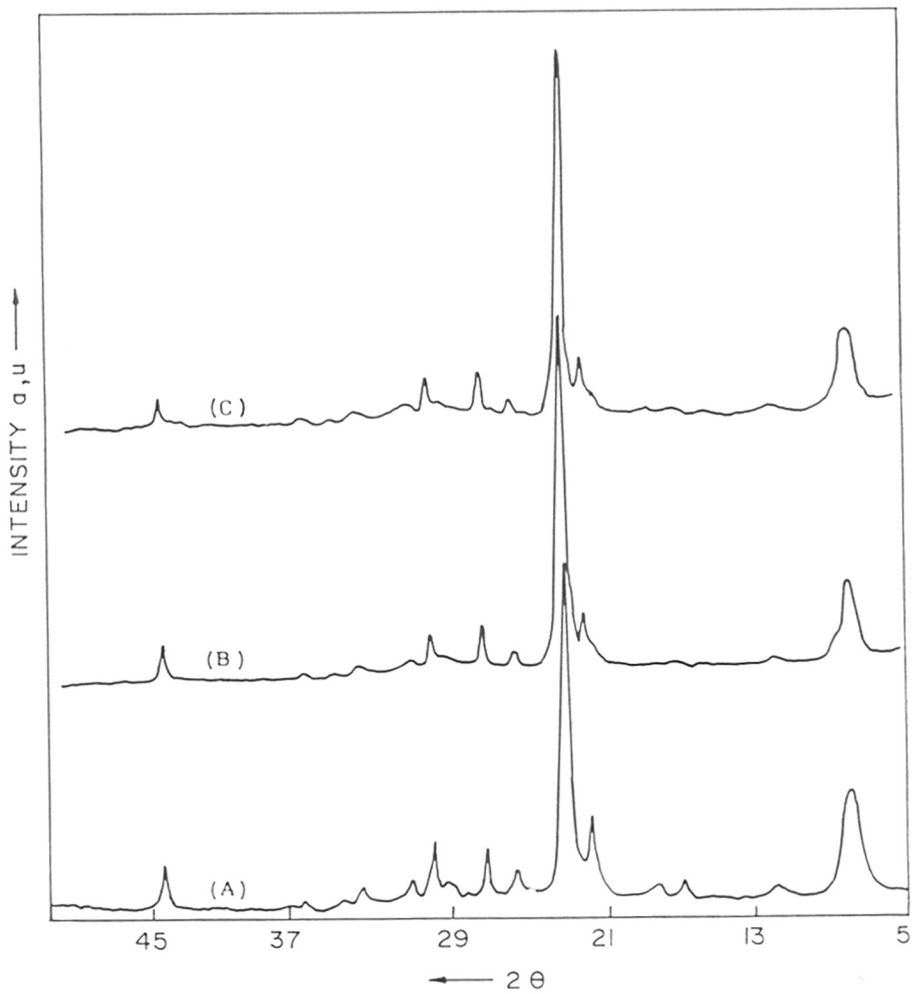
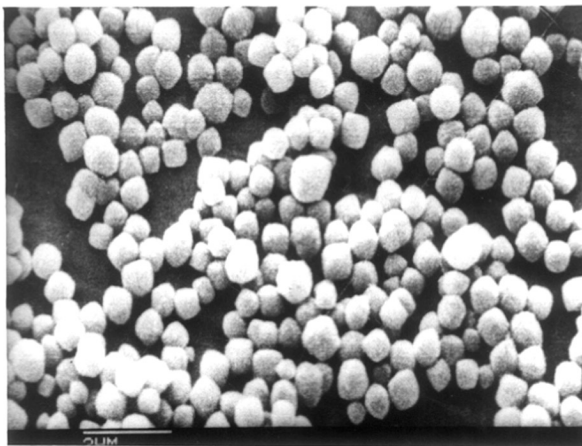
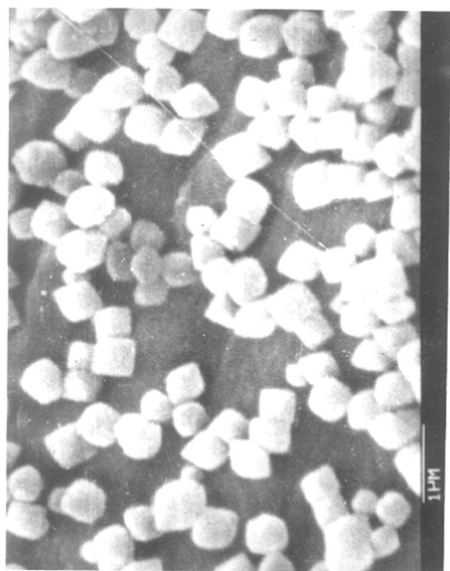


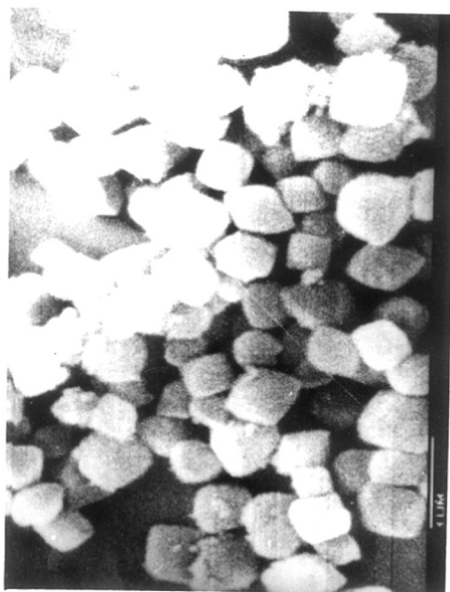
FIG.2.4A: X-RAY DIFFRACTION PATTERNS OF [Fe]BETA
 ZEOLITES $\text{SiO}_2/\text{Fe}_2\text{O}_3 = 25, 37$ and 59 (CURVES
 A, B AND C RESPECTIVELY)



A

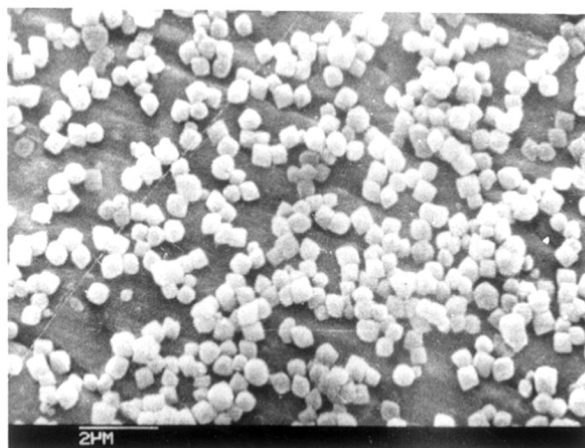


B

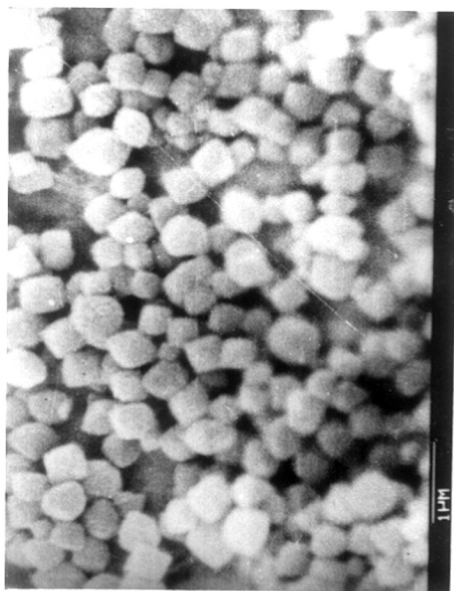


C

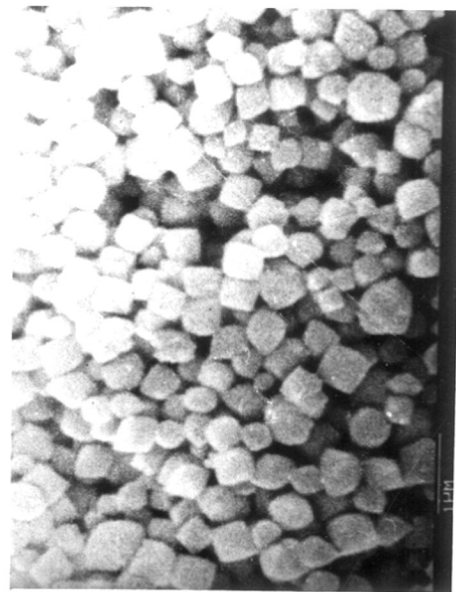
2.3B SEM PHOTOGRAPHS OF [A]BETA-28,45 AND 60 [A,B AND C RESPECTIVELY]



A



B



C

2.4B SEM PHOTOGRAPHS OF [Fe]BETA-25,37 AND 59 [A,B AND C RESPECTIVELY.]

Table - 2.3

The 'd' Values of [Al] Beta-28 and [Fe] Beta-25 as synthesized samples

Al			Fe	
hkl	2 θ	I/I ₀	2 θ	I/I ₀
-	7.85	20	7.75	23
-	11.7	2	11.65	2
004	13.4	1	13.3	1.5
-	16.7	2	16.6	2
300	21.6	13.0	21.45	12.0
302	22.65	100	22.45	100
304	25.45	5	25.28	4
008	26.95	10	26.75	10
-	28.9	2	28.7	2
306	29.75	11	29.5	10
330	30.7	3	30.5	3
334	33.65	2.5	33.4	2.5
-	43.9	5	43.65	5

The XRD patterns of Na- and [H]-**Beta** samples of both Al- and Fe showed the fully crystalline nature after thermal treatment as mentioned in 2-2.6 (Fig. 2.5).

2-3.2 The Influence of Synthesis Parameters

2-3.21 The Influence of the Reactivity of the Silica Source

The reactivity of the silica source often plays an important role in the synthesis of the zeolites since the dissolution of the silica is the first step in such cases. Under certain circumstances, this step can become rate controlling. To investigate the influence of the reactivity of silica on the crystallization of beta, three gels - (A), (B) and (C), described earlier (Table 2.1) were used. The results are shown in Table 2.4. Silica (A) with the maximum surface area ($400 \text{ m}^2 \text{ g}^{-1}$) also exhibited the maximum reactivity for the formation of pure zeolite beta. Hence, in all further experiments described below, silica gel (A) was used.

2-3.22 Effect of the Template Concentration

Figure 2.6 illustrates the influence of the concentration of tetraethyl ammonium hydroxide (TEAOH) in the gel mixture on the rates of synthesis. The gel composition was: $\text{SiO}_2/\text{Al}_2\text{O}_3 = 60$, $\text{OH}^+/\text{SiO}_2 = 0.1$, $\text{H}_2\text{O}/\text{SiO}_2 = 25$, $\text{TEA}^+/\text{SiO}_2 = 0.5$, 0.25 and 0.165 (curves 1-3, respectively). When the $\text{TEA}^+/\text{SiO}_2$ ratio was reduced to 0.1, another crystalline phase, large-pore mordenite, was formed. When the $\text{TEA}^+/\text{SiO}_2$ ratio was increased beyond 0.165 (curves 1 and 2) even though there is a minor reduction in the induction period, further crystallization is inhibited (Fig.2.6) suggesting that there exists a narrow range of optimum value of $\text{TEA}^+/\text{SiO}_2$ for the synthesis of zeolite beta. A similar type of observation (i.e. a narrow range of optimum R^+/SiO_2 values) in the crystallization of another high-silica, large-pore zeolite (ZSM-12) has been reported by Ernst et al.⁹² while using methyltriethylammonium cation as the organic molecule. However, at $\text{TEA}^+/\text{SiO}_2 = 0.25$ and 0.50, the gel could not crystallize completely, leading to around 80 and 60% crystalline material respectively (Fig.2.6, curves 1 & 2). This

FIG.2.5 : X-RAY DIFFRACTION PATTERNS OF Na- AND H-BETA OF Al AND Fe ZEOLITES (CURVES a,b,c AND d RESPECTIVELY)

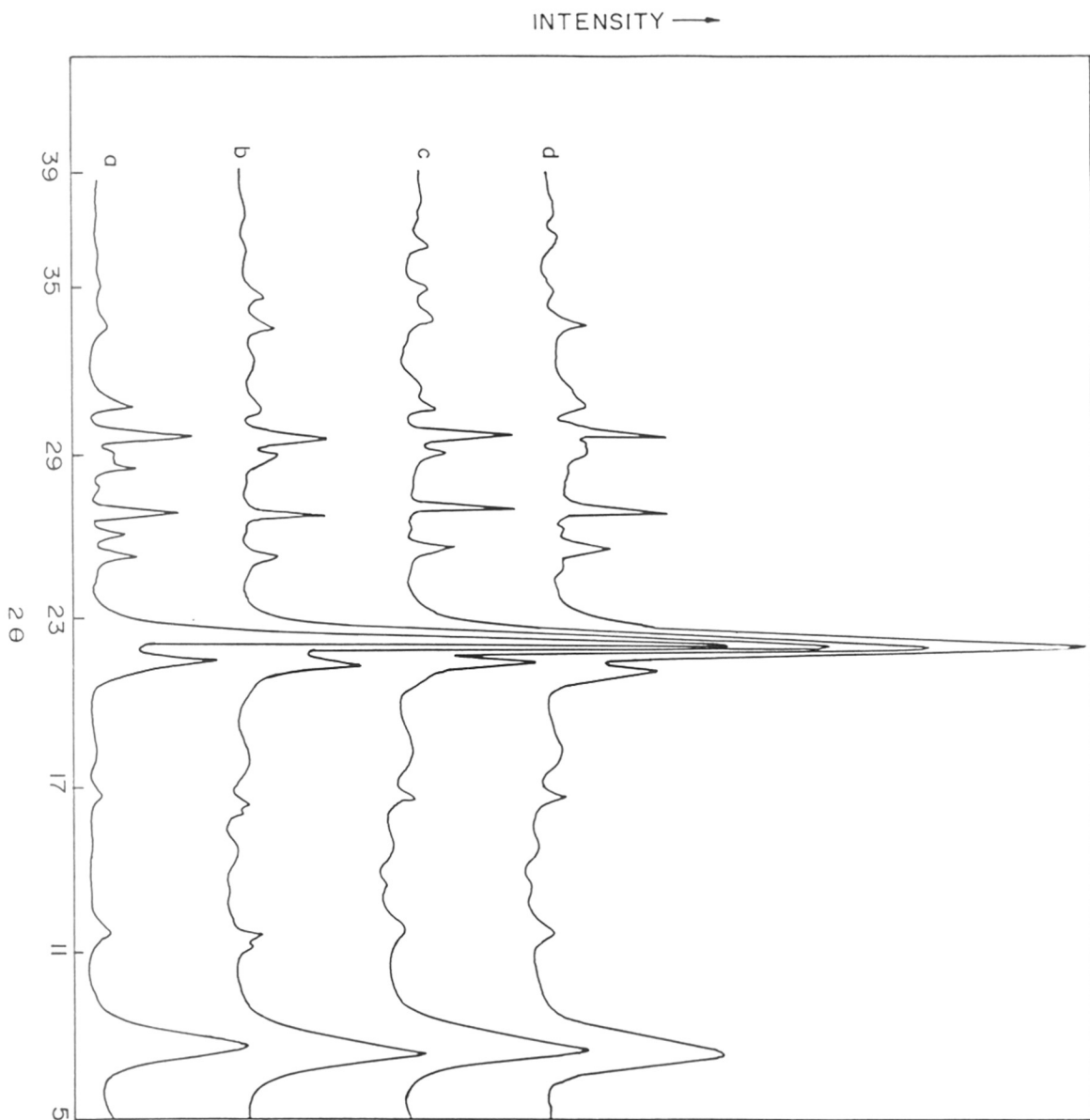


Table - 2.4

The influence of the silica source on the synthesis of zeolite beta

Gel ^a	Surface area (m ² g ⁻¹)	Zeolite	
		Phases	Crystallinity of beta (%)
A	400	Beta	100
B	200	Beta + ZSM-12	80
C	120	Beta + ZSM-5	50

^aMolar gel composition : TEA⁺/SiO₂ = 0.165,

OH⁻/SiO₂ = 0.1, Na⁺/SiO₂ = 0.1; H₂O/SiO₂ = 25

SiO₂/Al₂O₃ = 60; temperature = 423 K.

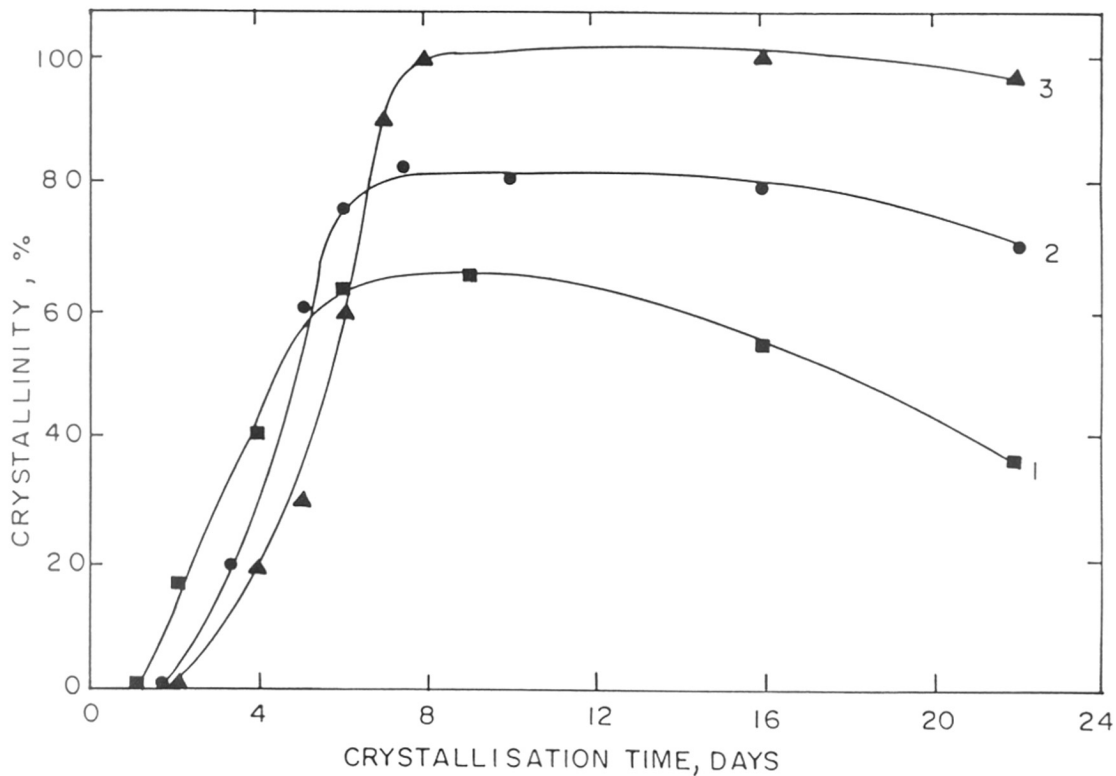


FIG.2.6 : THE INFLUENCE OF TEA^+/SiO_2 RATIO ON CRYSTALLIZATION OF BETA : [CURVES 1,2,3 CORRESPOND TO VALUES OF 0.5, 0.25 AND 0.165, RESPECTIVELY [$SiO_2/Al_2O_3=60$, $OH^-/SiO_2=0.1$, $H_2O/SiO_2=25$].

may, probably, be attributed to the highly alkaline nature of TEAOH used causing an increase in the gel pH, thereby inhibiting the complete crystallization, perhaps due to redissolution of the crystalline product.

2-3.23 The Effect of Alkalinity

The effect of alkalinity of the gel on the synthesis of beta is depicted in Fig.2.7. Alkalinity was varied by changing the concentration of NaOH in a gel of composition: $\text{TEA}^+/\text{SiO}_2 = 0.165$, $\text{H}_2\text{O}/\text{SiO}_2 = 25$, $\text{SiO}_2/\text{Al}_2\text{O}_3 = 60$ and variable OH^-/SiO_2 . The latter were calculated following Rollmann et al.⁹³. At low OH^-/SiO_2 values (curve 3), crystallization is very slow. At $\text{OH}^-/\text{SiO}_2 = 0.1$ (curve 2), the induction period is shortened and we get beta zeolite with 100% crystallinity. As the alkalinity increases still further (curve 1), the induction period is prolonged and the rate of crystallization decreases considerably. There exists an optimum value of the OH ion concentration which is just sufficient to depolymerize the silica gel and initiate the nucleation process but not enough to dissolve the zeolite precursors and retard crystallization.

2-3.24 Influence of Na^+/SiO_2

To study the influence of the concentration of sodium ions (independently of the OH^-/SiO_2 ratio) on the crystallization process, investigations were carried out by adding NaCl to the gel system while keeping the OH^-/SiO_2 ratio constant (Fig.2.8). Higher concentrations of sodium (curve 2, Fig.2.8) prolong the induction period without affecting the rate of crystallization. Moreover, at higher concentration of Na^+ , the ZSM-5 phase begins to appear at around 14 days, lowering the content of crystalline beta. Sodium cations apparently intervene mainly in the nucleation stage and in addition affect the relative stability of beta zeolite vis-a-vis the ZSM-5 system.

2-3.25 Influence of the Water Content

The influence of changes in the water content of the gel in the synthetic process is illustrated in Fig.2.9. There is no significant influence on the duration of the induction period.

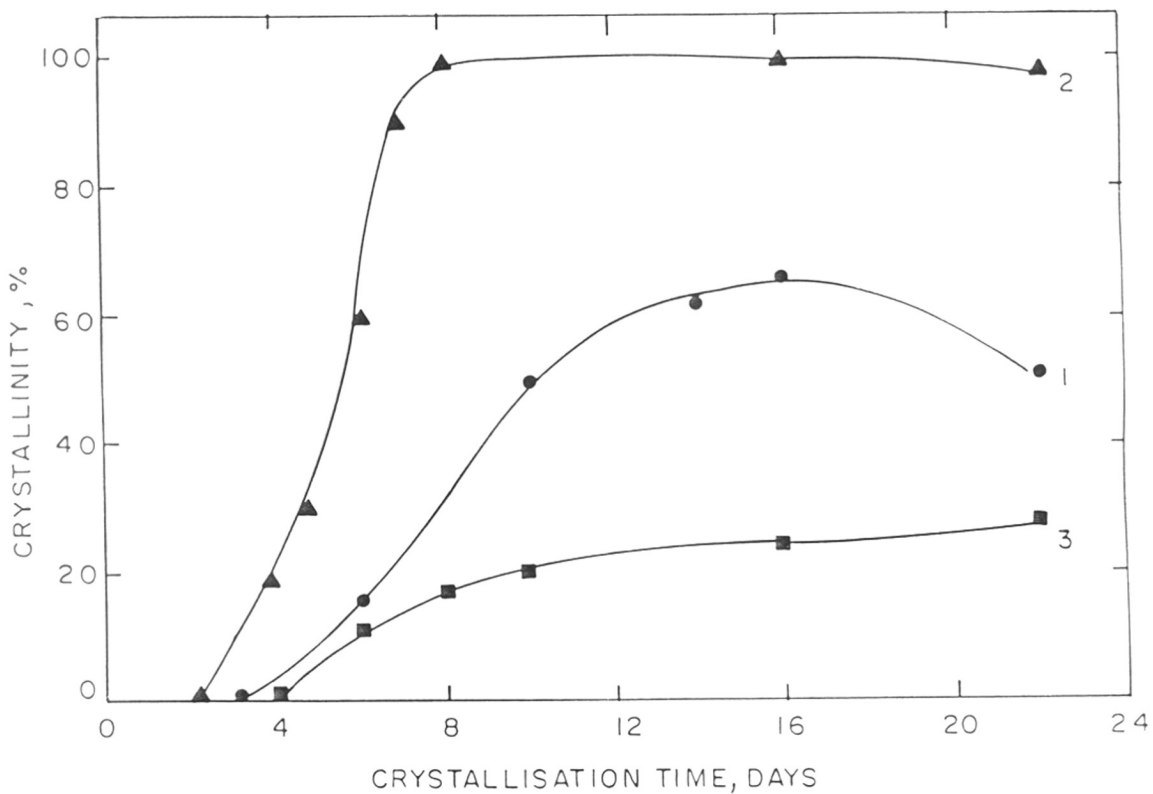


FIG.2.7 : THE INFLUENCE OF OH^-/SiO_2 RATION ON CRYSTALLISATION OF BETA: CURVES 1-3 CORRESPOND TO VALUES OF 0.2, 0.1 AND 0.067, RESPECTIVELY [$\text{SiO}_2/\text{Al}_2\text{O}_3=60$, $\text{TEA}^+/\text{SiO}_2=0.165$, $\text{H}_2\text{O}/\text{SiO}_2=25$].

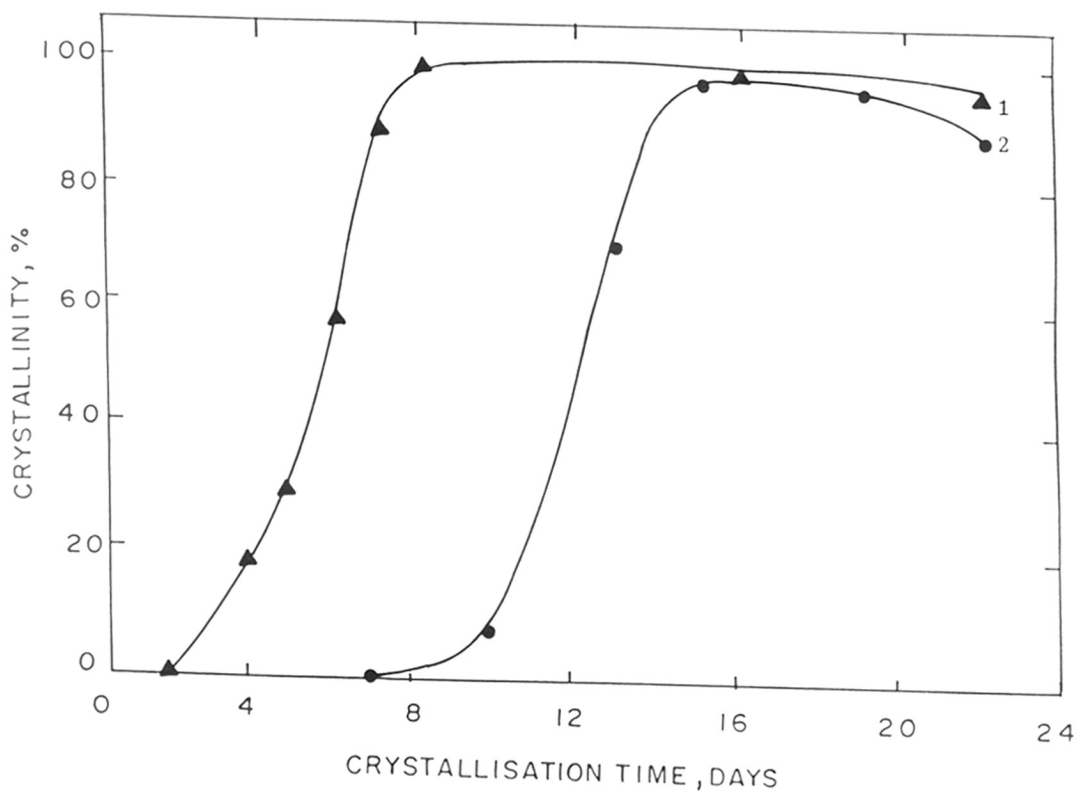


FIG.2.8 : THE INFLUENCE OF Na^+/SiO_2 RATION ON CRYSTALLISATION OF BETA: CURVES 1-2 CORRESPOND TO VALUES 0.1 AND 0.2, RESPECTIVELY $[\text{SiO}_2/\text{Al}_2\text{O}_3=60, \text{TEA}^+/\text{SiO}_2=0.165, \text{OH}^-/\text{SiO}_2=0.1, \text{H}_2\text{O}/\text{SiO}_2=25]$.

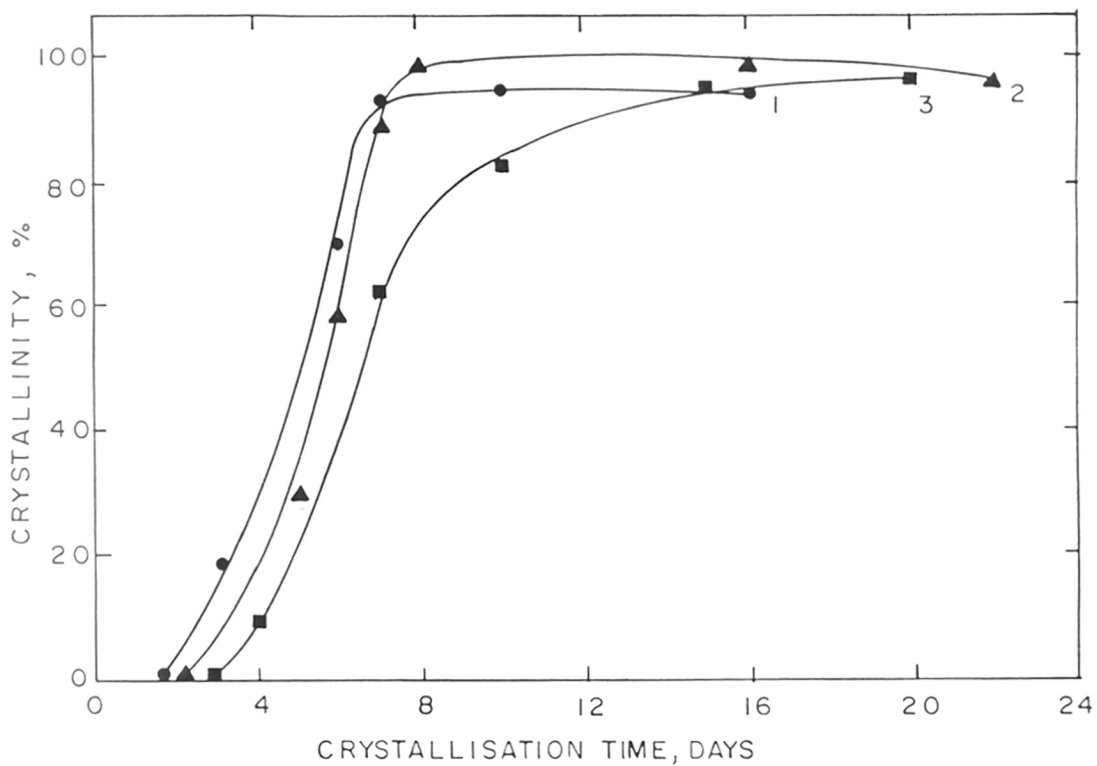


FIG.2.9 : THE INFLUENCE OF H_2O/SiO_2 RATIO ON THE CYRSTALLISATION OF BETA: CURVES 1,2,3 CORRESPOND TO VALUES 15, 25 and 35, RESPECTIVELY [$SiO_2/Al_2O_3=60$, $TEA^+/SiO_2=0.165$, $^-\text{OH} / SiO_2=0.1$].

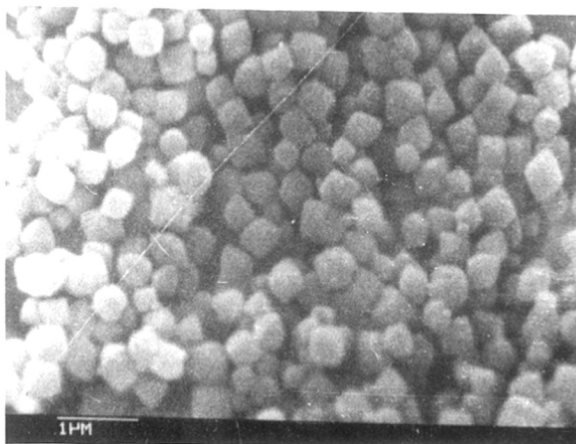
However, crystallization is faster in the more concentrated systems. A minor influence of dilution on the size of the beta crystals is observed. Scanning electron micrographs of the crystals of beta obtained from systems with varying concentration of water reveal that somewhat larger crystals (0.6-0.9 μ , Fig.2.10) are obtained from a system with $H_2O/SiO_2 = 35$ (curve 3, Fig.2.9) compared to those obtained from systems with $H_2O/SiO_2 = 25$ (0.4-0.6 μ , Fig.2.10 and curve 2, Fig.2.9) and $H_2O/SiO_2 = 15$ (0.3-0.5 μ , Fig.2.10, curve 1, Fig.2.9). There is however, no change in the shape of the crystals. They are cuboid in shape at all dilution levels studied. The faster rates of crystallization in the more concentrated systems and the larger crystal sizes obtained in dilute solutions are commonly observed in zeolite synthesis.

2-3.26 Influence of the SiO_2/Al_2O_3 ratio in the Gel

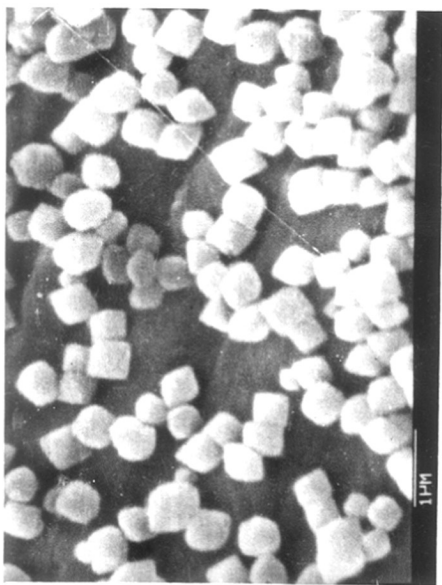
Figure 2.11 illustrates the influence of the SiO_2/Al_2O_3 ratio in the gel on the kinetics of crystallization of beta zeolite. As the concentration of SiO_2 in the gel increases, the induction period is shortened and the rate of crystallization increases. The correlation between the SiO_2/Al_2O_3 ratios in the gel and the solid beta zeolite as well as the yields of zeolite at various SiO_2/Al_2O_3 ratios is shown in Fig.2.12. It may be noted that, as the aluminium concentration in the gel increases, the incorporation of silicon in the zeolite framework is more efficient resulting in a higher yield of the zeolite. The presence of aluminium in the gel and the liquid phase thus seems to be necessary. In such a case, the relationship between the fractional yield of pure zeolite (Y) and the SiO_2/Al_2O_3 ratios in the zeolite and in the gel phases, respectively, may be expressed as:

$$Y = \frac{(SiO_2/Al_2O_3)_{zeolite}}{(SiO_2/Al_2O_3)_{gel}}$$

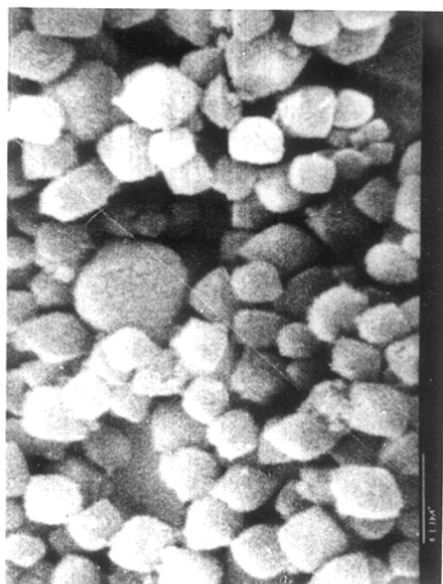
The values of the two (SiO_2/Al_2O_3) ratios should then become equal at $Y = 1.0$ (100% efficiency). Fig. 2.12 shows that it is indeed the case. The data points in Fig.2.12 are taken from Table 2.5. (For comparison, the data from Fig.2.7 and 2.8 of Perez- Pariente et al.⁹⁴ are also included). In this respect, the beta zeolite system differs from the ZSM-5 system where good yields of the



A



B



C

2.10 SEM PHOTOGRAPHS OF THE ZEOLITE BETA SAMPLES OBTAINED FROM THREE DIFFERENT CONCENTRATIONS OF WATER : $H_2O/SiO_2 = 15, 25$ AND 35 [A, B AND C RESPECTIVELY].

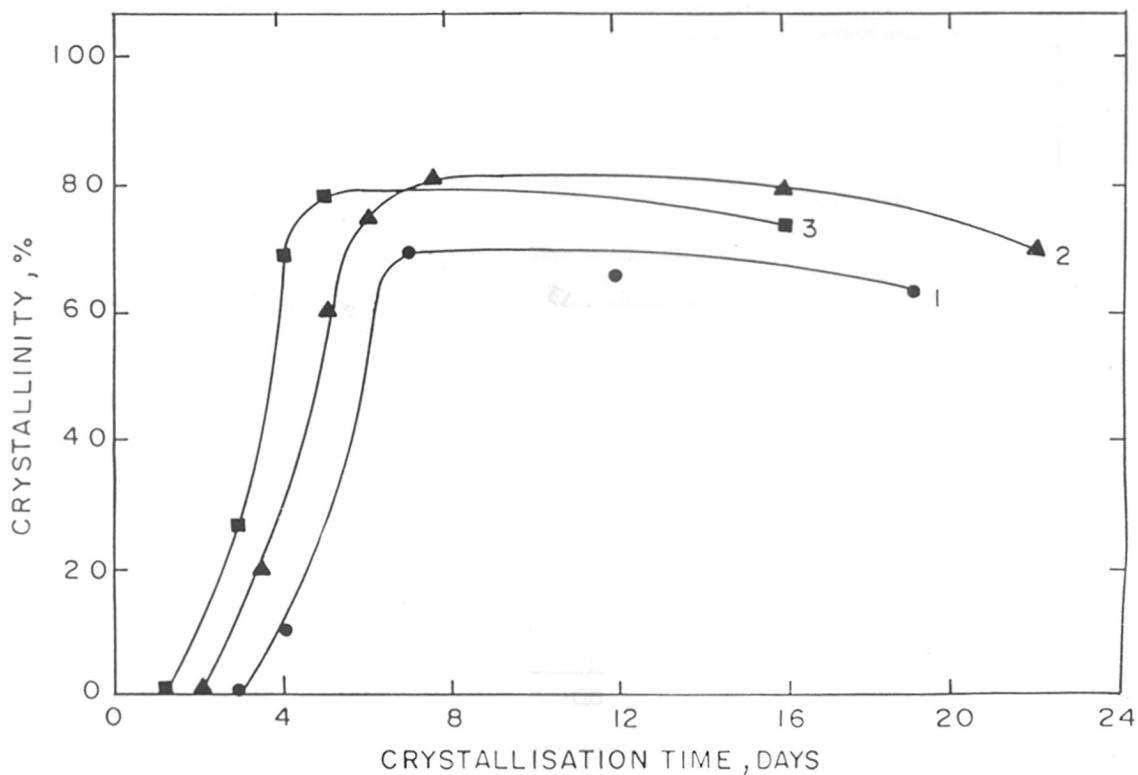


FIG.2.11 : THE INFLUENCE OF $\text{SiO}_2/\text{Al}_2\text{O}_3$ RATIO IN THE GEL ON CRYSTALLISATION OF BETA: CURVES 1-3 CORRESPOND TO $\text{SiO}_2/\text{Al}_2\text{O}_3$ RATIOS=30, 60 AND 90, RESPECTIVELY [$\text{TEA}^+/\text{SiO}_2=0.25$, $\text{OH}^-/\text{SiO}_2=0.1$, $\text{H}_2\text{O}/\text{SiO}_2=25$].

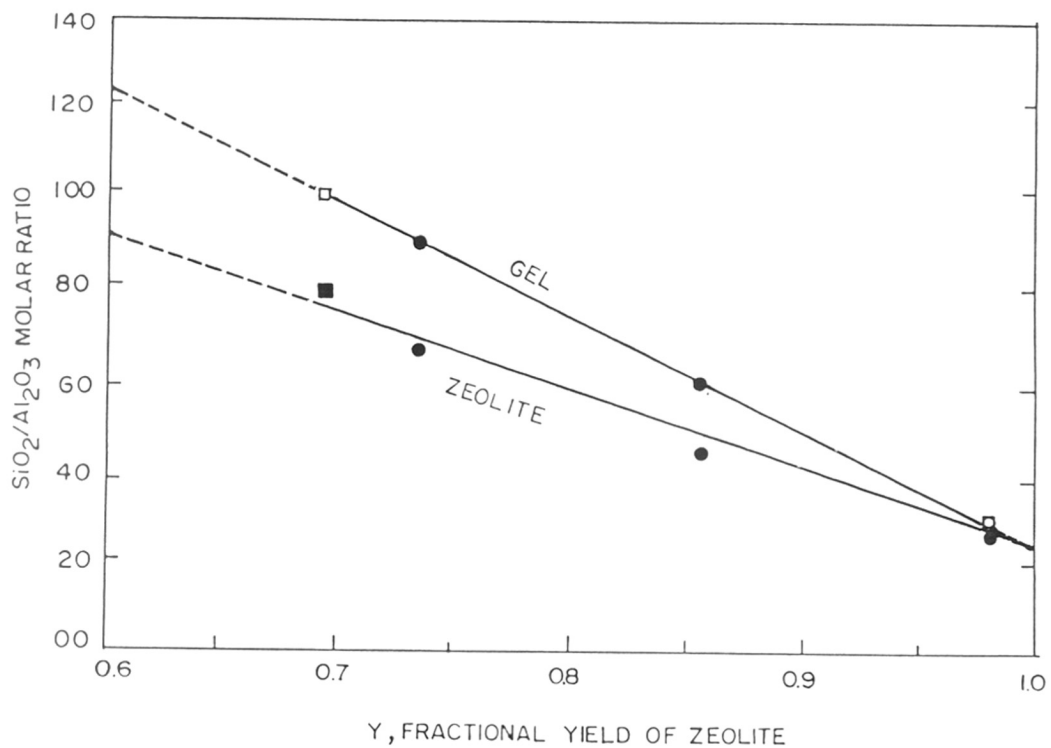


FIG.2.12 : RELATIONSHIP BETWEEN THE YIELD OF CRYSTALLINE BETA AND $\text{SiO}_2/\text{Al}_2\text{O}_3$ RATIO IN THE GEL AND FINAL ZEOLITE (DATA FROM REF.94 ARE ALSO INCLUDED).

zeolite could be obtained even in the absence of aluminium. Similar observations were made by Perez-Pariente et al.⁹⁵ who concluded that no zeolite beta can be made when using tetraethyl orthosilicate as the source of SiO₂ in an aluminium-free system.

2-3.27 Influence of the Temperature on Synthesis

In all the above-mentioned studies, the synthesis were done at 423K. Table 2.5 illustrates the consequences of carrying out the syntheses both above and below this value. At 443K, the ZSM-5 phase was formed as an impurity while at 403K, the crystallization was very slow and only a material with 35% crystallinity could be obtained even after 30 days. Using silica gel as the source of SiO₂ and under our synthesis conditions, 423K seems to be the optimum temperature for obtaining 100% crystalline beta in high yields. When using tetraethyl orthosilicate as the SiO₂ source, Perez-Pariente et al. observed that at 373K 100% crystalline beta was obtained as the sole crystalline phase, while ZSM-5 and cristobalite phase appear when the synthesis temperature was increased to 423K. This emphasizes the crucial role of the source of SiO₂ in the kinetics of the synthesis of zeolites.

2-4 CONCLUSIONS

The detailed procedures for the synthesis of Al- and Fe- beta zeolites has been described. The influence of various reaction parameters such as - reactivity of silica source, alkalinity, organic cation, water, temperature and silica-alumina ratio has been discussed in detail.

It is concluded that pure phase zeolite [Al]-**Beta** of high crystallinity can be obtained using silica gel of high surface area with optimum values of TEA⁺/SiO₂ = 0.165, OH/SiO₂ = 0.1, H₂O/SiO₂ = 25, temperature 423 K etc. An important relationship between the silica-alumina ratios in the final solid and in the starting gel is established, which in turn gives the percentage yield of pure zeolite beta. It is also brought out in this chapter that the difference between the Si/Al ratios in the starting gel and in the zeolite (product) increases with increasing silicon content and such zeolites can be obtained only in small yields. Pure silica polymorph of

Table - 2.5

The Influence of Temperature on the Synthesis of Beta Zeolite

Temperature (K)	Synthesis ^a time (days)	Zeolite	
		Phase	Crystallinity (%)
403	30	Beta	35
423	8	Beta	100
443	2	Beta, ZSM-5	-

^a Gel compositions: See Table (2.4) (using silica type A).

zeolite beta could not be synthesized.

Iron analogs of zeolite beta were also synthesized successfully using Al-free source of silicon and $\text{Fe}_2(\text{SO}_4)_3$ as the active source of iron. Lattice expansion observed in XRD peaks indicates the incorporation of Fe in the zeolite framework.

CHAPTER - 3

PHYSICOCHEMICAL CHARACTERIZATION OF BETA ZEOLITES

3-1 *EXPERIMENTAL*

3-1.1 Thermal Analysis

Thermal analysis of the synthesized samples was carried out on an automatic derivatograph (Netzsch, Model STA 490). Here simultaneous recording of TG/DTG and DTA thermograms is done. The thermograms of the samples were recorded under the following conditions:

Weight of the sample	- 50 mgs
Heating rate	- 10K/min
Sensitivity	-
TG	- 25 mg
DTA	- 0.1 mv
DTG	- 0.2 mv
Atmosphere	- Flowing air

In this experiment preheated and finely powdered α -alumina was used as the reference material.

3-1.2 Sorption Properties

The sorption experiments for water and hydrocarbons in the zeolite samples were carried gravimetrically with the help of automatic recording electromicro balance model Cahn-2000G, which is shown in Fig.3.1.

About 50 mgs of the sample was loaded in the sample pan and the exact weight of the sample was determined. Then the system was connected to high vacuum and the sample was activated in vacuum (10^{-6} torr) at 673K for 4 hrs. The sample was then cooled to the desired temperature. To study the equilibrium sorption, the sorbate was admitted to the sample at a

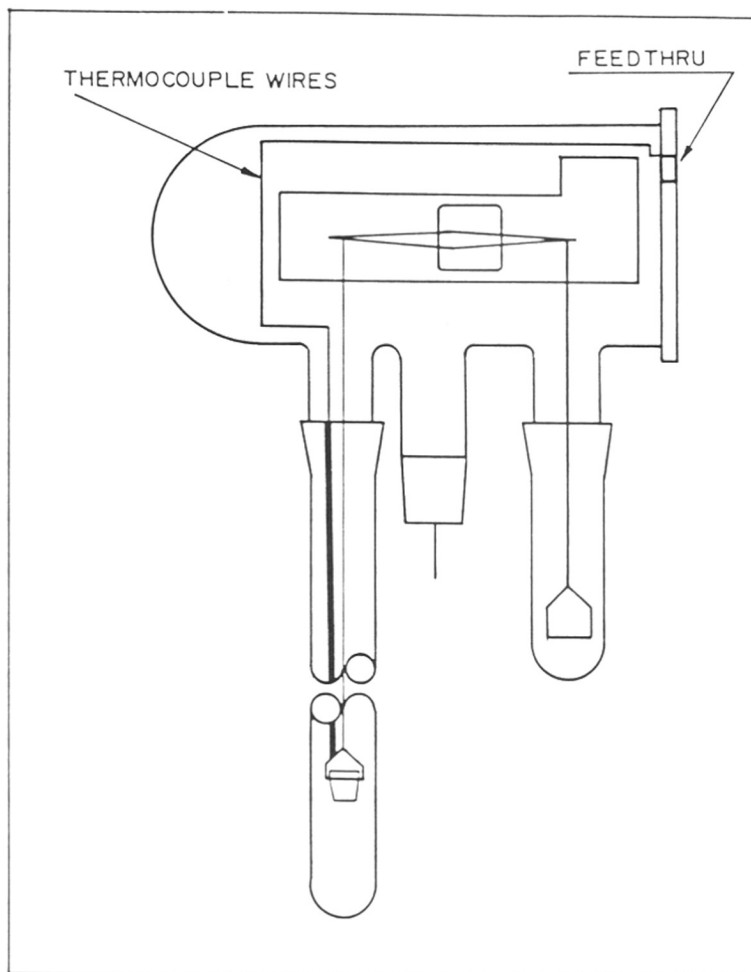


FIG.3.1: AUTOMATIC RECORDING ELECTROMICRO-
BALANCE [CAHN-2000G]

constant temperature and pressure, and the weight gained was recorded continuously as a function of time. After the completion of the experiment, the sample was evacuated and heated at 683 K at 10^{-6} torr and used for the next experiment.

Nitrogen adsorption at 77 K was studied volumetrically in a surface area analyser (Model micromeritics Accusorb 2000E). Sample was activated at 653K for 6 hrs in vacuum before the experiment. Micropore volume was estimated by employing Dubinin equation^{96,97}.

3-1.3 Temperature Programmed Desorption of Ammonia (TPD of NH_3)

This technique was used to determine the surface acidity and acid strength distribution of the [Al]Beta and [Fe]Beta samples. The experimental set-up used in this study is shown in Fig.3.2 The catalyst sample (10-20 mesh, 400 mgs) was loaded in the silica reactor which was connected to a sorptometer. After activation at 673K (10^{-6} torr) the sample was cooled to room temperature and adsorption isotherm of ammonia was determined, physically adsorbed ammonia was removed from the sample by evacuation and ammonia adsorption isotherm was once again determined. The difference in the 1st and 2nd saturation adsorption values gives the total chemisorbed ammonia. The sample was then evacuated at the same temperature and now connected on-line to a conventional gas chromatograph (Shimadzu GC-R1A) having a thermal conductivity detector and six port valve. The sample was heated at the rate of 10 K min^{-1} in the flow of (100ml/min) nitrogen. The concentration of desorbed ammonia as a function of temperature was recorded upto 823 K.

3-1.4 Infrared (IR) Spectroscopy

The infrared spectroscopic experiments were carried out on Nicolet 60 SXB FTIR spectrometer. For the experiments in the fundamental region of vibrations of zeolite framework ($1300\text{-}400 \text{ cm}^{-1}$), 1 mg of sample was ground and mixed with 300 mgs of high purity potassium bromide and pressed under vacuum into a transparent pellet (13 mm dia).

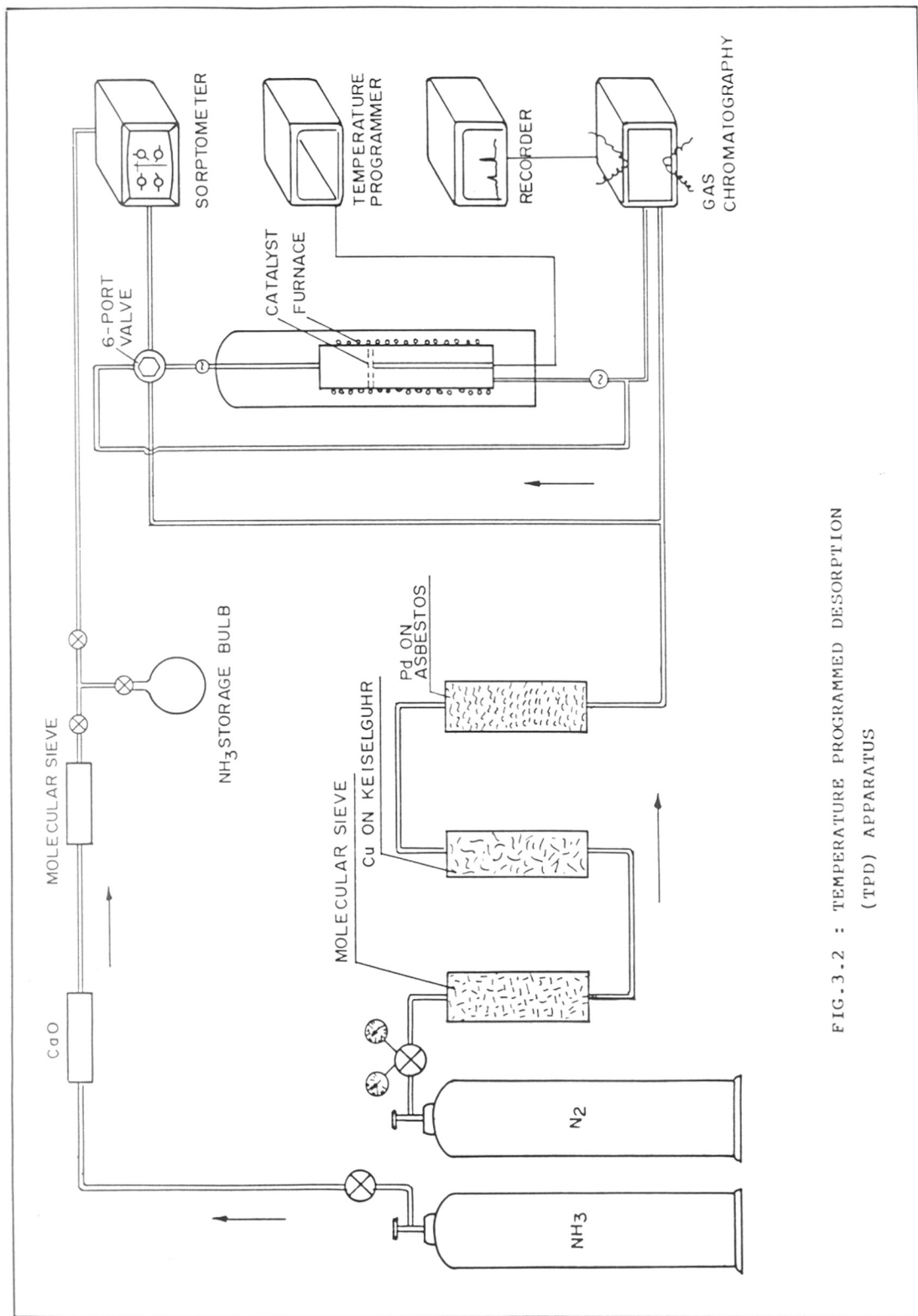


FIG. 3.2 : TEMPERATURE PROGRAMMED DESORPTION (TPD) APPARATUS

To study in the range of 4000-1300 cm^{-1} , self supported wafer technique was used. For in-situ studies a cell in which the temperature can be varied from liquid nitrogen temperature to 500°C while in the spectrometer beam, was fabricated and used. This cell was connected to a volumetric adsorption apparatus model micromeritics accurorb-2000E.

The cell is basically a DEWAR flask type with some modifications as shown in the Fig.3.3. The sample is pressed under pressure of 5 ton/inch² into a thin pellet (5-6 mgs/cm²) and mounted in the sample holder (SH). It was then placed inside the heating compartment of the cell (HC) and alligned in line with the IR beam. The cell was sealed from both the ends by potassium bromide windows (KW) with the help of elastomer "O" rings. A thermocouple placed in close vicinity of sample measures the temperature of the sample. The side tube at the top of the cell was connected to the high vacuum system. Cold water was constantly circulated through the cooling coil provided near the KBr windows. The sample was heated to 673K with a heating rate of 5K/min, under vacuum and maintained at this temperature for about 6 hrs. and then cooled down to 323K in vacuum. The spectra were recorded by averaging over 100 scans with 2 cm^{-1} resolution. Vapours of different reactants like water, pyridine, ammonia, benzene could be admitted to the sample through the adsorption manifold of the system.

3-1.5 Solid State MASNMR Spectroscopy

The high resolution MASNMR spectra for ²⁹Si were obtained at room temperature on a BRUKER MSL-300 spectrometer, operating in Fourier Transform mode, using "one cycle" type measurements. A 90° pulse with 3 seconds delay time was used for ²⁹Si nuclei and chemical shifts (δ) in ppm were measured with respect to tetramethyl silane (TMS) as an external reference. The rotor (sample holder) was spun at a rate of 4.0 KHz.

²⁷Al MASNMR spectra were obtained using a 45°C pulse with 1 second delay time. Chemical shifts in ppm were measured with respect to aqueous (0.1N) AlCl₃ as an external standard.

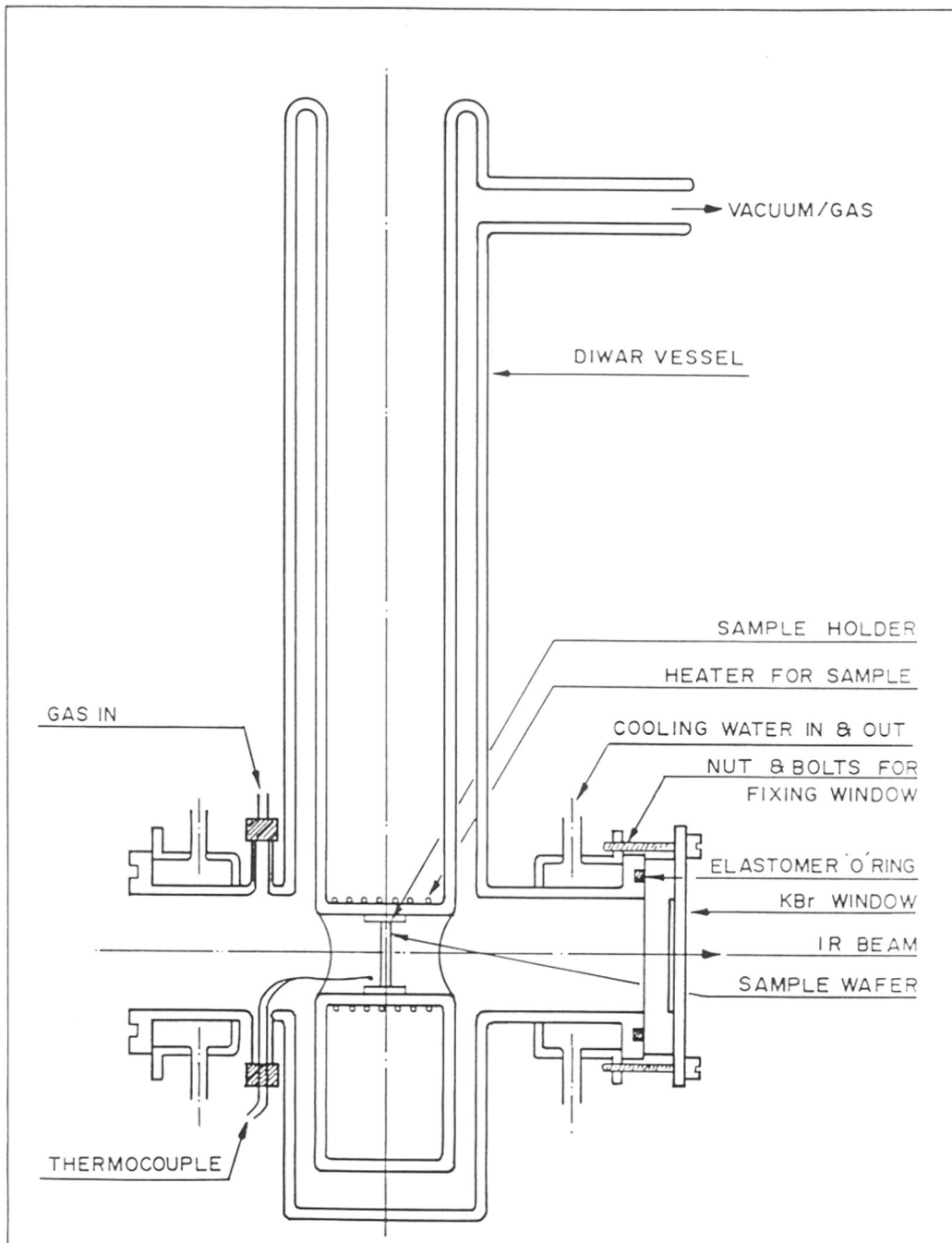


FIG.3.3 : FT-IR TRANSMITTANCE CELL

3-1.6 ESR Spectroscopy

The [Fe]Beta sample prepared in this study has been characterized for the presence of iron in the zeolite lattice by using Bruker-E2000 ESR spectrometer.

3-1.7 Magnetic Susceptibility

Magnetic susceptibility measurements were made in the temperature range of 94-297 K using a Faraday balance model "Cahn-Ventron, Cerritos, CA, U.S.A."

3-1.8 Mössbauer Spectroscopy

The Mössbauer measurements were performed with the conventional constant acceleration type Mossbauer spectrometer operating in multiscalar mode in the temperature range between room temperature (RT) and 4.2 K in the presence of externally applied magnetic field (4.13 T perpendicular to the γ -beam).

3-2 RESULTS AND DISCUSSION

3-2.1 Thermal Analysis

A typical thermogram of the as synthesized zeolite [Al]Beta-28 and [Fe]Beta-25 (100% crystalline) is shown in Fig.3.4(a&b). In this we find four distinct zones of exothermic weight loss in the dta/dtg curves of [Al]Beta with the peak maxima at 591, 650, 723 and 900K respectively. Perez-Pariente et al.⁹⁵ have reported three exothermic weight losses at 493-623,623-773, 773-973K respectively, in the decomposition of a TEA-beta zeolite. In the decomposition of TEA-ZSM-5 zeolite, Parker et al.⁹⁸ assigned the first two exothermic weight losses to the removal of occluded TEA-OH and TEA⁺ cations respectively. They also assigned the exothermic weight loss at 773-973K to the oxidative decomposition of residual coke formed by the decomposed template materials occluded in the zeolite channels. The results obtained in our study are similar to those of Perez-Pariente⁹⁵ et al., except for some variation in the region of 623-773K where two distinct and clear peaks at 650 and 773K were observed. Perez-Pariente et al.⁹⁵ reported only one peak at 700 K. Perhaps TEA-species are occluded in two energetically

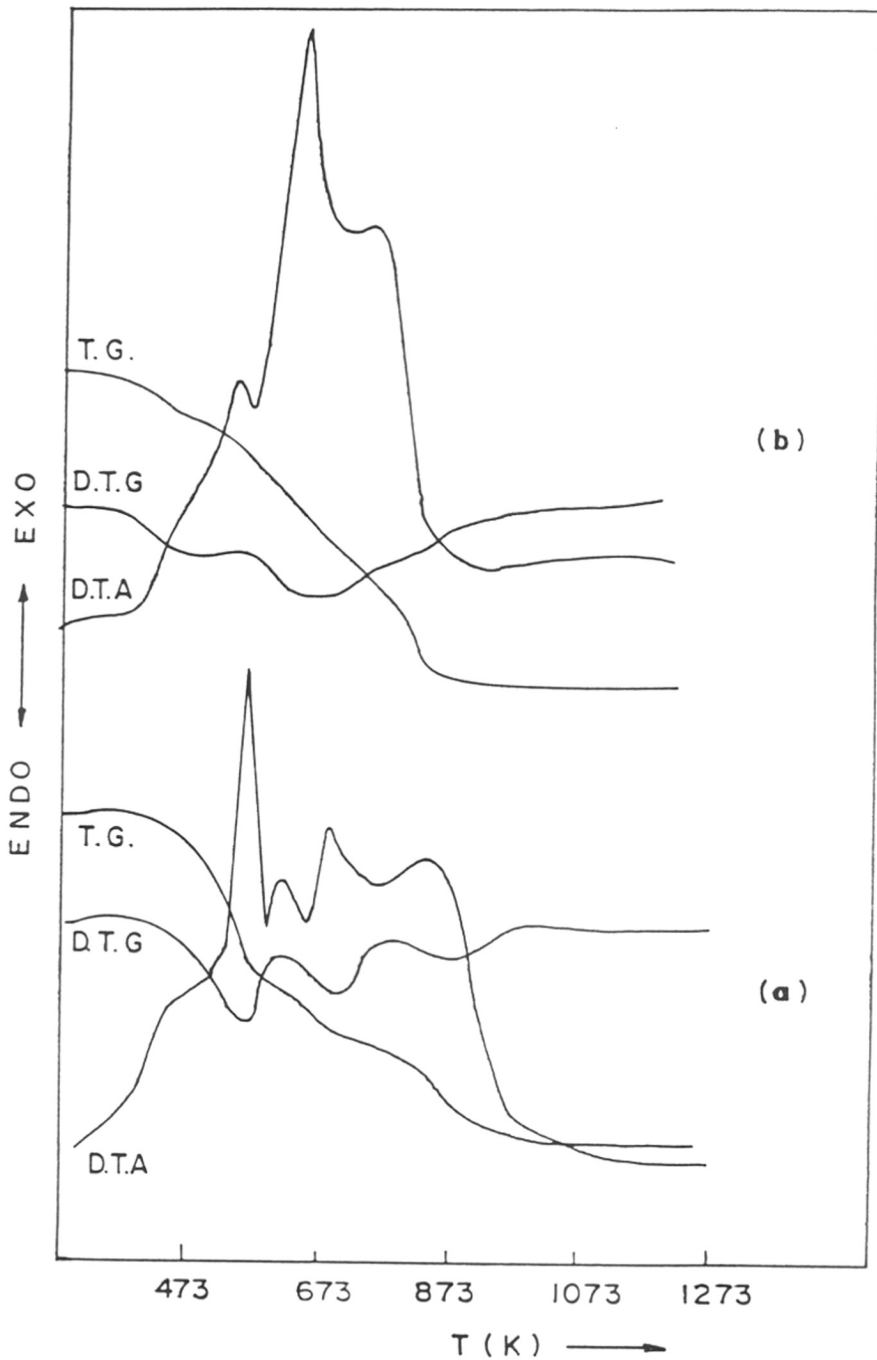


FIG.3.4 : TG,DTG AND DTA CURVES FOR TEA[Al]BETA-45(a) AND TEA[Fe]BETA-37(b)

different locations which give rise to these two peaks. This presumption can be supported by the additional observation that the DTG curve shows only a single, continuous and broad maximum around 700 K even though two maxima are seen in the DTA curve in the same region.

On substitution of Al by Fe, the exothermic weight losses due to the loss of occluded TEAOH and TEA⁺ cations are shifted to lower temperatures. The broad exothermic peak at 873K, assigned by Perez-Pariente⁹⁵ et al. to the oxidative decomposition of occluded organic template in the zeolite pores shifts to 773-823K in [Fe]Beta. The thermograms of the products obtained in 0,2,4,6,7 and 8 days from the reaction composition TEA⁺/SiO₂ = 0.165, OH/SiO₂ = 0.1, SiO₂/Al₂O₃ = 60 and H₂O/SiO₂ = 25 at 423 K, are presented in Fig.3.5,(curves a,b,c,d and e respectively), on the basis of oxidative decomposition pattern as observed in DTA, weight loss in the temperature range 525-975K was taken as the amount of occluded tetraethyl ammonium hydroxide. In the Table (3.1) the amount of organic material occluded in samples a to e, are presented together with the crystallinity estimated from X-ray powder diffraction. The amount of organic material occluded is directly proportional to the micropore volume and hence the zeolite content. It should be noted from the Table that for poorly crystalline materials, the XRD crystallinity is less than that obtained from TG. Gabelica and co-workers⁹⁹ have reported that X-ray powder diffraction does not show any crystallinity if [organic]-zeolite microcrystals are imbedded inside the non-zeolite aluminosilicate phase, because the crystallite size of such material is less than 5 nm.

3-2.2 Adsorption of Water and Hydrocarbons

On the basis of sorption results, Lok et al.¹⁰⁰ have shown that zeolite **beta** has an open structure with 12-ring windows. Bond et al.¹⁰¹ found that all C₈ aromatics (Xylenes, ethylbenzene) can enter zeolite **beta** at room temperature. 1,3,5-trimethylbenzene enters the zeolite but triisopropyl and the t-butyl analogs are not. Olson et al.¹⁰² have used these probing molecules to discriminate the 12-ring window from 10-ring window zeolites. Martens et al.¹⁰³ and Martens and Jacob¹⁰⁴ have carried out n-decane conversion reaction on zeolite **beta** and found that **beta**

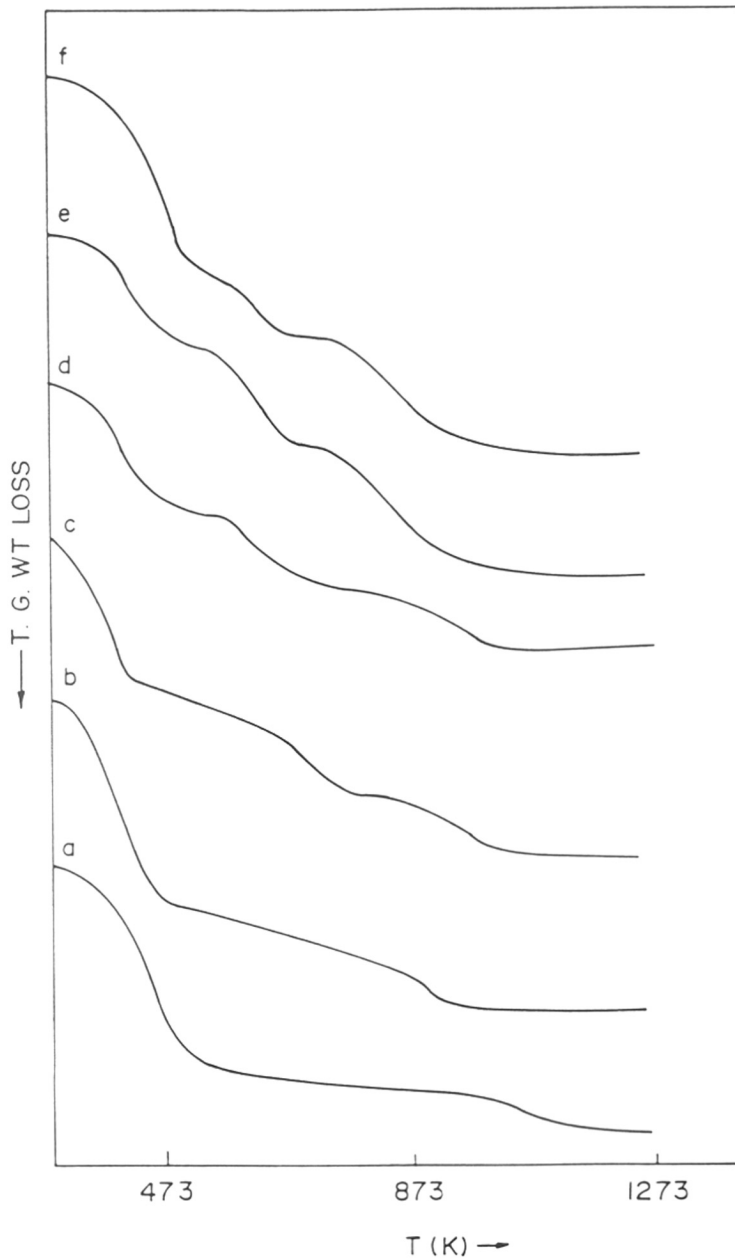


FIG.3.5 : THE THERMOGRAMS OF [Al]BETA-45 SAMPLES OBTAINED IN 0,2,4,6,7 AND 8 DAYS (CURVES a TO f RESPECTIVELY)

TABLE - 3.1

Thermogravimetric data of different crystallinity samples of TEA[Al]Beta-45

Sample	Wt. loss below 550 K	Wt. loss between 550-975 K	Total wt. loss
XRD Crystallinity			
100	3.2	16.5	19.7
90	3.9	14.55	18.45
60	5.1	11.2	16.3
50	6.7	10.1	16.8
20	10.6	6.0	16.6
0	12.3	2.8	15.1

zeolite has 12-ring pore systems. Sorption data also provide information about the absence of secondary cage structure. The measured sorption capacities of a typical **beta** zeolite for water and cyclohexane were 17.0% and 13.4% respectively¹⁰⁵. All the volume accessible to water is also accessible to cyclohexane.

In Table 3.2, adsorption results on [Al] and [Fe]**Beta** zeolites are presented. Pore volumes of fully crystalline materials determined by adsorption of n-hexane, cyclohexane, o-, m-,p-xylenes, and 1,3,5-Trimethylbenzene vapors were 0.24 ± 0.02 ml/g of zeolite. The adsorption value of n-hexane in [Al]**Beta**-45 samples prepared in 0,2,4,6,7 and 8 days from the reaction composition $\text{TEA}^+/\text{SiO}_2 = 0.165$, $\text{OH}/\text{SiO}_2 = 0.1$, $\text{SiO}_2/\text{Al}_2\text{O}_3 = 60$ and $\text{H}_2\text{O}/\text{SiO}_2 = 25$ at 423 K are given in Table 3.3. In Fig.3.6, percentage crystallinity with respect to 100% crystalline material calculated on the basis of n-hexane adsorption, template loss in thermogravimetric experiments and intensity of 520 cm^{-1} band in mid-IR spectra were plotted against XRD crystallinity. Thus crystallinity calculated from adsorption, TG and IR methods follow a similar trend and shows that about 18% crystalline material is present in 0% X-ray crystalline material.

3-2.3 Temperature Programmed Desorption of Ammonia (TPD of NH_3)

The results of T.P.D. of NH_3 are presented in Fig.3.7 and Table (3.4). General features of T.P.D. curves are typical of any high silica zeolite. Temperature of peak maxima are listed in Table 3.4. T_{max} of strongest acid sites for [Al]**Beta** zeolite are found to be higher than those of [Fe]**Beta** for comparable silica to alumina ratio. T_{max} 638, 615 and 603 K for [Al]**Beta**-28, 45 and 60 (Curves a,b and c) are to be compared with 613, 598 and 573 K for [Fe]**Beta**-25,37 and 59 (Curves d,e and f) respectively. The total amount of ammonia adsorbed was found to be in excess of the number of Al or Fe atoms/u.c, indicating that part of the adsorbed NH_3 is physically adsorbed on sites like silanol groups. Only the last peaks e.g., with maximum around 633-673 K for [Al]**Beta** and 600-650 K for [Fe]**Beta** were found to correlate with the Al or Fe atoms, acidity and catalytic activity. Beyond 773 K for [Al]**Beta** and beyond 700 K for [Fe]**Beta** zeolite, the rising portion of the T.P.D. peak is due to dehydroxylation as no NH_3 is detected in

TABLE 3.2

Adsorption Properties of H[Al]Beta-45 And H[Fe]Beta-37

Adsorbate*	N ₂	H ₂ O	n-H	c-H	o-X	m-X	1,2,4-TMB
Kinetic dia. Å	3.4	2.65	4.3	6.0	7.0	6.8	7.5
Sample	Adsorption (Wt %)						
[Al]Beta							
28		19.2	15.9	18.3	20.0	22.7	17.1
	(0.23)	(0.2)	(0.24)	(0.23)	(0.23)	(0.26)	(0.20)
44		18.24	16.6	17.5	21.74	21.82	17.6
	(0.22)	(0.19)	(0.25)	(0.22)	(0.25)	(0.25)	(0.195)
60		16.2	16.6	18.3	19.15	22.6	17.95
	(0.25)	(0.17)	(0.25)	(0.23)	(0.22)	(0.26)	(0.21)
[Fe]Beta							
23		20.1	15.2	19.1	20.8	21.0	15.4
	(0.24)	(0.21)	(0.23)	(0.24)	(0.24)	(0.24)	(0.18)
37		18.2	17.3	19.9	22.6	21.8	15.4
	(0.21)	(0.19)	(0.26)	(0.25)	(0.26)	(0.25)	(0.18)
59		18.2	16.6	19.1	21.74	22.5	14.55
	(0.23)	(0.19)	(0.25)	(0.24)	(0.25)	(0.26)	(0.17)

* n-H = n-Hexane, c-H = cyclo-Hexane, m-X = meta-Xylene,
o-X = ortho-Xylene, 1,2,4-TMB = 1,2,4-Trimethylbenzene.

Adsorption conditions: P/P₀ = 0.5, Temperature = 298 K.

() Figures in bracket indicate pore volume (ml/g)

TABLE - 3.3

Adsorption properties of Na[Al]Beta having different crystallinity

Adsorbate	Kinetic** diameter $\overset{\circ}{\text{A}}$	XRD Crystallinity of sample (%)					P.V.#
		20	30	60	90	100	
N ₂	-	-	-	-	-	-	-
Water	2.6	8.8	11.0	12.4	15.8	19.2	0.19
n-Hexane	4.3	6.4	7.9	10.4	14.3	15.7	0.23
c-Hexane	6.0	6.1	7.7	11.5	14.6	17.2	0.22
m-Xylene	7.0	8.6	8.8	12.8	18.8	19.6	0.22

* Temperature = 293 K

$$P/P_0 = 0.5$$

** Values of the kinetic diameter ($\overset{\circ}{\text{A}}$) are taken from Handbook of Chemistry and Physics, College Edition, 1968.

P.V. = Pore volume of the 100% crystalline sample (ml/g) for the adsorbate.

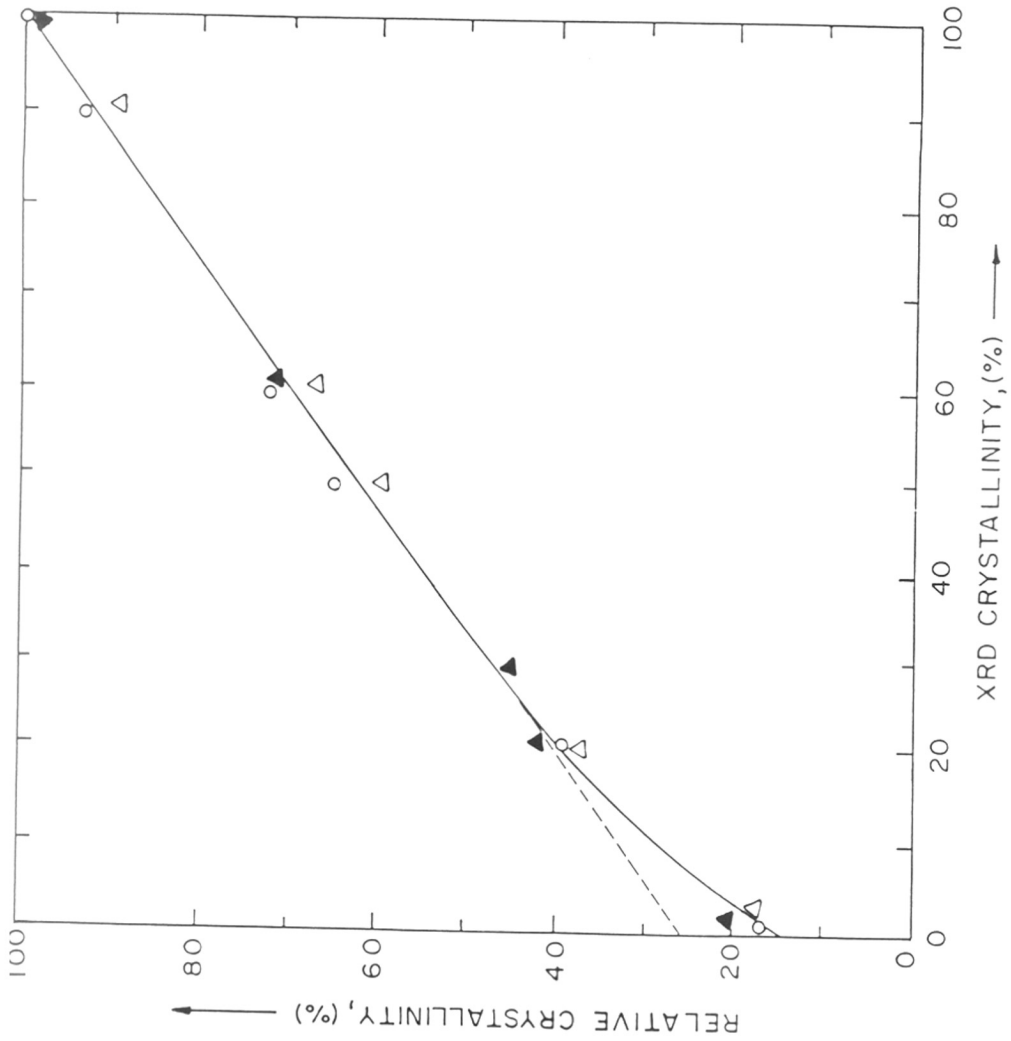


FIG. 3.6 : CORRELATION BETWEEN XRD CRYSTALLINITY AND RELATIVE CRYSTALLINITY ESTIMATED FROM IR SPECTROSCOPY (-▲-), THERMAL ANALYSIS (-○-), AND ADSORPTION OF n-HEXANE (-△-) RESPECTIVELY

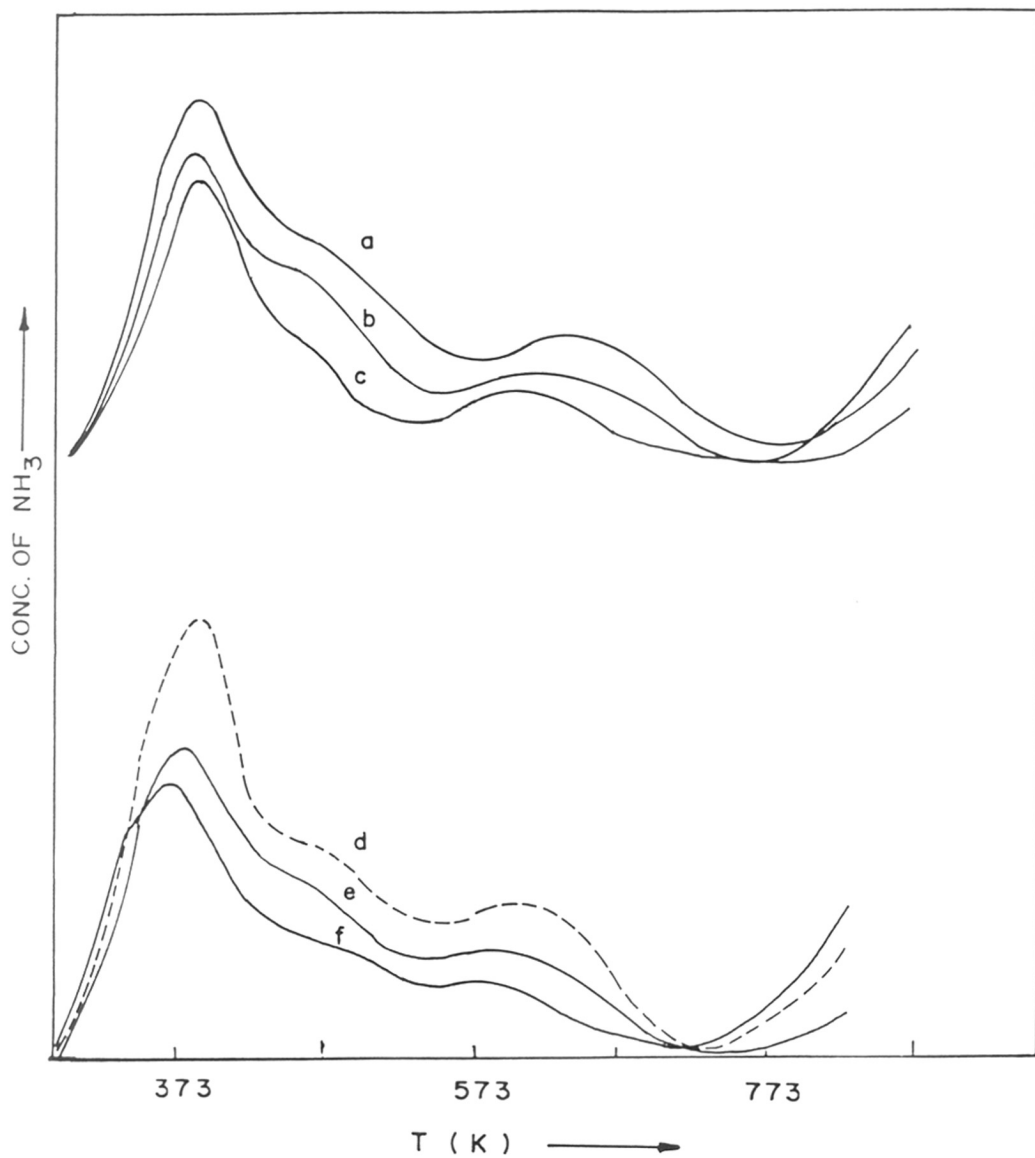


FIG.3.7 : TPD SPECTRA OF NH₃ FROM H[Al]BETA-28,45 AND 60 (CURVES a,b AND c , H[Fe]BETA-25,37 AND 59 (CURVES d,e AND f) RESPECTIVELY

TABLE - 3.4

TPD results for [Al]Beta and [Fe]Beta zeolites

Sample	Peak Maxima (K)				
	α -Peak	β -Peak	NH ₃ in ($\alpha + \beta$) (mol/u.c)	γ -Peak	NH ₃ in γ (mol/u.c)
H[Al]Beta-28	360	450	11.27	638	3.92
H[Al]Beta-45	360	450	8.84	615	2.21
H[Al]Beta-60	360	450	6.5	603	1.8
H[Fe]Beta-23	383	460	10.9	613	3.6
H[Fe]Beta-37	383	450	8.4	598	2.6
H[Fe]Beta-59	337	450	4.68	573	1.63

the desorbate and only H₂O is detected. Lower temperature of onset of dehydroxylation for [Fe]Beta compared to [Al]Beta shows that structural hydroxyl groups on [Fe]Beta are less stable than those of [Al]Beta. Kotasthane et al.¹⁰⁶ have observed similar difference in acidity of [Al]ZSM-5 and [Fe]ZSM-5 series. Chu et al.¹⁰⁷ reported similar results while discussing B, Fe, Ga and Al substituted ZSM-5 zeolites. However, there is an important difference in the T.P.D. curves of zeolite beta and those observed for H-ZSM-5. The peak maximum in the case of [Al]ZSM-5 for strongly adsorbed NH₃ associated with strong acidic sites occurred at 773-823 K. It is shifted to lower temperature (633-673 K) for [Al]Beta zeolite. For [Fe]ZSM-5, this particular peak occurs at (700-750 K) whereas for [Fe]Beta of comparable silica to ferric oxide ratio, it is observed in the range (600-650 K). This indicates that in both [Al] and [Fe] forms, beta zeolites have weaker acidic sites compared to those of ZSM-5 zeolites.

Lok et al.¹⁰⁸ reported the T.P.D. spectra for NH₃ desorbing from zeolite-Y and L. NH₃-Y had three NH₃ T.P.D. peaks located at 393, 489 and 553 K. Another sample of Si enriched NH₃-Y had two not well-resolved NH₃ peaks located at 586 and 705 K. The stronger acidity of latter sample (due to higher Si/Al ratio) was reflected by the increased temperature for NH₃ desorption. The NH₃ T.P.D. chromatogram of a fresh NH₃ K-L sample showed three peaks located at 385, 691 and 821 K. The last peak being associated with the partial decomposition of the catalyst. In this respect, beta zeolite is more similar to zeolites with 12-membered rings like Y and L rather than 10-membered ring zeolite like ZSM-5. The similar acidity of the (OH) groups in beta to those in Y zeolite is further supported by their similar selectivity in gas oil cracking¹⁰⁹

3-2.4 Infrared Spectroscopy

a) Framework Spectra

The typical mid-infrared spectra determined by KBr pellet technique for the as-synthesized forms of [Al]Beta-45 samples obtained after 0,2,4,6 and 8 days of crystallization with 0,20,30,60 and 100 % crystallinity are shown in Fig.3.8, (Curves a-d) respectively, and Table 3.5.

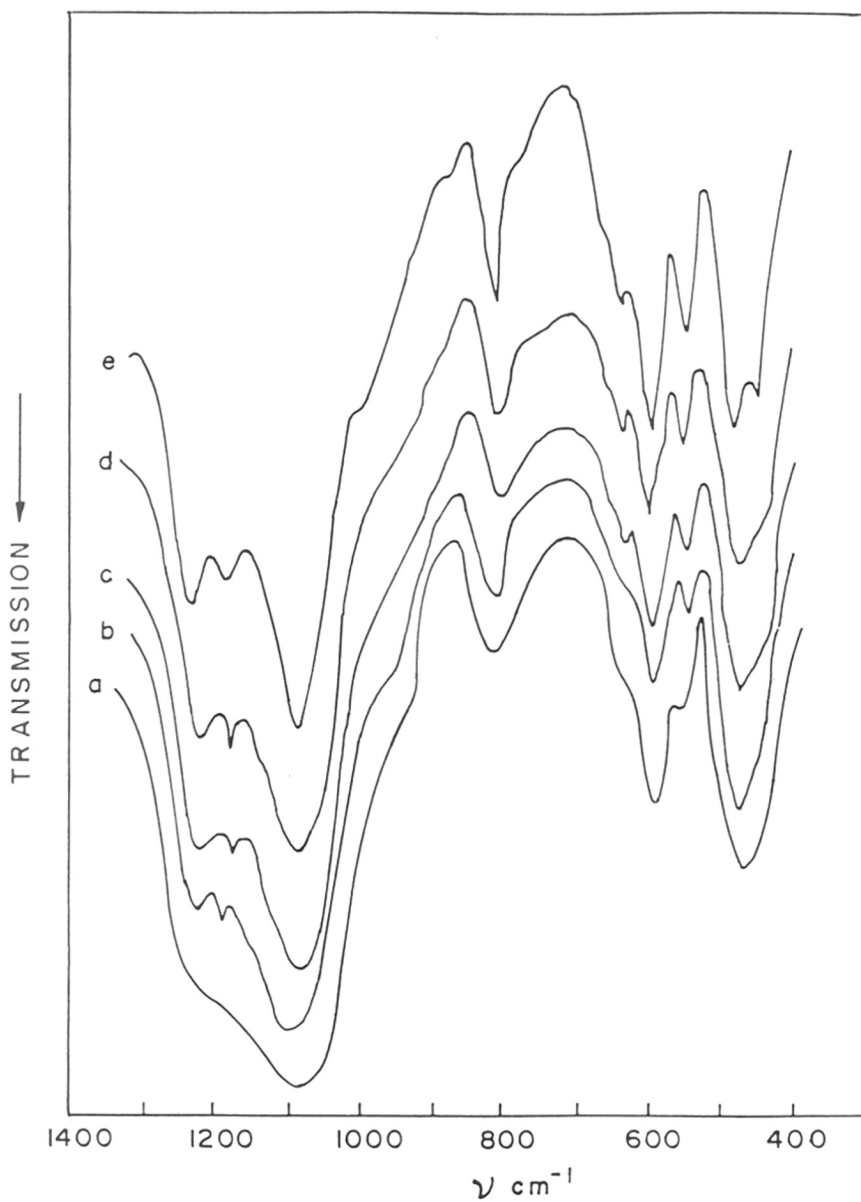


FIG.3.8 : FT-IR SPECTRA OF TEA[Al]BETA-45 HAVING 0,20,30,60 AND 100% XRD CRYSTALLINITY (CURVES a,b,c,d AND e RESPECTIVELY)

Table - 3.5

FT-IR Framework Vibration Frequencies of Beta Zeolites(vcm^{-1})

TEA [Al] Beta					TEA [Fe] Beta
*	0%	20%	30%	60%	100%
	1224	1220	1217	1218	1216
	1172	1170	1173	1170	1172
	1086	1084	1084	1080	1080
	782	780	784	783	782
	609 (Sh)	609 (Sh)	609 (Sh)	610 (Sh)	620 (w.)
	564	565	567	566	568
					548
	522	522	522	524	524
	460	460	455	457	464
	-	-	440 (Sh)	435 (Sh)	430
					430

(Sh) = Shoulder

* Indicates XRD Crystallinity of the sample

Infrared spectra in Fig.3.8 are comparable in band positions and spectral features to those published⁹⁵. The specific IR absorption at 575 and 525 cm^{-1} which are typical for zeolite **beta** are similar to those for zeolites having 4 and 6-membered double-ring vibrations like faujasite. Wolf et al¹¹⁰. used the chain frequency IR band at 575 cm^{-1} to determine crystallographic stability of A and X type zeolites. The intensity of that band (D-4 ring) correlated with loss in crystallinity determined by XRD and adsorption measurements. The intensity of the peak at 525 cm^{-1} was chosen in the present study for such correlation. From Figure 3.6 the presence of X- ray amorphous zeolite **beta** nuclei to the extent of about 18% can be seen in the sample with 0% XRD crystallinity.

Mid-infrared spectroscopy is also applicable in studies involved in framework modifications by changing aluminium concentration or isomorphous substitution. Typical spectra for as synthesized fully crystalline samples of TEA[Al]Beta-28 and TEA[Fe]Beta-25 are plotted in Fig.3.9 (Curves a,b) and in the Table (3.4) the band positions are summarized for the same. We have not observed any significant shift in band positions on decreasing [Al] or [Fe] content in the zeolite sample. However, remarkable differences in band positions are observed on comparing the spectra of [Al]Beta and [Fe]Beta of comparable ratios (Fig 3.9). The bands due to external linkages which are structure sensitive have shifted to lower wave numbers. This provides strong evidence for the framework incorporation of iron in zeolite **beta**. Szostak¹¹¹ and co-workers have considered iron incorporation in ZSM-5 framework and attributed the band shift to the change in reduced mass of the $-(\text{Si-O-Fe})_n-$ compared to $-(\text{Si-O-Al})_n-$ harmonic oscillator. Contributions from such vibrations in [Fe]Beta compared to [Al]Beta framework is illustrated as shaded area in Fig.3.9. This is manifested in the 1080, 568 and 524 cm^{-1} bands in [Al]Beta shifting to 1068, 548 and 508 cm^{-1} respectively for [Fe]Beta (Fig 3.9).

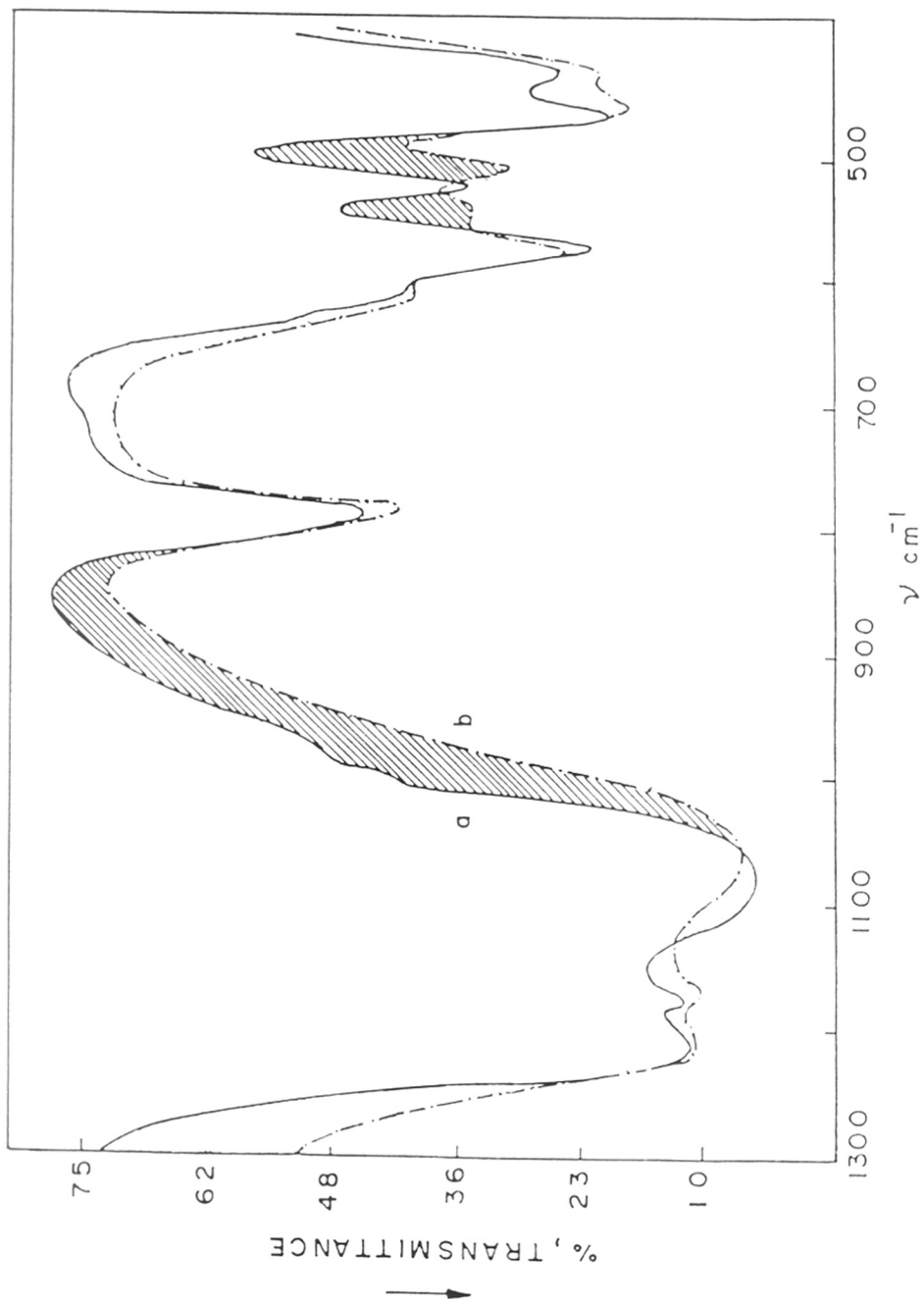


FIG.3.9 : FT-IR SPECTRA OF TEA[Al|BETA-28(a)] AND TEA[Fe|BETA-25(b)]

b) *Spectra of Surface Groups*

i) **TEA- and Na-Beta**

The difference FT-IR spectra obtained by subtracting the spectra of the as-synthesized samples TEA[Al]Beta-28,45 and 60 from that of the Na[Al]Beta-28,45 and 60 are shown in Fig.3.10 (Curves a,b and c respectively). Spectra for TEA [Al]Beta were taken after heating the samples at 450 K in vacuum (10^{-4} torr) for 3 hrs (i.e., without removing the TEA-cation) and those of Na[Al]Beta after in-situ oxidative decomposition in flowing dry air at 723 K, ensuring the complete removal of the occluded organic material, and evacuating at 10^{-6} torr for 3 hrs. The absorption bands in the region of 2800-3000 cm^{-1} (appearing as negative peaks in the difference spectra) are due to the asymmetric and symmetric C-H stretching vibrations. In the figure, three types of (OH) absorption bands can be distinguished: two sharp bands at 3740 and 3605 cm^{-1} and a third broad band with a maximum around 3540 cm^{-1} . The bands at 3740 and 3540 cm^{-1} are more intense for the sample with a higher silicon content (sample [Al]Beta-60) whereas the band at 3605 cm^{-1} is more intense for sample [Al]Beta-28 with a higher Al content.

Woolery et al.¹¹² have obtained very similar results for H-ZSM-5 systems. Three types of (OH) groups were distinguished absorbing at 3740, 3610 and around 3500 cm^{-1} and assigned them to free SiOH groups (both terminal and internal), Bronstead acid sites associated with Al (bridging hydroxyl), and hydrogen-bonded SiOH groups respectively. They also observed that the intensity of the bands at 3740 and 3500 cm^{-1} increased with the silicon content of the zeolite whereas that of the band at 3610 cm^{-1} was proportional to the Al-content. The (OH) bands in Fig. 3.10 are also assigned to similar species in zeolite beta. There is however, a significant difference between the results of H-ZSM-5 and of H-Beta (Fig.3.10). The band around 3500 cm^{-1} was absent in the Na-ZSM-5 zeolites and appeared only when Na^+ ions were replaced by

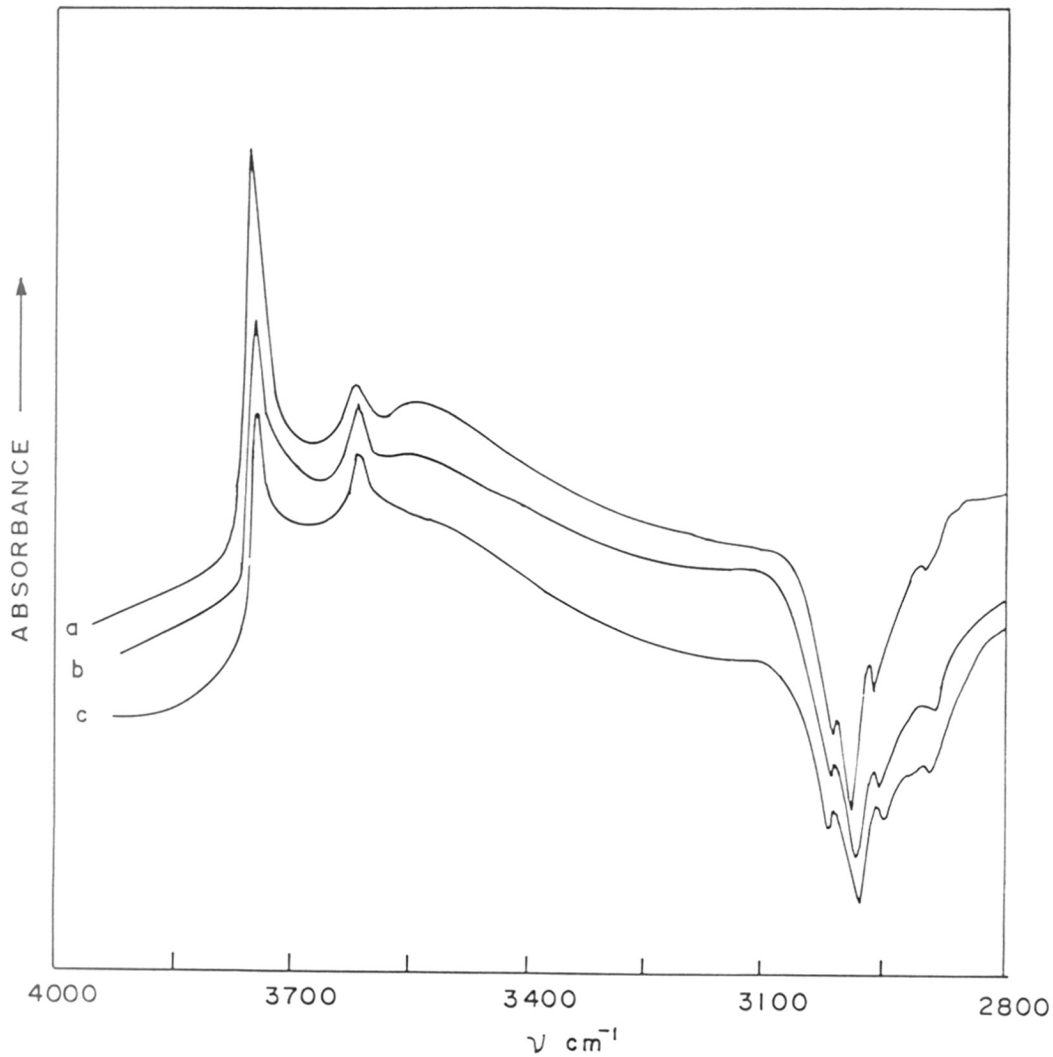


FIG.3.10 : FT-IR DIFFERENCE SPECTRA [$\text{TEA}^+ - \text{Na}^+$] OF ZEOLITE [Al]BETA-28,45 AND 60 (CURVES a,b AND c RESPECTIVELY)

protons. In the case of zeolite **beta** (Fig.3.10), the 3540 cm^{-1} band is present even in Na-**Beta**. Its occurrence at a higher frequency (3540 instead of 3500 cm^{-1}), is indicative of a lower hydrogen bonded character.

In the Fig.3.11, curves a and b represent IR spectra of TEA[Fe]**Beta**-37 after treating at 450 and 575 K for 3 hrs in vacuum (10^{-4} torr) respectively. Absorption bands due to SiOH groups at 3740 cm^{-1} , due to hydrogen bonded SiOH groups at 3540 cm^{-1} and due to C-H stretching vibrations at $3000\text{-}2800\text{ cm}^{-1}$ are observed. On oxidative decomposition of remaining TEA at 640K in air and subsequent evacuation, (Curve c in Fig.3.11) a sharp band at 3632 cm^{-1} and a broad low intensity band around 3100 cm^{-1} developed and is assigned to Bronstead acid sites associated with [Fe] bridging hydroxyls and to residual coke in the sample respectively. The color of the sample was grey at this stage. On further oxidative decomposition of this residual coke at 675 K in air and subsequent evacuation (Curve d in Fig.3.10), the band at 3100 cm^{-1} disappeared, and intensity of bands at 3740 cm^{-1} increased, whereas band at 3632 and 3540 cm^{-1} decreased considerably. The color of the sample turned white at this stage. It indicates that a minimum temperature of 675 K is needed for oxidative decomposition of TEA-cations in [Fe]**Beta** zeolite. Between 640 K and 675 K some of the bridging hydroxyl groups in [Fe]**Beta** are removed by dehydroxylation. In this respect, acid sites in [Fe]**Beta** are less stable than those of [Al]**Beta** zeolite.

ii) NH_4^+ -**Beta**

The sodium forms of the [Al] and [Fe]**Beta** samples (whose spectral characteristics were described above) were next converted into their respective ammonium forms by procedures described in Experimental Section. Fig.3.12 illustrates the changes in the FT-IR spectra of sample NH_4 [Al]**Beta**-45 on decomposition, in-situ, at various temperatures. After decomposition at 423 K (curve a), apart from the bands at $3000\text{-}3400\text{ cm}^{-1}$ due to N-H stretching vibrations, there is a sharp band at 3740 cm^{-1} (due to internal and terminal, SiOH) in addition to broad bands around 3680 and 3540 cm^{-1} . On progressive decomposition at

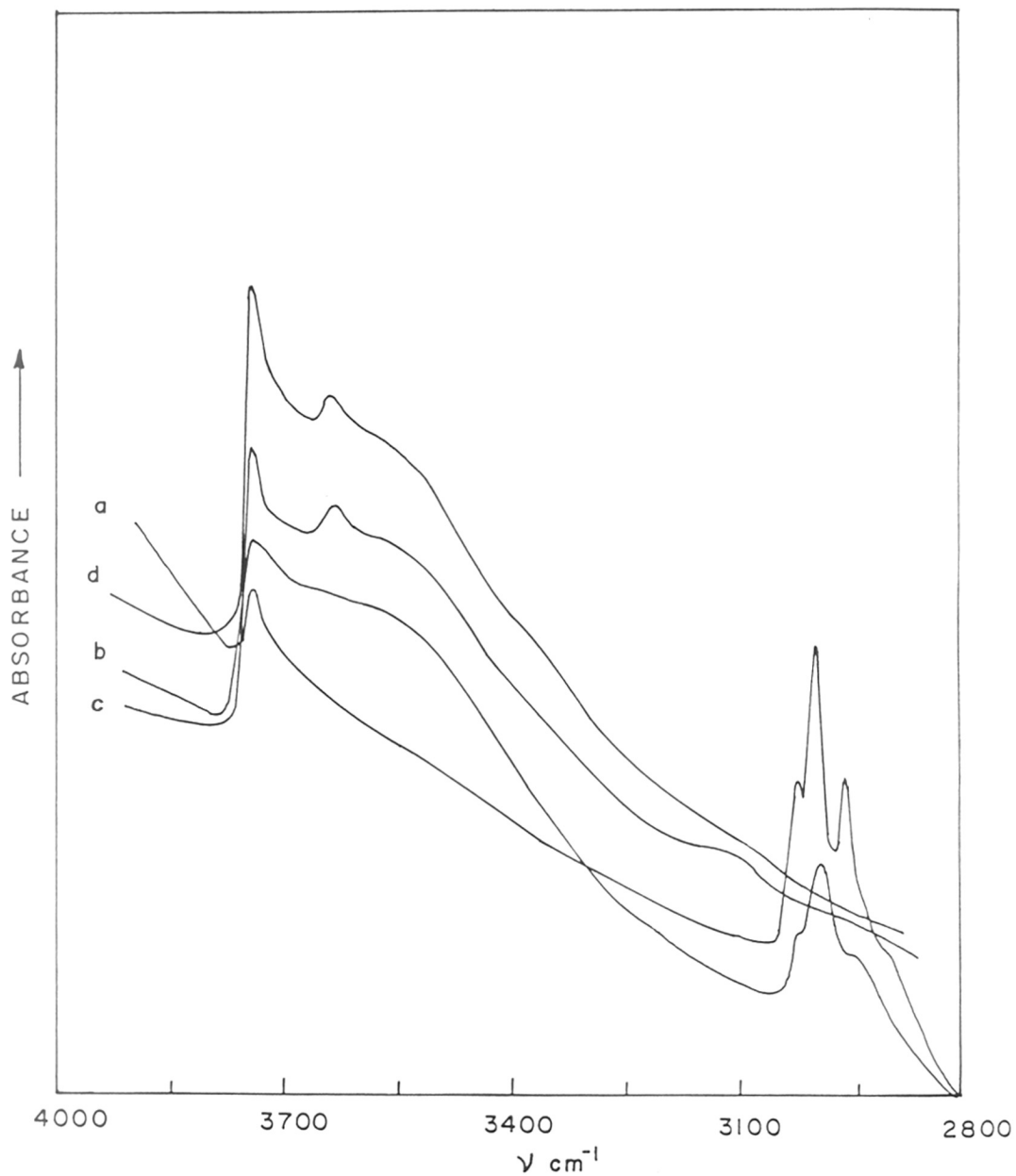


FIG.3.11 : FT-IR SPECTRA OF TEA[Fe]BETA-37 TREATED AT 450,575,653 AND 673 K (CURVES a TO d RESPECTIVELY)

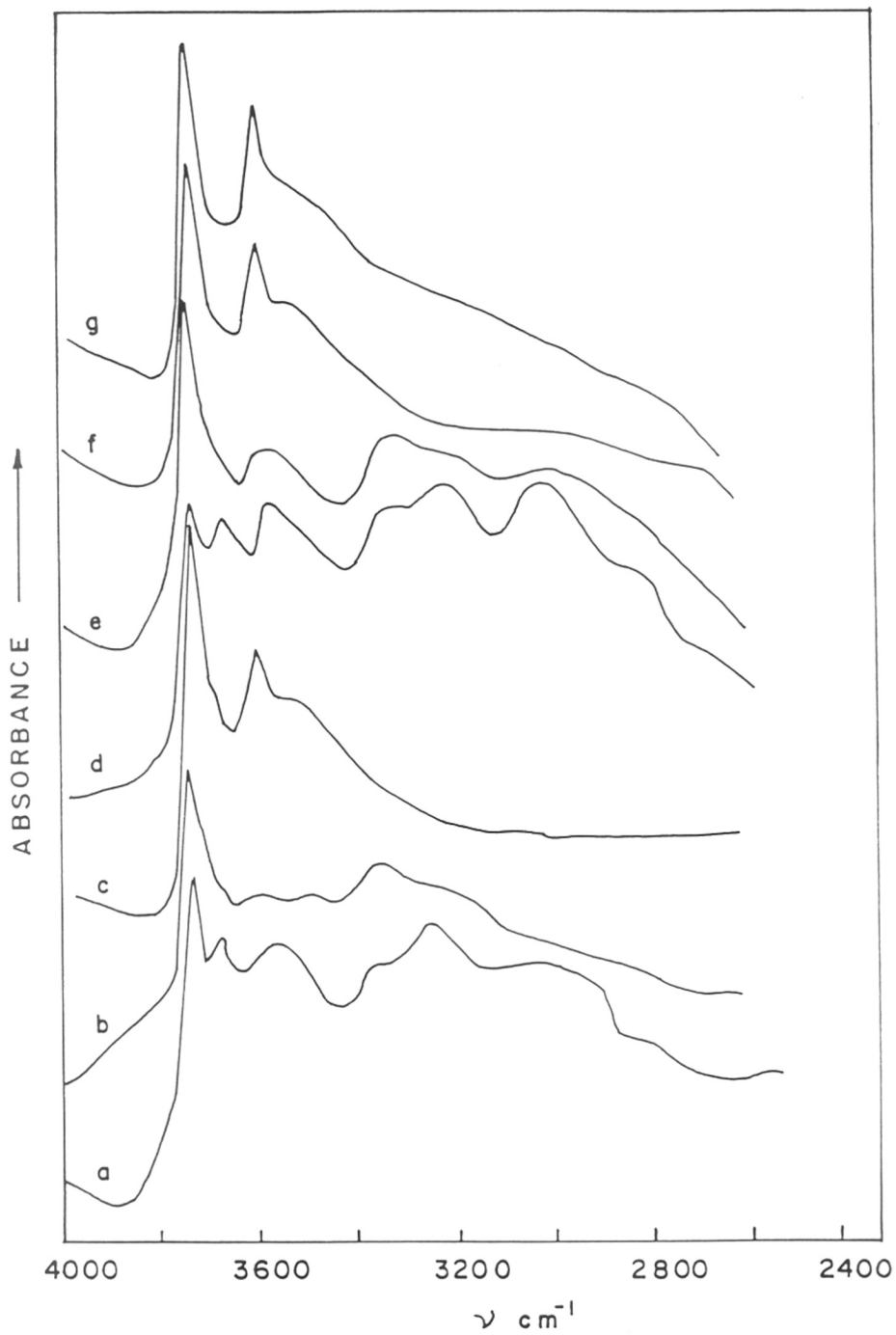


FIG.3.12 : FT-IR SPECTRA OF $\text{NH}_4[\text{Al}]\text{BETA-45}$ DECOMPOSED AT 473, 573 AND 773 K (CURVES a, b AND c) AND OF $\text{NH}_3\text{-H}[\text{Al}]\text{BETA-45}$ DESORBED AT 423, 573, 723 AND 823 K (CURVES d TO g) RESPECTIVELY

higher temperatures (curves a-c, Fig.3.12) the bands due to N-H vibrations disappear. After decomposition at 723 K (Curve c), in addition to the bands at 3740, 3605 and 3540 cm^{-1} observed above, (Fig.3.12) a shoulder appears at 3680 cm^{-1} . A similar peak at 3680 cm^{-1} was observed in the spectra of ZSM-5 by Woolery et al.¹¹²

Fig.3.13 illustrates the changes in FT-IR spectra of sample $\text{NH}_4[\text{Fe}]\text{Beta}$ -37 on decomposition, in-situ, at various temperatures. At 423 K (Curve a) the spectrum is similar to that for $[\text{Al}]\text{Beta}$ (Fig.3.12, Curve a). At 573 K (Curve b), N-H stretching vibrations at 3000-3400 cm^{-1} have almost disappeared. In addition to bands at 3740, 3632 and 3540 cm^{-1} , a shoulder at 3680 cm^{-1} is clearly visible. At 723 K, (Curve c) bands at 3000- 3400 cm^{-1} due to N-H stretching vibrations are absent and all the bands at 3680, 3632 and 3540 cm^{-1} reduce in intensity compared to those in curve b. Therefore, at 723 K, considerable dehydroxylation of bridging hydroxyl groups in $\text{H}[\text{Fe}]\text{Beta}$ zeolite occurs. Thus, the stability of Bronstead acid sites on $[\text{Fe}]\text{Beta}$ is less than that of $[\text{Al}]\text{Beta}$ zeolites.

iii) NH_3 Adsorption On H-Beta

The ammonium forms of $[\text{Al}]\text{Beta}$ -45 and $[\text{Fe}]\text{Beta}$ -37 samples were converted to the protonic forms by procedures described before and $\text{H}[\text{Al}]\text{Beta}$ -45 and $\text{H}[\text{Fe}]\text{Beta}$ -37 samples were obtained. Adsorption of NH_3 on these samples was studied by FT-IR spectroscopy. NH_3 was adsorbed at room temperature on samples evacuated at 673 K for $\text{H}[\text{Al}]\text{Beta}$ and at 643 K for $\text{H}[\text{Fe}]\text{Beta}$ respectively. FT-IR spectra were recorded after decomposition of ammonia at 423, 573, 723 and 823 K for $[\text{Al}]\text{Beta}$ and at 423, 573, 623 and 723 K for $[\text{Fe}]\text{Beta}$ respectively. They are illustrated in Fig.3.12 (Curve d-g) and Fig.3.13 (Curve d-g) respectively. As expected the spectra in Fig.3.12 (Curve d-g) and in Fig.3.13 (Curve d-g) are similar to those in Fig.3.12 (Curve a-c) and in Fig.3.13 (Curve a-c) respectively. It should be noted that for $[\text{Al}]\text{Beta}$ sample evacuated at 673 K and for $[\text{Fe}]\text{Beta}$ samples evacuated at 623 K, no trace of NH_3 was detected. The absorption bands (1) at 3605 for $\text{H}[\text{Al}]\text{Beta}$ sample evacuated at 823 K, (2) at 3632 for $\text{H}[\text{Fe}]\text{Beta}$ sample evacuated at 723 K and (3) at 3540 cm^{-1} due to hydrogen bonded hydroxyl

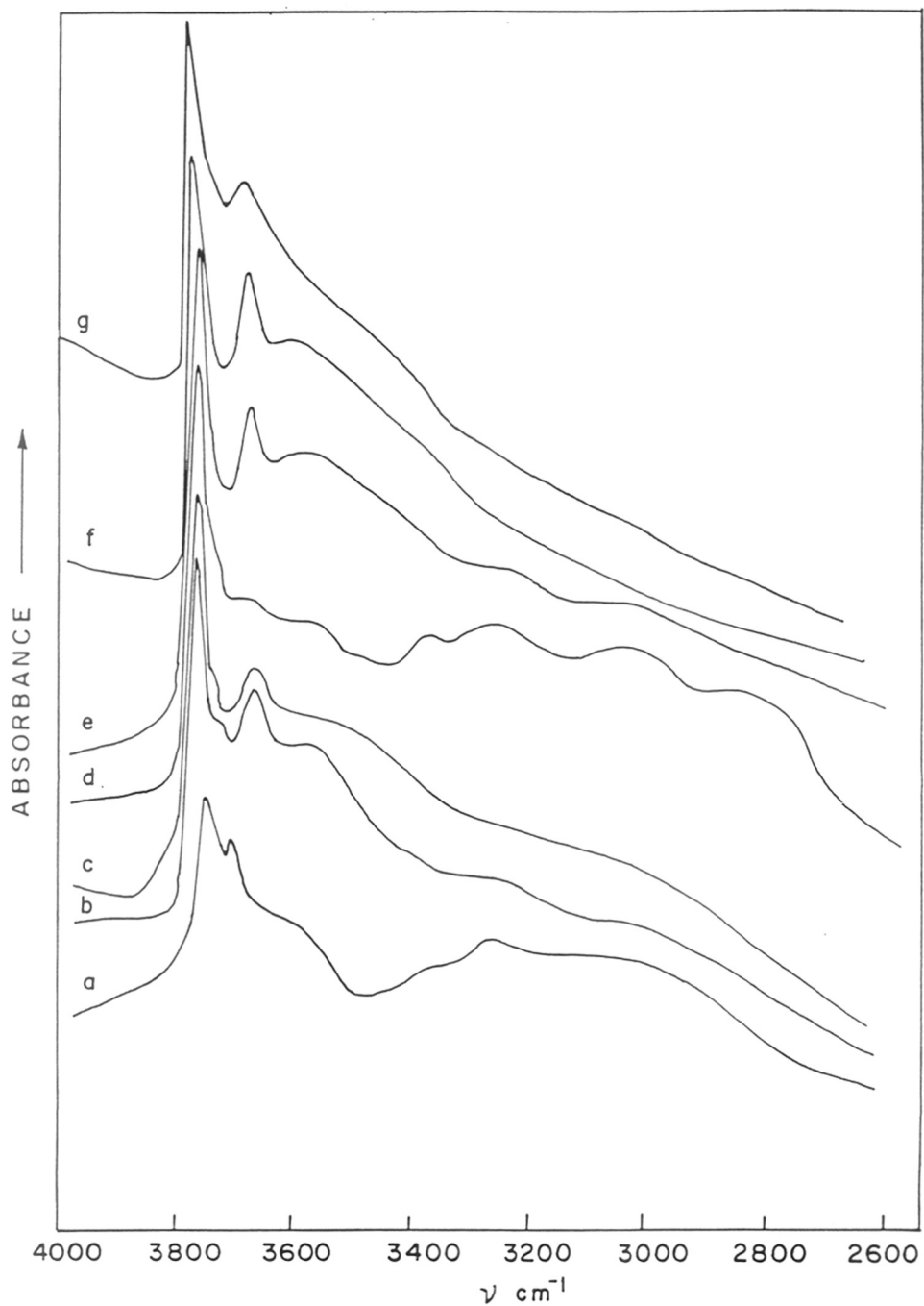
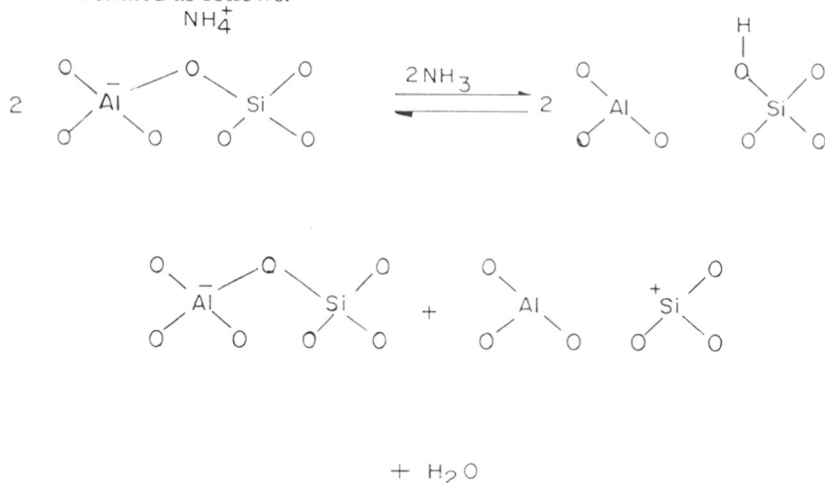


FIG.3.13 : FT-IR SPECTRA OF $\text{NH}_4[\text{Fe}]\text{BETA-37}$ DECOMPOSED AT 423,573 AND 773 K (CURVES a,b AND c) AND $\text{NH}_3\text{-H}[\text{Fe}]\text{BETA-37}$ DESORBED AT 423,573,623 AND 723 K (CURVES d TO g) RESPECTIVELY

groups in both the samples have lower intensity indicating their removal via dehydroxylation. The nature of TPD spectra in Fig.3.7 beyond 773 and 723 K respectively agrees with these FT-IR observations.

Thermochemical changes occurring on heating $\text{NH}_4\text{-Beta}$ zeolites at different temperatures can be illustrated as follows.



Thermal stability of surface hydroxyl groups of $[\text{Fe}]\text{Beta}$ zeolites are at least 50 K less than those of $[\text{Al}]\text{beta}$ zeolites.

iv) D_2O , C_6H_6 (H-BETA)

In order to confirm that absorption bands at 3740, 3605 and 3632 cm^{-1} on the surface of beta zeolite are indeed, due to (OH) groups situated at locations accessible to probe molecules and to assess the relative acidity of these (OH) groups, the shift in the (OH) frequencies on adsorption of D_2O Fig.3.14 and benzene (Fig.3.15) was evaluated. Samples $\text{H}[\text{Al}]\text{Beta-45}$ and $\text{H}[\text{Fe}]\text{Beta-37}$ were studied. Exposure of $\text{H}[\text{Al}]\text{Beta}$ and $\text{H}[\text{Fe}]\text{Beta}$ (previously activated at 673 K and 643 K respectively) to D_2O vapors followed by desorption at 423 K led to the decrease in intensity of the bands at 3740 and 3540 cm^{-1} for $[\text{Al}]\text{Beta-45}$ and $[\text{Fe}]\text{Beta-37}$ samples. Bands at 3605 and 3632 cm^{-1} respectively were totally absent. New bands due to surface O-D

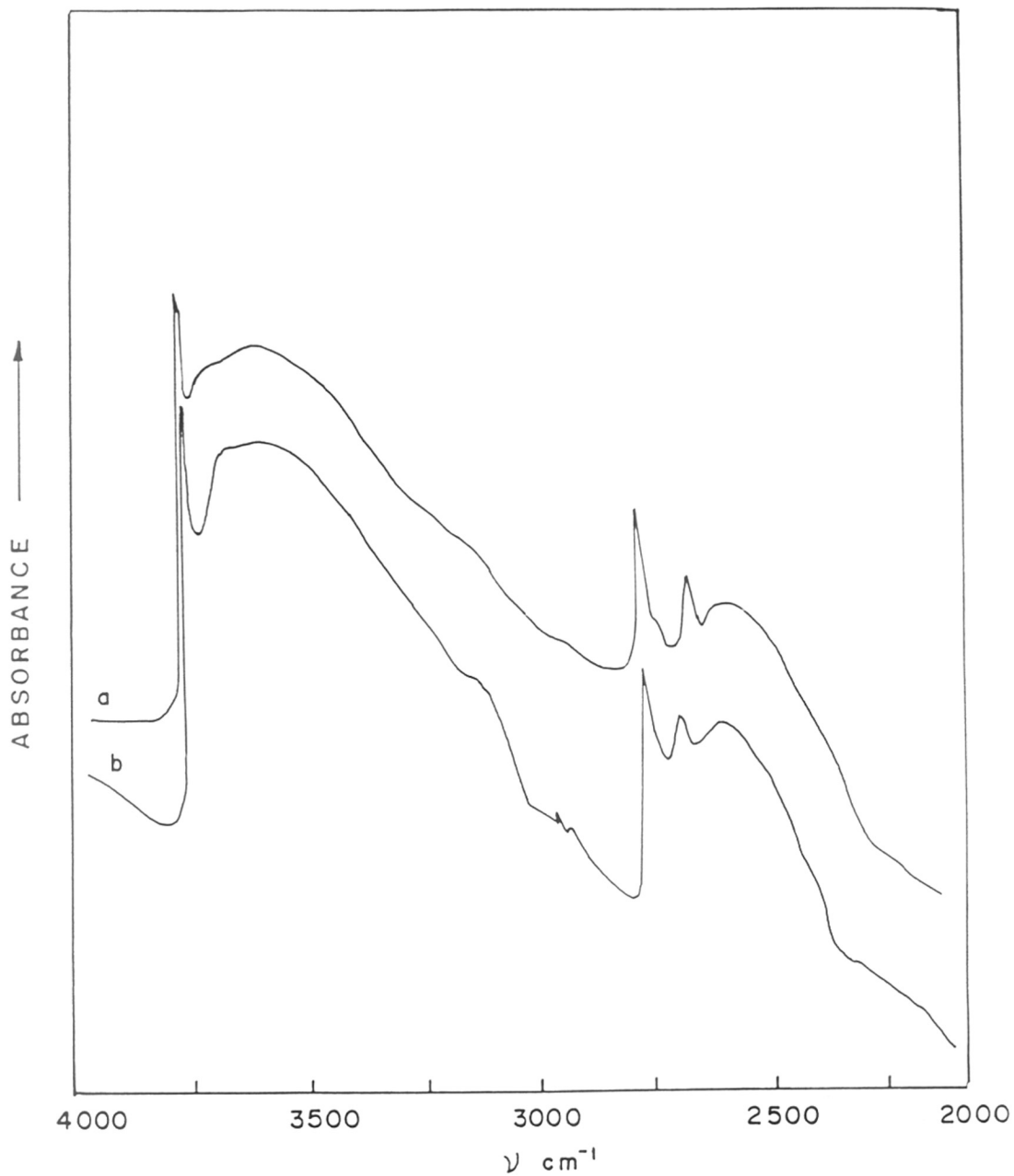


FIG.3.14 : FT-IR SPECTRA OF H[Al]BETA-45 (a) AND H[Fe] BETA-37 (b) WITH ADSORBED D_2O

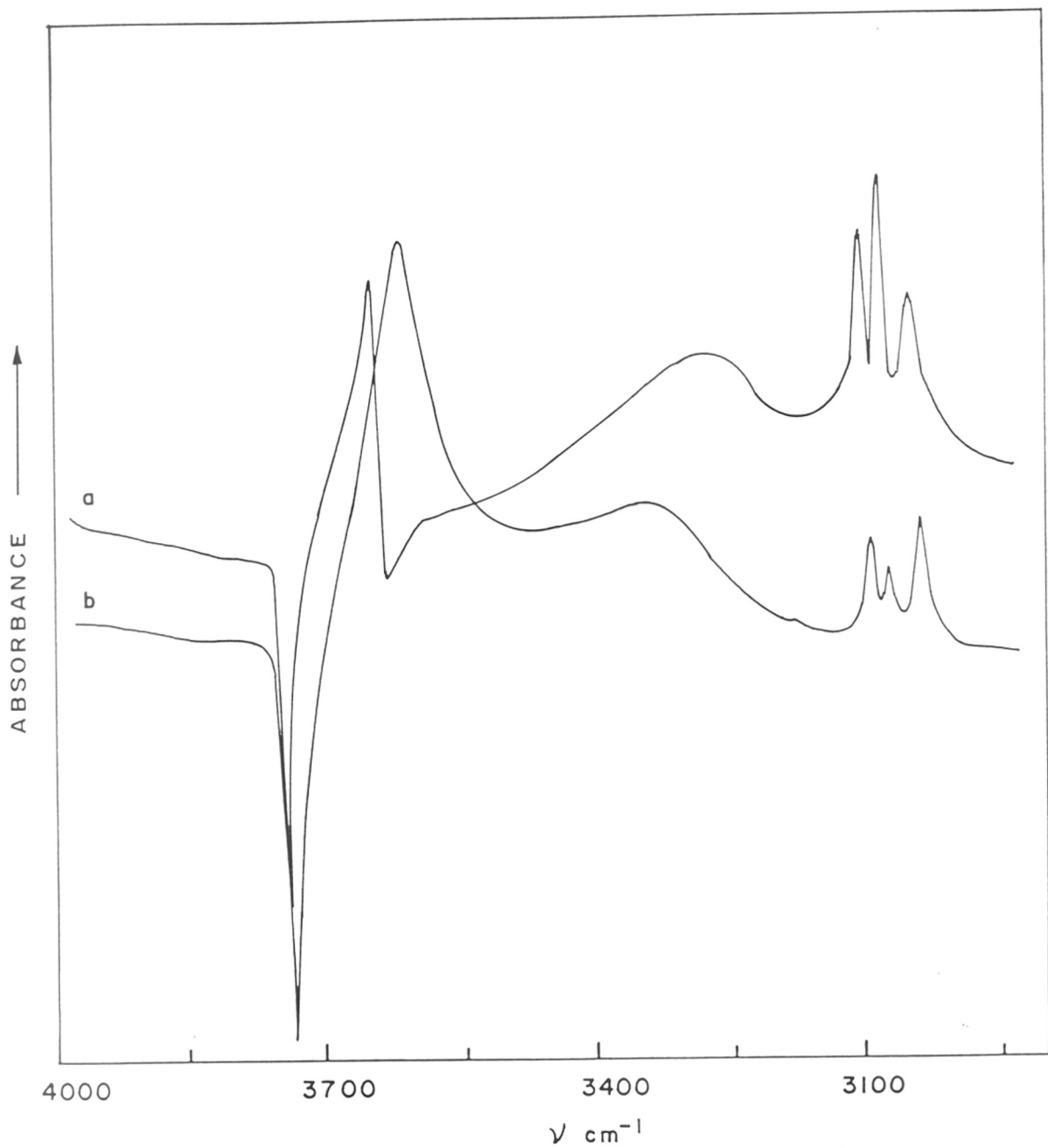


FIG.3.15 : FT-IR DIFFERENCE SPECTRA OF [SAMPLE WITH BENZENE -
SAMPLE] H[Al]BETA-45 (a) AND H[Fe]BETA-37 (b)

groups at 2763, 2713 and 2545 cm^{-1} for [Al]Beta and at 2763, 2733 and 2545 cm^{-1} for [Fe]Beta were observed. The rapid displacement (of OH by OD) and the expected frequency shift suggest that OH groups are located at easily accessible positions.

It is known that when H-bonded complexes of OH groups with weakly adsorbed bases are formed, the IR bands of OH groups with acidic properties are shifted towards lower frequencies¹¹³. The extent of the shift is the characteristic of the strength of the Bronsted acidic sites^{113,114}. On adsorption of benzene at 423 K on H[Al]Beta-45 (Fig.3.15) (previously activated to 673 K) O-H band at 3740 cm^{-1} is shifted to 3640 cm^{-1} (negative peak at 3740 cm^{-1} and positive peak at 3640 cm^{-1}) in the difference spectrum. The O-H band at 3605 cm^{-1} disappears and a new broad band at 3265 cm^{-1} (frequency shift 337 cm^{-1}) appears. The bands around 3000 cm^{-1} are due to aromatic C-H vibrations (Fig.3.15, Curve a). For H[Fe]Beta-37 sample (Fig.3.15, Curve b) the disappearance of bands at 3740 and 3632 cm^{-1} was clearly seen as negative peaks and were shifted to 3610 (apparent frequency shift 130 cm^{-1}) and to 3322 cm^{-1} (frequency shift 310 cm^{-1}). The corresponding frequency shifts for adsorption of benzene on H[Al]ZSM-5, H[Fe]ZSM-5 and H-Y are 350, 330 and 300 cm^{-1} respectively¹¹⁴. The strength of the Bronsted acid sites in zeolite beta is hence intermediate between that of H-ZSM-5 and H-Y.

v) Pyridine-H (Beta)

Fig.3.16 shows the IR spectra of pyridine retained at 673 K on samples Na[Al]Beta-45, H[Al]Beta-45, Na[Fe]Beta-37 and H[Fe]Beta-37 (Curves a,b,c and d respectively). Vedrine et al¹¹⁵. reported the IR spectra of pyridine adsorbed on H-ZSM-5. Absorption bands due to adsorbed pyridine were observed at 1640, 1628, 1550, 1495 and 1450 cm^{-1} . The bands at 1640 and 1550 cm^{-1} were ascribed to the pyridinium ions. The bands at 1628, 1495 and 1450 cm^{-1} were assigned to pyridine molecules coordinated to Lewis acid sites. A similar assignment can be made for the spectra in Fig.3.16. The bands at 1633 and 1546 cm^{-1} are assigned to pyridinium ions, whereas the bands at 1618, 1500 and 1450 cm^{-1} are assigned to a Lewis site bound pyridine.

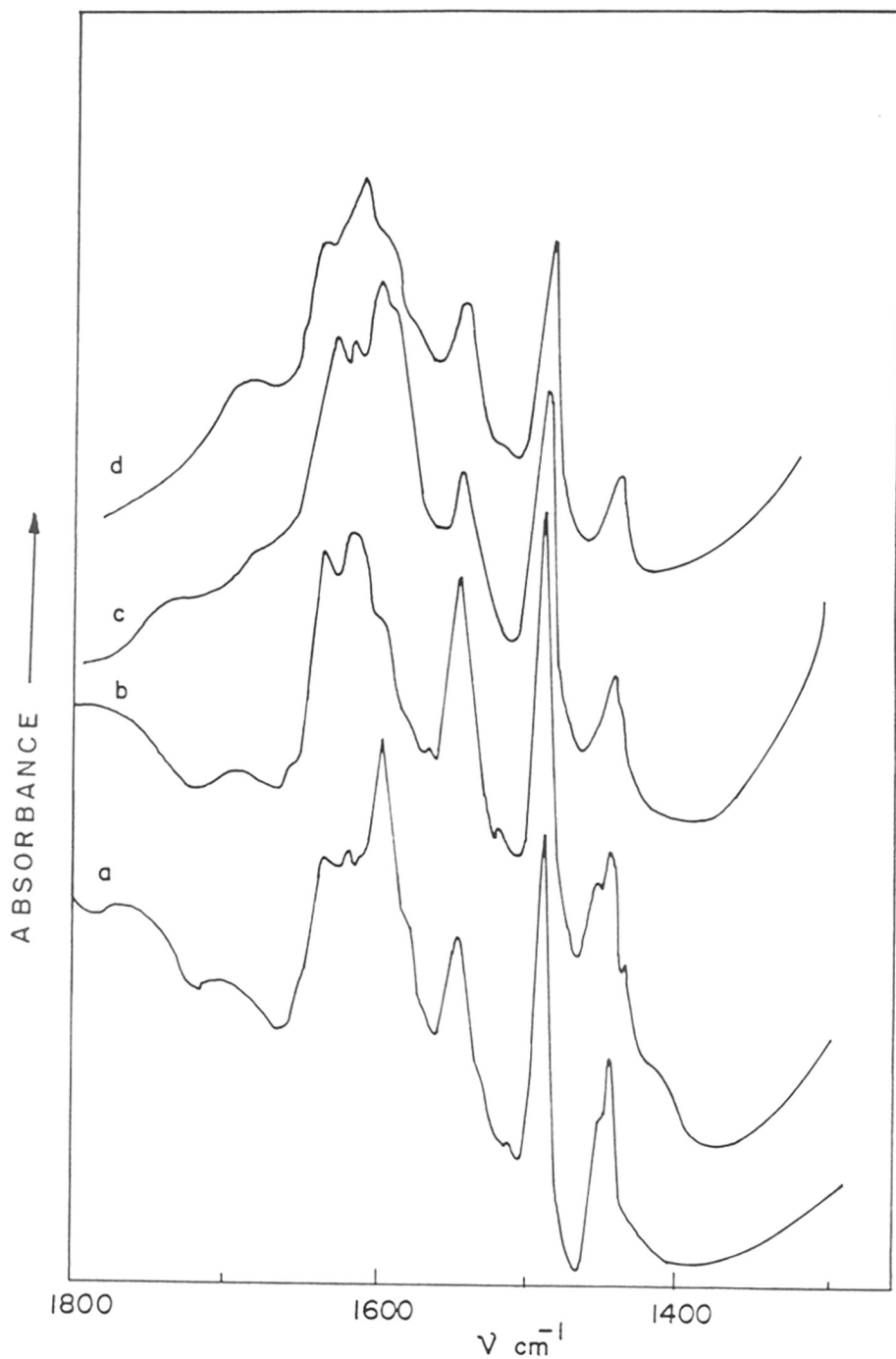


FIG.3.16 : FT-IR SPECTRA OF PYRIDINE CHEMISORBED ON H[Al]BETA-45, Na[Al]BETA-45, H[Fe]BETA-37 AND Na[Fe]BETA-37 (CURVES a TO d RESPECTIVELY)

The bands at 1443 and 1600 cm^{-1} are also present which are due to hydrogen bonding. At 673 K H[Fe]Beta zeolite contains less number of Bronstead and Lewis acid sites compared to H[Al]Beta, as can be seen from the Fig.3.16.

3-2.5 MASNMR Spectroscopy

The ^{29}Si and ^{27}Al MAS NMR of as-synthesized TEA[Al]Beta-45 and TEA[Fe]Beta-37 are given in Fig. 3.17, Curves a&b respectively. The ^{27}Al spectra of TEA[Fe]Beta shows absence of Al in the sample. Spectrum of ^{29}Si for [Fe] sample is broadened compared to that for [Al] sample. It arises from Si-O-Fe nuclear electron coupling in [Fe] zeolite.

3-2.6 E.S.R. Spectroscopy

Although an e.s.r. signal around $g = 4.3-4.4$ cannot be used to confirm the presence of Fe^{3+} in zeolite lattice positions, the observation of such a signal is a necessary consequence of such a presence and may, hence, lend additional support to any postulate of isomorphous substitution of Al by Fe. The e.s.r. spectra of the [Fe]Beta samples Fig.3.18 reveal two main signals at $g = 2.0$ and 4.4 , respectively. The latter is assigned to tetrahedral Fe^{3+} possibly in lattice positions. The enhanced intensity of this signal at lower temperatures as well as its relative insensitivity to oxidation-reduction treatments suggests that it arises from Fe^{3+} ions in tetrahedral lattice positions rather than nonframework positions.

3-2.7 Magnetic Susceptibility

Magnetic susceptibility measurements were done for the as-synthesized TEA[Fe]Beta-37, sample between 94 and 297 K. The values were 5.8 and 5.5 Bohr Magneton at 94 and 297 K, respectively. Non-interacting Fe^{3+} ions in a diamagnetic matrix are expected to have a magnetic moment below about 6 B.M. The observed values of 5.5-5.8 B.M. for [Fe]Beta sample and relative insensitivity of these values to temperature changes indicate the absence of a significant concentration of iron-oxide phases. The latter, if present, would exhibit much higher values of the magnetic moment (depending on the degree of agglomeration of the iron-oxide

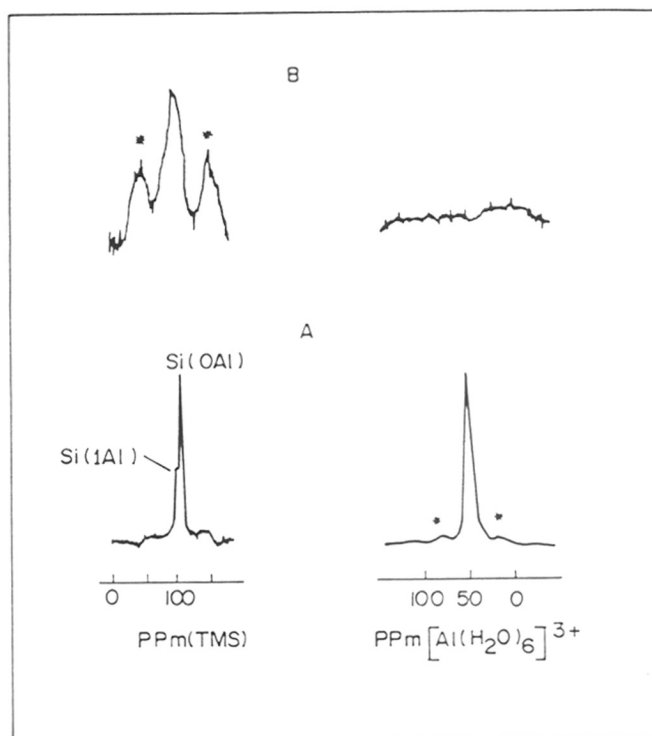


FIG.3.17 : MASNMR OF [Al]BETA-45 AND [Fe]BETA-37 (A and B SHOWN RESPECTIVELY) * SPINNING SIDE BANDS

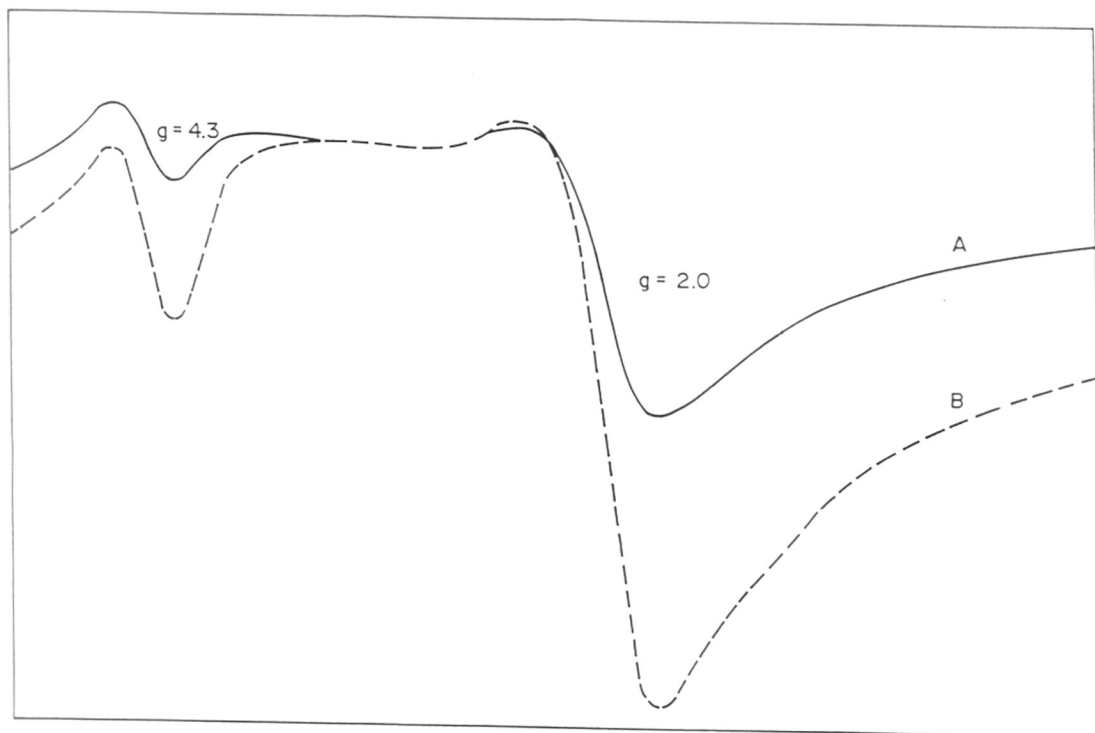


FIG.3.18 : ESR SPECTRA OF [Fe]BETA-37 AT 297 AND 94 K
(CURVES A AND B RESPECTIVELY)

phase). In addition, the values of the magnetic moments would also increase markedly at lower temperature. Hence the magnetic susceptibility data indicate that (i) iron-oxide phases like Fe_2O_3 or Fe_3O_4 are absent in the sample of [Fe]Beta and (ii) that the Fe^{3+} ions are present in a magnetically dilute environment. These observations support that Fe^{3+} ions are isomorphously substituted in the zeolite beta lattice.

3-2.8 Mössbauer Spectroscopy

Fig.3.19 represents the Mossbauer spectrum of TEA[Fe]Beta- 37 obtained at 300 K. It is nearly Lorentzian in shape, with $\Gamma = 2.3$ mm/s which could not be resolved into three mutually consistent pairs of Lorentzian lines, showing the absence of quadrupoles splitting. The isomer shift was found to be 0.22 ± 0.03 mm/s.

The Mossbauer spectrum at 4.2 K without and with internally applied magnetic field (Fig. 3.20, Curves a & b) shows an isomer shift of 0.32 mm/s. Quadrupoles splitting did not change with applied magnetic field showing that the electronic ground state of ferric ions is the high spin $\text{Fe}^{3+}(6s)$. These parameters are characteristic of tetrahedral Fe^{3+} ions^{116,117}. The absence of well-defined hyperfine splitting even at 4.2 K indicates that Fe^{3+} is in a very dilute paramagnetically well dispersed state. The Mossbauer spectrum at 4.2 K with applied external magnetic field (Fig.3.19, Curve b) shows hyperfine splitting arising due to three crystal field split states $1 \pm 5/2 >$, $1 \pm 3/2 >$, and $1 \pm 1/2 >$ of $6s$ Fe^{3+} ions. The average value of the internal magnetic field $H(\text{int}) = 46.8$ T is within the range specified for tetrahedrally coordinated iron ions. All these observations rule out the possibilities of presence of $\gamma\text{-Fe}_2\text{O}_3$ and Fe_3O_4 impurities in the sample.

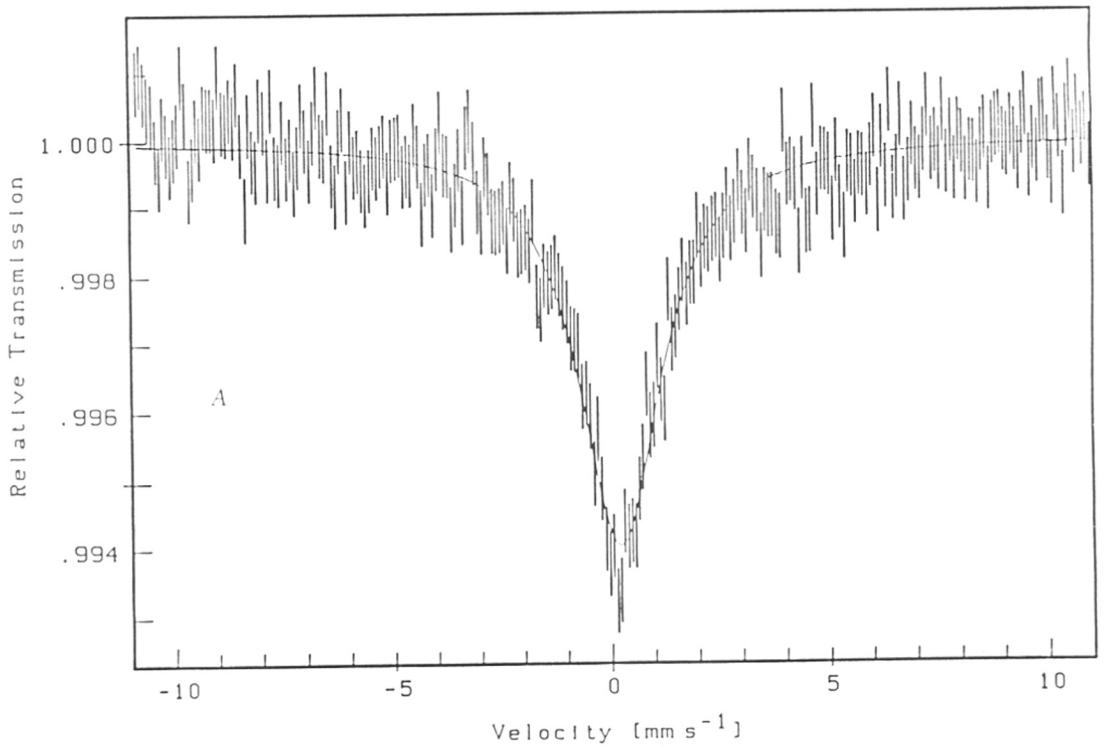
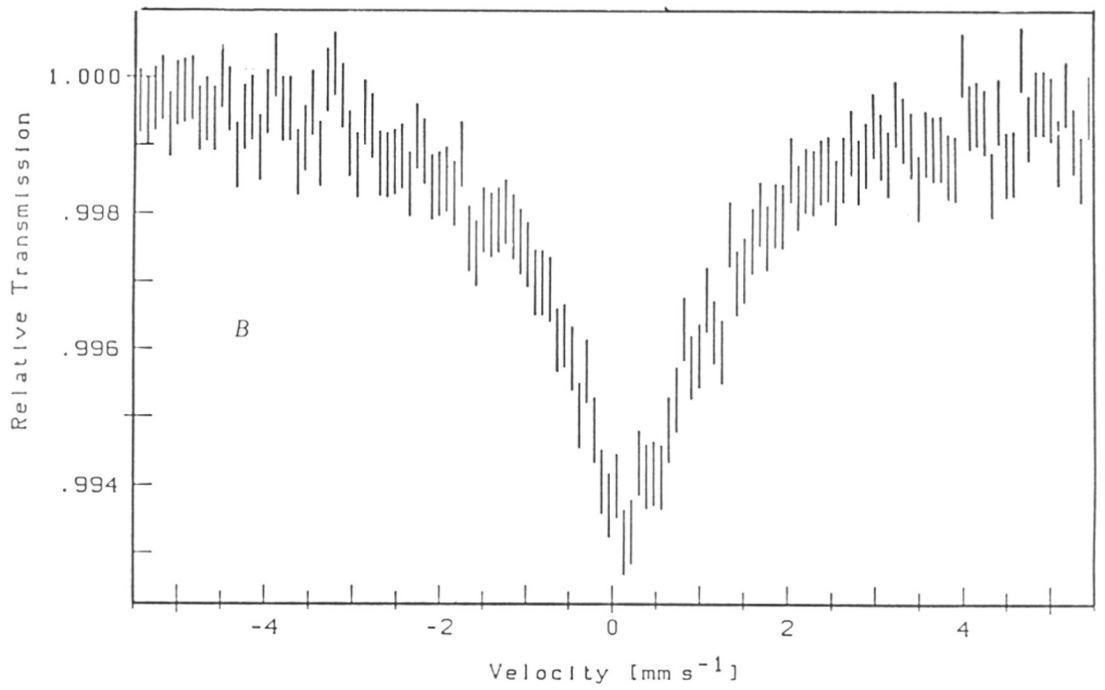


FIG.3.19 MOSSBAUER SPECTRA OF T EA [Fe]BETA AT 300 K (A) NORMAL SCALE (B) EXPANDED SCALE

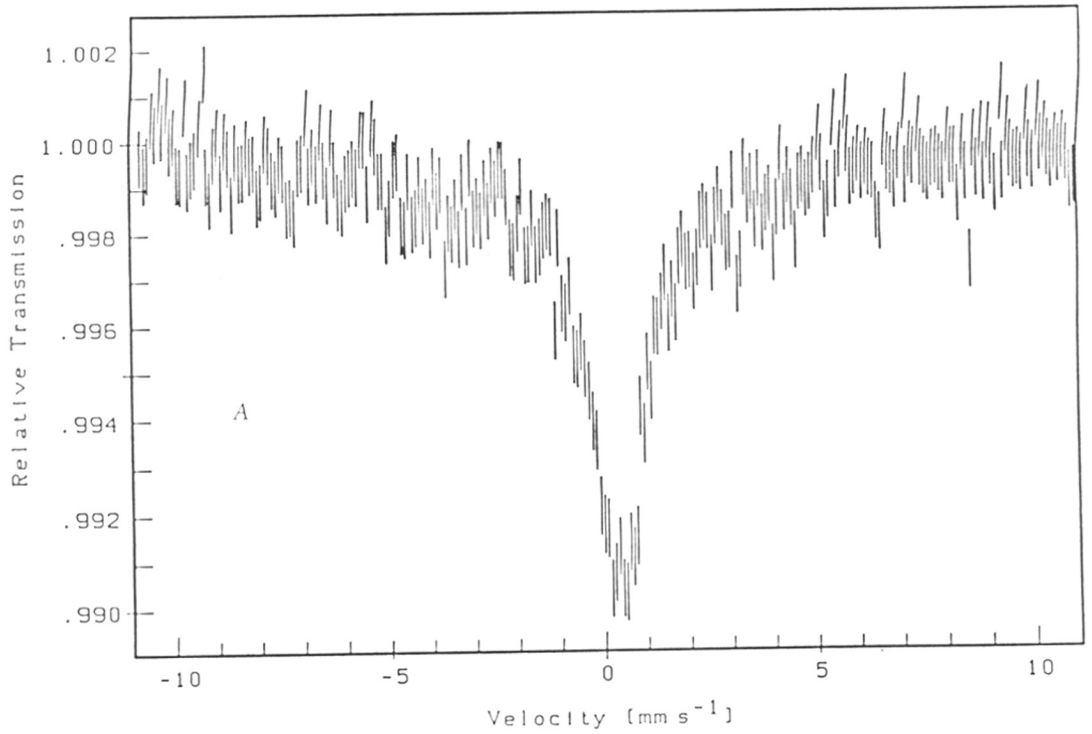
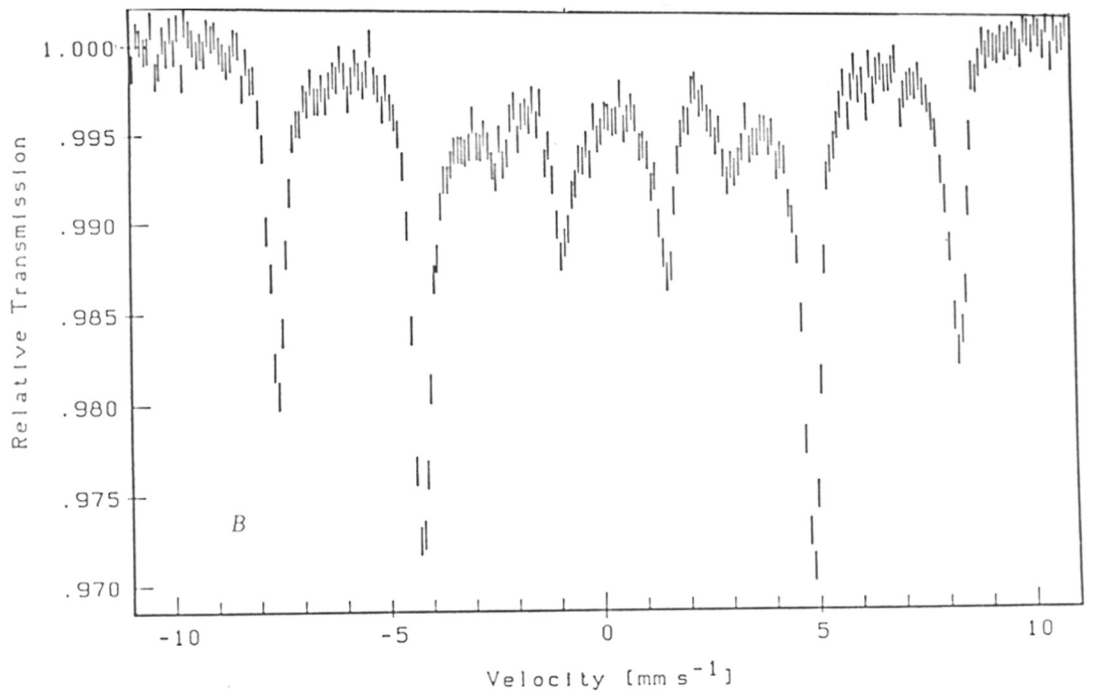


FIG.3.20 MOSSBAUER SPECTRA OF TEA [Fe]BETA AT (A) 4.2K AND (B) 4.2K WITH AN EXTERNALLY APPLIED MAGNETIC FIELD 4.17T.

3-3 CONCLUSIONS

- 1) X-ray amorphous nuclei of **beta** zeolite could be detected by thermal analysis, adsorption and IR studies.
- 2) Adsorption pore volume of [Al] and [Fe]**Beta** is about 0.22 ± 0.03 ml/g of zeolite.
- 3)
 - a) Mid-IR frequency due to asymmetric stretching vibrations of $-(\text{Si-O-Fe})_n-$ units in TEA[Fe]**Beta** is shifted to lower wave numbers compared to $-(\text{Si-O-Al})_n-$ units in TEA[Al]**Beta** zeolite.
 - b) The solid state MASNMR ^{29}Si spectrum of TEA[Fe]**Beta** is broadened compared to TEA[Al]**Beta** arising from Si-O-Fe nuclear-electron coupling in [Fe] zeolite.
 - c) Magnetic susceptibility of TEA[Fe]**Beta** zeolite is 5.8 and 5.5 B.M., at 94 and 293 K respectively, indicative of Fe^{3+} ions in magnetically dilute environment.
 - d) The room temperature Mossbauer isomer shift (0.32 mm/s), the absence of hyperfine splitting at 4.2 K, and crystal field splitting into $1 \pm 5/2 >$, $1 \pm 3/2 >$, $1 \pm 1/2$ of $6s$ state of Fe^{3+} ion, and internal magnetic field = 46.8 T are well within the range for tetrahedral co-ordination for Fe^{3+} ions by oxide ions.
- 4) Bronsted acid sites (bridging hydroxyl groups for [Al] and [Fe]**Beta** zeolite gave bands at 3605 and 3632 cm^{-1} respectively. Frequency shift of these vibrations on benzene adsorption was 337 and 310 cm^{-1} respectively showing that [Fe]**Beta** has weaker acidity compared to [Al]**Beta**.
- 5) The thermal stability of surface hydroxyl groups of [Fe]**Beta** is less than those of [Al]**Beta** zeolite.

CHAPTER - 4

CATALYSIS

4-1 INTRODUCTION

This chapter presents the results of the studies on the catalytic properties of [Al]-Beta and [Fe]-Beta. The studies reported are :

Interconversion of aromatics

- 1) Meta-xylene conversion
(isomerization and disproportionation)
- 2) Toluene methylation
- 3) Toluene transalkylation
- 4) Toluene disproportionation, and
- 5) Alkylation of benzene with long chain linear olefins.

Interconversion of aromatics.

The conversion of meta-xylene provides information regarding the structural features of zeolites. There are three important parameters which can rank medium and large pore zeolites according to their pore openings and void space. These parameters are:

- a) **para-/ortho-xylene ratio** - ranks medium pore zeolites according to their product shape selective properties.
- b) **Isomerization/Disproportionation ratio** - ranks zeolites according to their void space. (restricted transition state shape selectivity)
- c) **1,3,5-/1,2,4-trimethyl benzene ratio**- distinguishes between medium and large pore 10-membered ring and 12-membered ring zeolites.

4-2 *EXPERIMENTAL*

4-2.1 Atmospheric Pressure Reactor

An on-line reaction analysis set up was used to carry out catalytic studies. It consisted of a fused silica reactor of 1.5 cm inner diameter (i.d.) and 30 cm length with a provision for feeding reactants and carrier gas at the top. It had a thermowell which carried a thermocouple for sensing the reaction temperature. The catalyst powder was pressed, pelleted, crushed and sieved to obtain 15-20 mesh size particles. 1.0 g (on anhydrous basis) of this catalyst was charged in the centre of the reactor in such a way that the catalyst bed was sandwiched by inert porcelain beads. The upper portion of the reactor, serving as a vaporiser-cum-preheater was packed with inert porcelain beads. The reactor was placed in a two-zone furnace (Fig. 4.1). Before the reaction, the catalyst was activated in a stream of dry air at 723K for about 8 hrs. The catalyst was then flushed with dry nitrogen and cooled to reaction temperature. The reactants were passed at the required rate into the reactor. The liquid reactant was fed by a syringe pump (SAGE Instruments - Model 352). The flow rates of gaseous reactants were controlled by needle valves, and monitored by calibrated flow meter. A Shimadzu gas chromatograph with six port heated gas sampling valve was used. At fixed intervals samples were injected into a G.C. through the 6-port valve for on-line analysis (G.C. model Shimadzu R-1A FID detector). A two metre long stainless steel column packed with Bentone-34 and diisodecylphthalate (10%) was used for separation of the components of the products.

4-2.2 Regeneration of the Catalyst

After the completion of reaction, feed injection was stopped and the catalyst was flushed first with nitrogen and then a mixture of nitrogen and air (60:40 volume ratio approximately) was passed over the catalyst at 523 K (approx.). The temperature was raised slowly to 723 K. The regeneration was carried out at this temperature for 8 hrs. Then the catalyst was flushed again by dry nitrogen and cooled down to reaction temperature for further use.

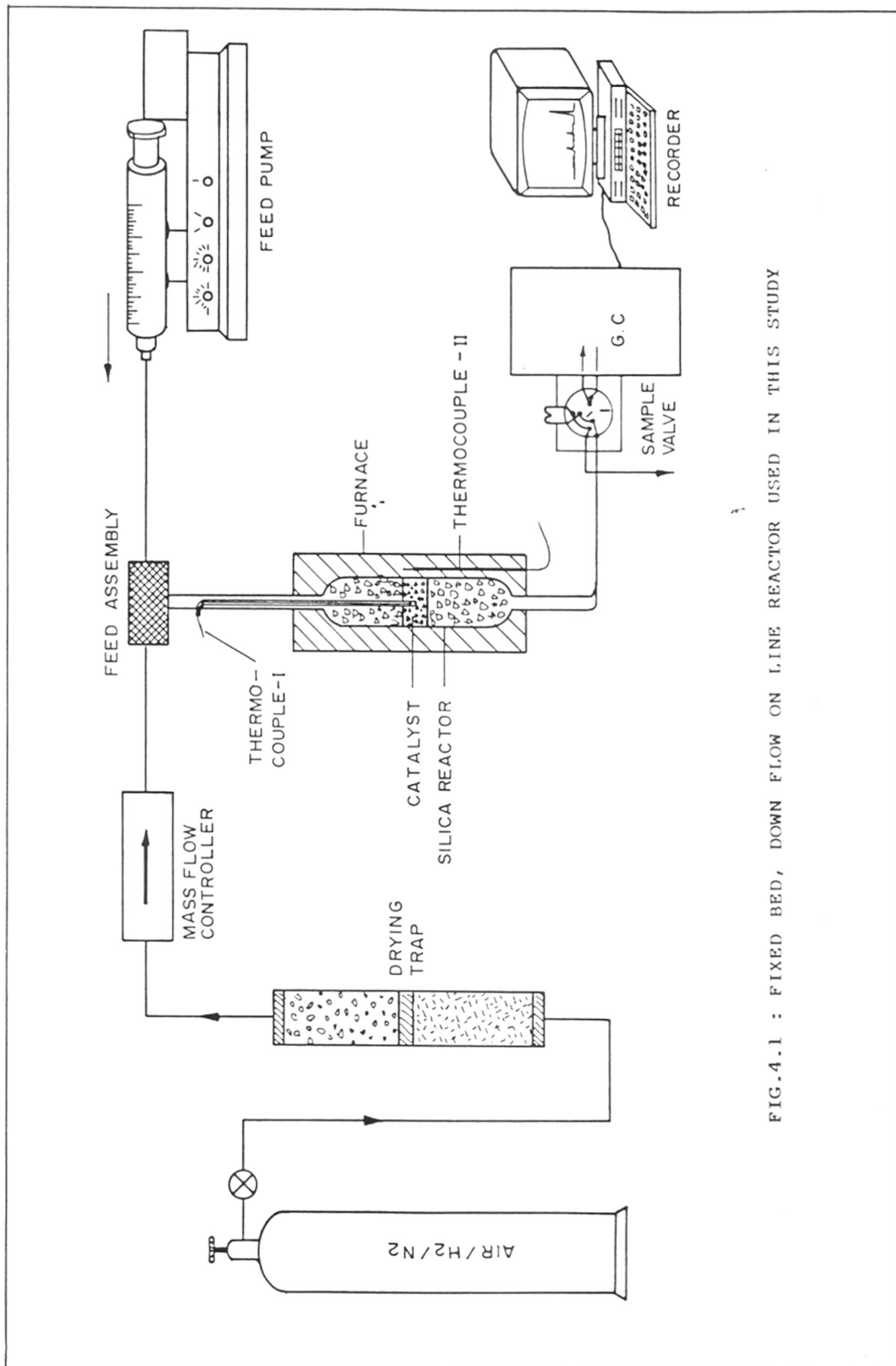


FIG.4.1 : FIXED BED, DOWN FLOW ON LINE REACTOR USED IN THIS STUDY

4-2.3 High Pressure Reactor

A high pressure reactor (Model BL-2), supplied by M/s. Geomecanique, Paris, France was used in this study. The reactor had a total volume of 220 ml, and was made up of SS-316 and was 88.5 cm long with i.d. of 19 mm. It had a thermowell running all along the length of the reactor (o.d. = 6 mm). Four thermocouples could be inserted through the thermowell to measure the reactor temperature at different points. The furnace was made up of 5 shells (zones), whose temperatures could be independently controlled with five temperature controllers. Gases were introduced via mass flow controllers, while the outgoing gases were measured by a wet gas flowmeter. About 60-80 g catalyst (1.5 x 3 mm) was used in high pressure reactions. The catalyst was activated in flowing dry air at 723 K, then purged with nitrogen and cooled to 373 K. The hydrogen was introduced at the rate of 200 ml/min at required pressure and the temperature was raised to desired reaction temperature. After adjusting all the parameters the feed was injected at the desired rate. Samples were collected periodically (liquid as well as gas). A diagram of the reactor is shown in Fig.(4.2).

4-2.4 Regeneration of Catalyst

After the completion of the reaction, the catalyst was flushed with dry nitrogen with a rate of 250 ml/min at 373K for one hour. Later a mixture of N₂ and O₂ (90:10 N₂:O₂ ratio approximately) was introduced and the temperature was slowly raised to 723 K. After 1 hr, dry air was passed and regeneration continued for 8 hrs. The catalyst was flushed in nitrogen and cooled to desired reaction temperature.

Some of the other zeolites used in this study were prepared as per the recipe given in the references and are tabulated in Table 4.1

The feed(s) used in this study, their source and purity are given in Table 4.2.

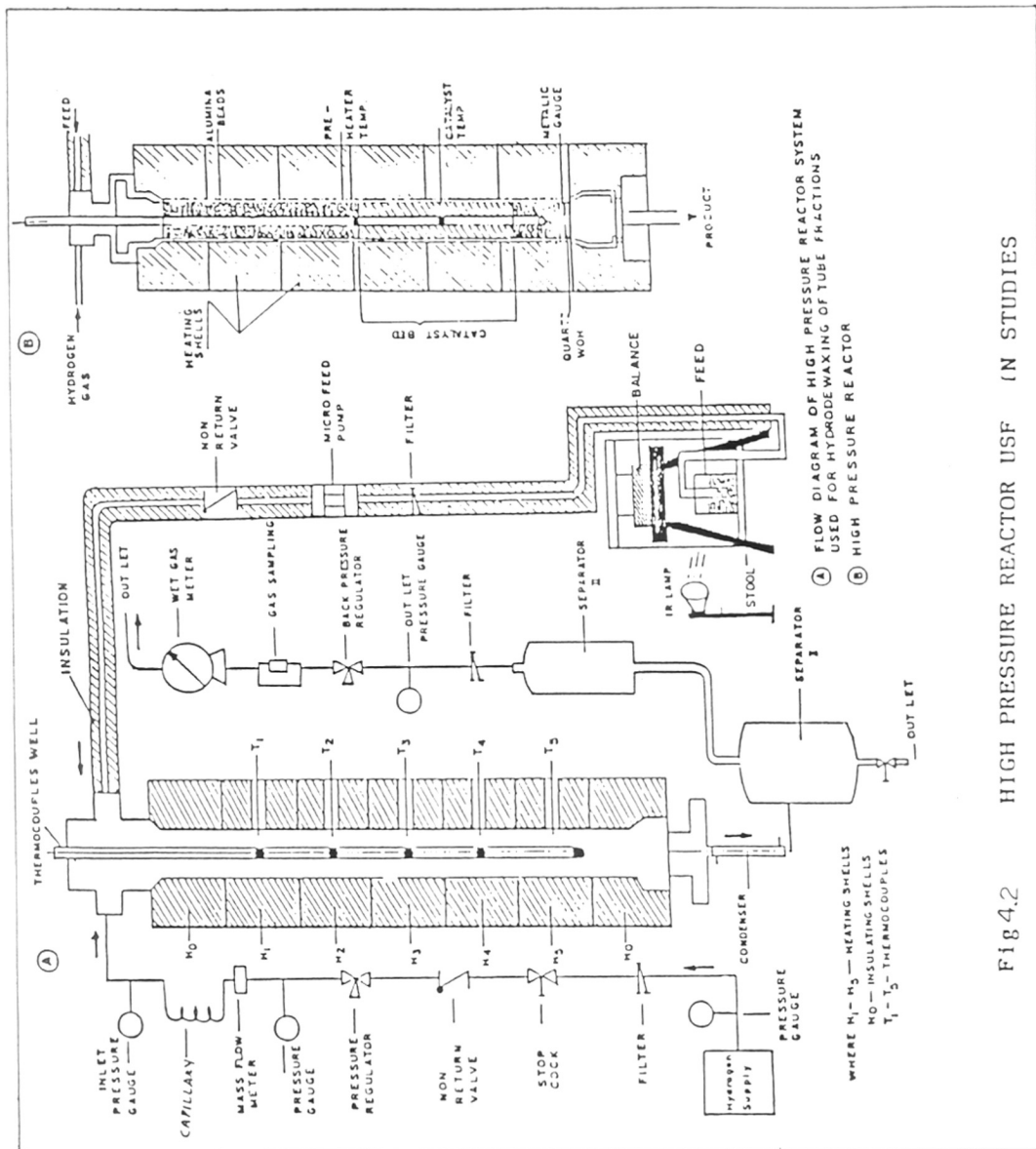


Fig 4.2 HIGH PRESSURE REACTOR USE IN STUDIES

Table - 4.1

Details of the zeolites used in this study

Zeolite	Si/Al Ratio	Reference for recipe
ZSM-23	55	118-120
ZSM-48	80	121,122
ZSM-5	33	123,124
ZSM-50	58	125,126
ZSM-12	150	127
Mordenite	4.8	Supplied by Norton zeolon-900
Zeolite-Y	2.4	Union Carbide (Linde Division)

Table - 4.2

Reactant feed (s), their source and purity

Feed	Source	Purity
Benzene	Loba Chemie, India	99.8% (AR)
m-Xylene	Aldrich, U.S.A.	99.9% (AR)
Toluene	Loba Chemie, India	99.8% (AR)
Methanol	BDH, India	99.8% (HPLC grade)
Isomer feed	IPCL, Vadodara India	C ₈ aromatic cut
Linear long chain olefins	Reliance Inds. Ltd. Patalganga, India	10% Olefins of LAB plant (C ₁₀ - C ₁₃) (rest paraffins)

4-3 RESULTS AND DISCUSSION

4-3.1 Conversion of meta-Xylene

The effect of $\text{SiO}_2/\text{Al}_2\text{O}_3$ of zeolite **beta** on its catalytic activity and selectivity in m-Xylene isomerization is shown in Table-4.3. With the increase in $\text{SiO}_2/\text{Al}_2\text{O}_3$, the activity (conversion of meta-xylene) of the catalysts decreases due to the concomitant decrease in the density of the active Bronsted acid sites. The results on the influence of reaction parameters like temperature and space velocity on the activity and selectivity are recorded in Table 4.4 and 4.5 respectively. As expected, the conversion of meta-xylene increased with the increase of reaction temperature or decrease in WHSV.

4- 3.11 para-Xylene/ortho-Xylene (p-X/o-X) ratio

It has been demonstrated^{128,129} that the value of the p-X/o-X mainly depends upon pore openings of zeolites, particularly in 10-membered (medium pore) ones. In the case of 12-membered ring (large pore) zeolites, this ratio generally follows the thermodynamic value, suggesting that there are no diffusional restrictions on xylene isomers in large pore zeolites. So, as expected, the value of p-Xylene/o-Xylene ratios, obtained in the isomerization of meta-xylene over zeolite **beta** having different $\text{SiO}_2/\text{Al}_2\text{O}_3$ ratios, at all conversion level closely followed the thermodynamic values (i.e., 1 ± 0.1 , Fig.4.3). For comparison, the p-xylene/o-xylene ratios exhibited by some medium pore zeolites (such as ZSM-48, ZSM-23, ZSM-5) are also plotted against conversion in Fig.4.4. The approach to equilibrium of xylene isomers in the m-Xylene conversion over zeolite **beta** and other medium pore zeolites is compared in Fig.4.3. While 10-ring zeolites follow the para selective path, zeolite **beta** strictly follows the equilibrium path.

4-3.12 Isomerization/Disproportionation (I/D) ratio

Unlike the isomerization, the disproportionation of m-xylene is controlled by the restricted transition state shape selectivity (rtss) exerted by the void space available around

Table - 4.3

Isomerization of m-Xylene over H [Al]Beta: Influence of SiO₂/Al₂O₃Feed = m-xylene + H₂ (1:4 mole)WHSV = 3.5 hr⁻¹, Temperature = 488 K

	SiO ₂ /Al ₂ O ₃		
	28	45	60
Conversion (%)	15.0	10.12	7.70
Products (Wt%)			
Toluene	2.4	1.4	0.7
p-Xylene	5.8	3.35	4.42
m-Xylene	85.0	89.88	92.3
o-Xylene	4.8	3.96	3.42
1,3,5 TMB ^a	0.5	0.335	0.192
1,2,4 TMB	1.3	0.968	0.565
1,2,3 TMB	0.2	0.097	0.06
1,3,5-/1,2,4 TMB	0.38	0.35	0.34
I/D Ratio	0.167	0.169	0.123

^a = Trimethylbenzene.

Table - 4.4

Isomerization of m-xylene over H-[Al]-Beta-28: Influence of temperature

Feed = m-xylene + H₂ (1:4 mole).WHSV : 3.5 hr⁻¹

Temp. K	473	488	518	548	578
Conversion (%)	5.6	15.0	22.3	36.5	15.9
Products (Wt. %)					
Toluene	0.6	2.4	3.5	6.8	12.9
p-xylene	2.3	5.8	7.7	11.1	13.2
m-xylene	94.4	85.0	77.7	63.5	48.1
o-xylene	2.2	4.8	7.1	10.6	12.3
1,3,5 TMB ^a	0.1	0.5	1.1	2.2	3.7
1,2,4 TMB	0.4	1.3	2.6	5.2	8.7
1,2,3, TMB	0.0	0.2	0.3	0.6	1.1
1,3,5-/1,2,4 TMB	0.25	0.38	0.42	0.42	0.42
D/I ^b	0.098	0.0167	0.239	0.326	0.468

a = Trimethyl Benzene

b = Disproportionation/isomerization

Table - 4.5

Isomerization of m-xylene over H-[Al]Beta -28: Influence of WHSV

Feed = m-xylene + H₂ (1:4 mole)

Temperature = 518 K

WHSV (hr ⁻¹)	3.5	5.2	7.0	8.7	13.0
Conversion (%)	22.3	16.9	15.3	11.1	8.1
Products (wt. %)					
Toluene	3.5	2.6	2.2	1.6	1.0
p-xylene	7.7	6.2	5.5	4.2	3.0
m-xylene	77.7	83.1	84.7	88.9	91.9
o-xylene	7.1	5.4	4.9	3.7	2.8
1,3,5 TMB ^a	1.1	0.7	0.7	0.4	0.3
1,2,4, TMB	2.6	1.8	1.8	1.1	0.9
1,2,3, TMB	0.3	0.2	0.2	0.1	0.1
1,3,5-/1,2,4 TMB	0.42	0.39	0.39	0.36	0.33
D/I ^b	0.240	0.210	0.220	0.178	0.182

a = Trimethyl benzene

b = Disproportionation/isomerization

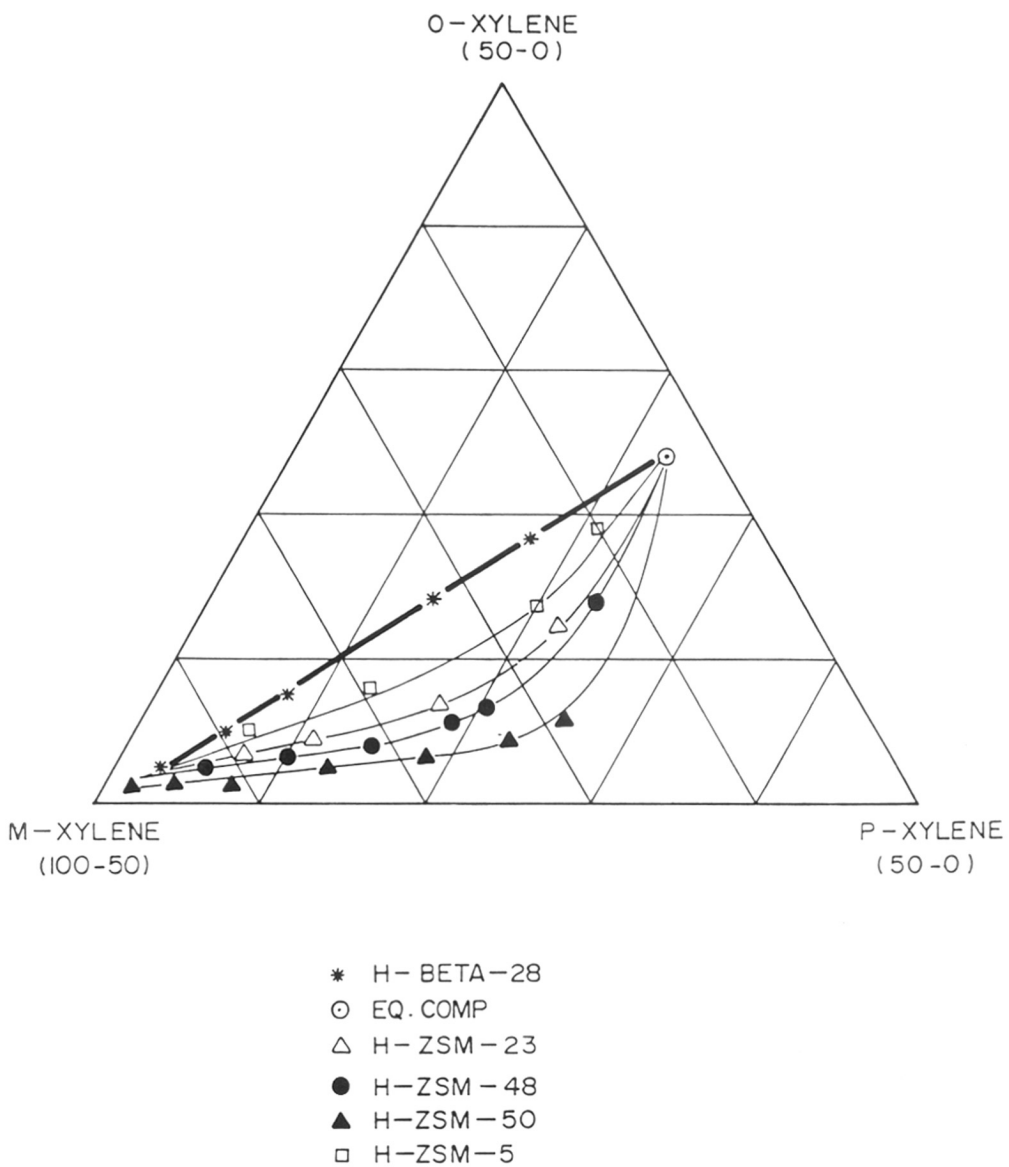
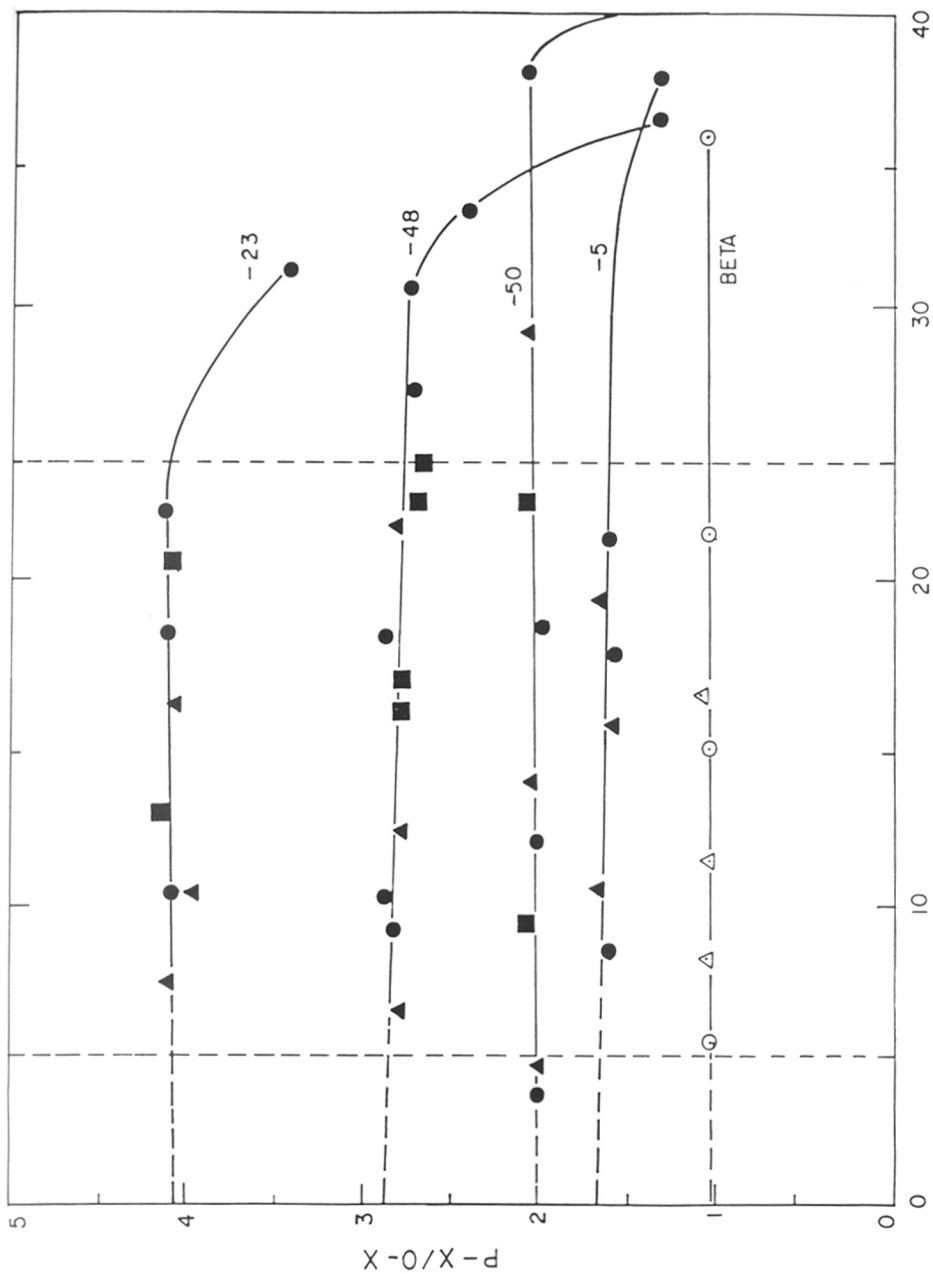


FIG.4.3 : REACTION PATHS FOR THE m-XYLENE ISOMERIZATION OVER ZEOLITE BETA AND OTHER MEDIUM PORE ZEOLITES LEADING TO EQUILIBRIUM POINT



M-XYLENE CONVERSION, %

FIG.4.4 : PX/OX RATIO AGAINST M-XYLENE CONVERSION OBTAINED BY CHANGING TEMPERATURE (●,○), WHSV (▲,△) AND TIME ON STREAM, TOS, (■,□), FILLED AND EMPTY SYMBOLS REPRESENT MEDIUM AND LARGE PORE ZEOLITES RESPECTIVELY. NUMBERS FOLLOWED BY "-" REPRESENT ZEOLITE ZSM-

active sites in the zeolites^{130,131}. The value of I/D at extrapolated to zero m-xylene conversions, can be used to rank zeolites according to their void space. The tendency of zeolite [Al]Beta to disproportionate (rather than isomerize) the xylenes is compared with that of other zeolites in Table 4.6. The value of I/D exhibited by zeolite beta falls in between that for mordenite and zeolite Y, indicating that zeolite beta has quite large void space in agreement to its structure¹³¹. In Fig.4.5, Log (I/D) has been plotted against meta-Xylene conversion. For comparison, other small and large pore zeolites data are also included. For most of the zeolites, log(I/D) strongly depends upon m-xylene conversion.

The disproportionation of m-xylene into toluene and trimethylbenzenes, TMBs, is a bimolecular reaction involving large diphenyl methane-type intermediate complexes which are bulkier than both reactant and products¹³⁷. The results in Table 4.4. indicate^{138,139} that the I/D selectivity largely depends on the intracrystalline void space of zeolites, example is zeolite ZSM-50, a medium pore zeolite with very large deep side pockets off the main 10-membered unidimensional nonintersecting channels. ZSM-50 (similar to EU-1) exhibits a high product shape selectivity Fig.(4.3) in agreement with its 10-membered ring pore openings. However,¹⁴⁰ its log (I/D) value (Fig.4.5) is comparable to those observed over large pore zeolites like mordenite¹⁴⁰.

4-3.13 1,3,5-/1,2,4 TMB ratio

Martens et al.¹³⁷ have discussed the accommodation of possible diphenylmethane type intermediate complexes in the channels of a variety of zeolites. The size of the complex required to form the 1,2,4 TMB¹³⁷ is smallest. The ratio of 1,3,5-/1,2,4-TMB exhibited by zeolites and other medium pore and large pore zeolites is plotted in Fig.(4.6) as a function of meta-xylene conversion. For all the 10-membered ring zeolites, the 1,3,5/1,2,4 TMB ratio is very low and becomes zero at zero conversion. In 10-membered ring zeolites the 1,3,5-isomer

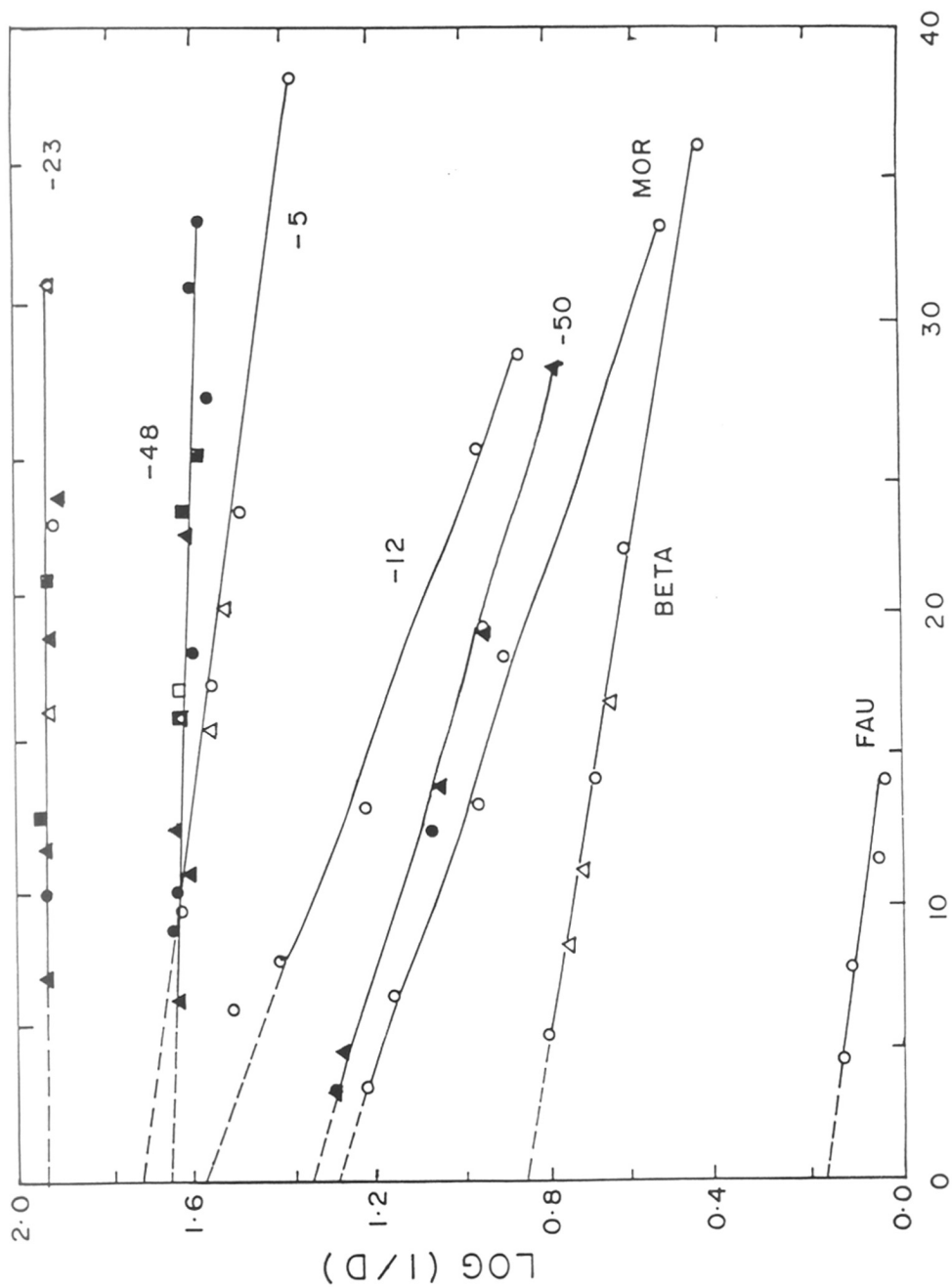
Table - 4.6

Influence of pore geometry on shape selectivity in the
isomerization of m-xylene

Feed = m-xylene + H₂ (1:4 mole)

Zeolite	Pore diameter (nm)	Characteristics	Disp./Isom.
12-Membered ring pores			
Faujasite	0.74 (132)*	Three dimensional	0.68
Beta	0.73 x 0.60 (133)	Linear channels	0.135
	0.56 x 0.65	Tortuous channels	
Mordenite	0.7 x 0.67 (132)	Unidimensional	0.05
	0.57 x 0.29		
ZSM-12	0.61 x 0.57 (132)	Unidimensional	0.027
10-Membered ring pores			
ZSM-50	0.58 x 0.41 (134)	Unidim. elliptical	0.044
	0.68 x 0.58	channel, side	
	x 0.81	cavities	
ZSM-5	0.54 x 0.56 (132)	Circular, straight:	0.022
	0.55 x 0.51	elliptical	
		sinusoidal,	
		bidim. with large	
		intersections	
ZSM-48	0.53 x 0.56 (135)	Unidim. circular	0.021
ZSM-23	0.56 x 0.45 (136)	Unidim. tear drop	0.008
ZSM-22	0.55 x 0.45 (132)	Unidim. elliptical	0

* Figures in brackets indicate references.



M - XYLENE CONVERSION, %

FIG. 4.5 : LOG (1/D) AGAINST M-XYLENE CONVERSION OBTAINED BY CHANGING TEMPERATURE (●,○), WHSV (▲,△) AND TIME ON STREAM, TOS, (■,□), FILLED AND EMPTY SYMBOLS REPRESENT MEDIUM AND LARGE PORE ZEOLITES RESPECTIVELY. NUMBERS FOLLOWED BY "-" REPRESENT ZEOLITE ZSM-

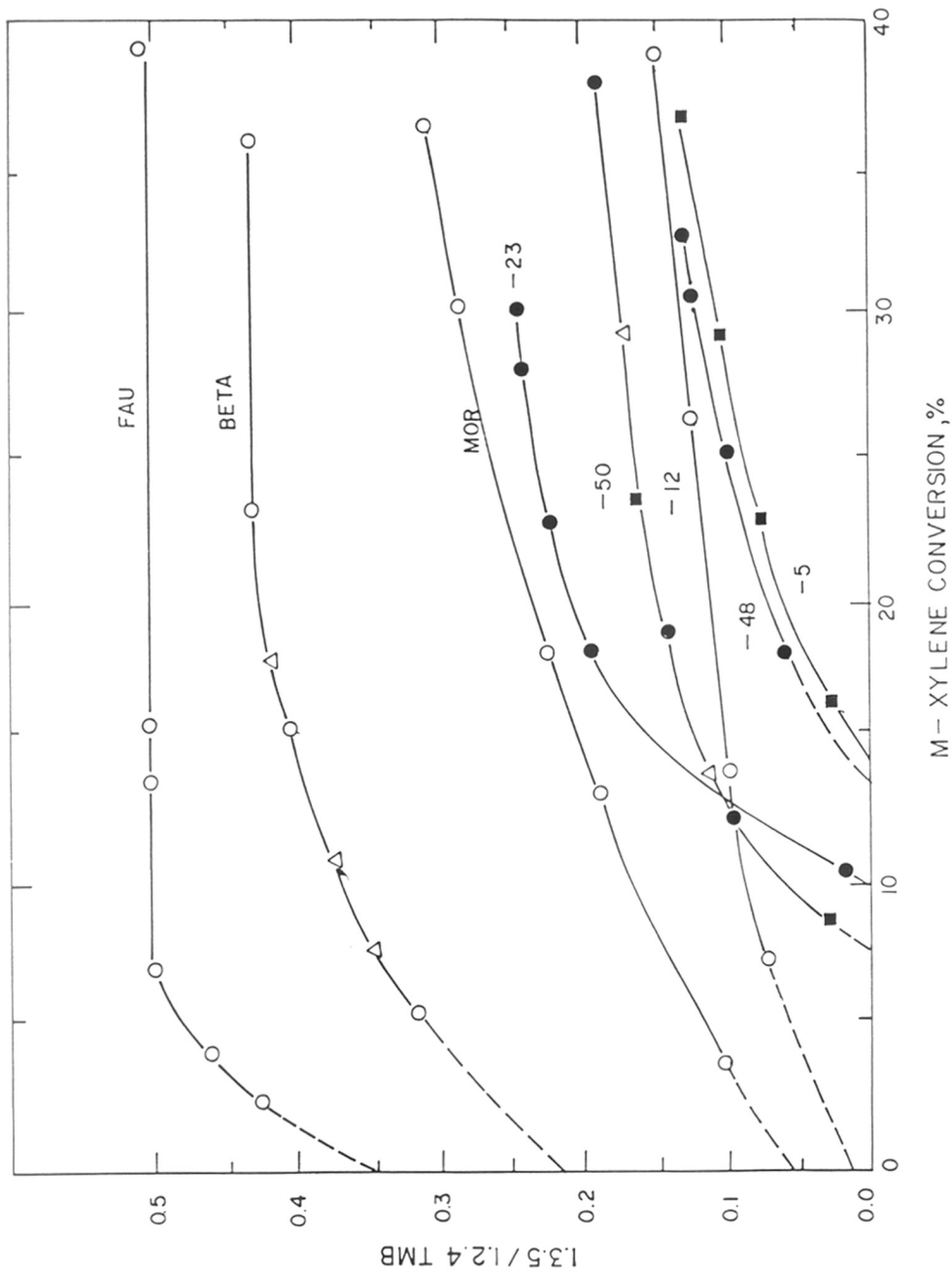
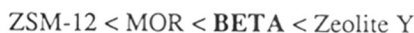


FIG.4.6 : 1.3.5-/1.2.4 TMB RATIO AGAINST M-XYLENE CONVERSION OBTAINED BY CHANGING TEMPERATURE (●,○), WHSV (▲, △) AND TIME ON STREAM, TOS, (■, □), FILLED AND EMPTY SYMBOLS REPRESENT MEDIUM AND LARGE PORE ZEOLITES RESPECTIVELY. NUMBERS FOLLOWED BY "-" REPRESENT ZEOLITE ZSM-

is probably formed as a secondary product via isomerization of the 1,2,4-isomer, formed in disproportionation. For large pore zeolites the 1,3,5/1,2,4-TMB ratio increases with the increase in channel size of the zeolites in the order:



The methylation of toluene over H[Al]-Beta-45 is shown in Table 4.7. As expected no shape selectivity is observed in the xylenes' fractions. However, among the trimethylbenzene isomers, the formation of the bulkiest 1,3,5 isomer is suppressed. The 1,2,4 isomer with minimum cross section is formed predominantly. A similar trend could also be seen in isomerization of m-xylene (Tables 4.4 and 4.5). The 12-membered channels of zeolite beta, while unable to discriminate among xylene isomers, are able to do so for the trimethylbenzenes. In the industrial process for xylene isomerization, the feed stock contains significant amount of ethylbenzene. Babu et al.¹⁴¹ had studied the reactions undergone by an industrial isomer feed over ZSM-5 catalyst. The performance of zeolite beta ($\text{SiO}_2/\text{Al}_2\text{O}_3 = 45$) is compared with ZSM-5 ($\text{SiO}_2/\text{Al}_2\text{O}_3 = 50$) based catalyst and the results are given in Table(4.8). The zeolite and platinum contents in both the samples were similar. The two catalysts were compared at

- constant ethylbenzene conversion levels of 49% (Columns I and IV), and
- constant reaction conditions (Column II and III).

At a similar activity level, the xylene loss is higher over zeolite beta than over ZSM-5. But at similar reaction conditions beta is more active than ZSM-5. The higher activity of zeolite beta may be due to the lower diffusional resistance encountered by the reactant molecules in its large, three dimensional pore system. The large void space of beta facilitates the disproportionation of xylene.

Table - 4.7

Methylation of toluene over H-[Al]Beta -45 :

Influence of temperature

Feed = Toluene + Methanol (4:1 mole)

WHSV = 3.5 hr⁻¹ Pressure:atmospheric

Temp. (K)	548	598	648
Toluene conversion (%)	17.4	26.0	27.2
Methanol conversion (%)	100	100	100
Products (Wt. %)			
Aliphatics	0.5	0.3	0.3
Benzene	0.4	1.0	2.1
Toluene	79.5	71.3	70.1
p-xylene	4.4	5.3	5.0
m-xylene	4.4	10.7	11.3
o-xylene	5.1	4.9	4.7
p-ethyltoluene	0.1	0.1	0.1
m-ethyltoluene	0.1	0.2	0.1
o-ethyltoluene	-	-	-
1,3,5 TMB	0.9	1.5	1.5
1,2,4 TMB	2.8	3.5	3.7
1,2,3 TMB	0.4	0.5	0.5
Durene	1.4	0.7	0.6
1,3,5-/1,2,4 TMB	0.32	0.43	0.40

Table - 4.8

The xylene isomerization process:
Comparison of H-[Al]Beta-45 with ZSM-5

Zeolite	Feed	H[Al]Beta-45		HZSM-5 -(50)	
		I	II	III	IV
Pressure (bar)		6	6	6	18
WHSV (hr ⁻¹)		6	10	10	10
EB conversion (wt. %)		49	43	21	49
Xylene loss (wt. %)		3.4	1.8	0.7	2.1
Composition (wt. %)					
C ₈ ⁻ aliphatics	8.0	10.5	11.3	11.4	17.2
Benzene	3.6	4.8	4.3	4.9	6.2
Toluene	6.0	8.2	7.0	5.1	4.6
Ethylbenzene	22.4	11.3	12.8	17.6	11.4
p-xylene	8.8	13.1	13.0	12.8	12.9
m-xylene	47.4	31.5	33.7	35.0	32.3
o-xylene	3.7	12.0	11.4	11.9	13.2
Ethyltoluene	-	1.5	1.4	-	-
1,3,5 TMB	-	1.0	0.7	-	-
1,2,4 TMB	0.1	2.7	1.9	0.1	0.4
1,2,3 TMB	-	1.2	1.1	0.8	1.1
C ₁₀ ⁺ aromatics	-	1.7	1.3	0.1	0.2

Temperature : 655 K, H₂/oil (mole) = 6.

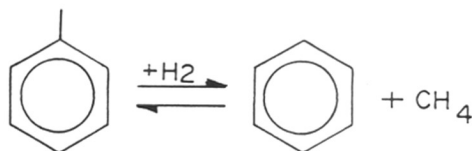
4-3.2 H-[Fe]-Beta-37

The isomerization of m-xylene over H-[Fe]-Beta-37 was carried out and the results are compared with H-[Al]-Beta-45 (Table 4.9). The Fe-analog was less active than its Al-analog. The $\text{SiO}_2/\text{Al}_2\text{O}_3$ and $\text{SiO}_2/\text{Fe}_2\text{O}_3$ ratios of Al- and Fe-Beta was 45 and 37 respectively. Sivasanker et al.¹⁴² and Rao et al.¹⁴³ have also observed similar results in the case of iron analogs of other zeolites. In all the cases the para-xylene/ortho-xylene ratio was found to be 0.9 (around 1.0) close to the thermodynamic values. For [Fe]-Beta, the concentration of 1,3,5-Trimethylbenzene (TMB) is around 20% among the three TMB isomers, which is lower than equilibrium value¹⁴⁴. For the [Al]-Beta this value is 27%. This reaction is known to be catalyzed by Bronsted acid sites¹⁴⁴, and these sites can be generated only by protons associated with Fe^{3+} in lattice positions.

4-4 TOLUENE DISPROPORTIONATION

In addition to toluene disproportionation the following side reactions may also take place,

- 1) Hydrodealkylation of toluene into benzene and methane,



- 2) Disproportionation of xylenes, produced during the main reaction, into toluene and trimethylbenzene.

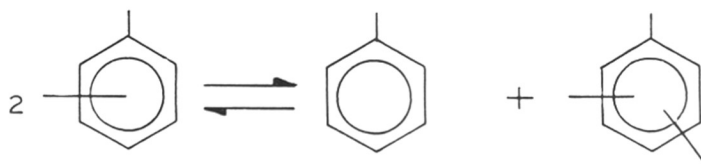


Table - 4.9

Isomerization of m-xylene over H-[Fe]Beta-37 and H-[Al]Beta-45

Feed = m-xylene + H₂ (1:4 mole)WHSV = 3.5 hr⁻¹ ; Pressure = atmospheric

Zeolite	H-[Fe]Beta (SiO ₂ /Fe ₂ O ₃ = 37)					H-[Al]Beta (SiO ₂ /Al ₂ O ₃ = 45)				
Temp. (K)	623	643	663	683	703	473	488	518	548	558
Conversion (%)	5.1	14.5	18.2	24.0	30.3	5.3	14.7	23.8	33.4	38.6
<u>Products</u> <u>wt %</u>										
Toluene	0.4	1.3	2.0	2.9	3.8	0.6	2.0	3.5	6.5	10.9
Ethylbenzene	0.2	0.1	0.2	0.2	0.1	-	-	-	-	-
p-xylene	1.8	5.1	6.4	8.0	9.7	2.0	5.4	8.1	10.3	10.2
m-xylene	94.9	85.5	81.8	76.0	69.7	94.7	85.3	76.2	66.6	61.4
o-xylene	2.2	5.6	7.0	9.2	10.8	1.9	5.1	8.0	9.9	9.9
1,3,5 TMB ^a	0.1	0.5	0.6	0.8	1.3	0.2	0.6	1.1	1.8	2.2
1,2,4 TMB	0.4	1.7	1.8	2.6	4.1	0.6	1.5	2.9	4.4	4.7
1,2,3 TMB	-	-	0.2	0.2	0.5	-	0.1	0.2	0.5	0.6
1,3,5-/1,2,4 TMB	0.20	0.23	0.23	0.22	0.22	0.25	0.27	0.26	0.27	0.29
Sel. isom. ^b	0.78	0.74	0.73	0.71	0.67	0.74	0.71	0.67	0.60	0.52

a = Trimethylbenzene

b = Sel. Isomerization (p-Xylene + o-Xylene/m-Xylene converted).

In the present section, the results obtained in the toluene disproportionation over zeolite H-[Al]-Beta-28 are presented. The effect of reaction temperature on the product distribution (mole%) and conversion of toluene over H-[Al]-Beta-28 ($\text{SiO}_2/\text{Al}_2\text{O}_3 = 28$) is depicted in the Fig 4.7A. Similar data obtained over H-[Al]-Beta-45 ($\text{SiO}_2/\text{Al}_2\text{O}_3 = 45$) are presented in Fig.4.7B.

As expected¹⁴⁵⁻¹⁴⁷, the conversion of toluene increased with the reaction temperature. The benzene/xylene mole ratio (an indication of the dealkylation/disproportionation ratio) was near unity at lower temperatures. However, with the increase in temperature, the relative concentrations of benzene vis-a-vis xylenes increased, suggesting that at higher temperatures the dealkylation of toluene into benzene was facilitated. The fraction of trimethylbenzenes (TMBs) remained between 1-3 mole%. No significant increase in the TMBs concentration was observed with the increase in reaction temperature.

Fig.4.8A and 4.8B illustrate the influence of space velocity (WHSV) on toluene conversion and product distribution. Though the conversion of toluene decreases with the increase in WHSV, (i.e. decrease in contact time), the molar distribution of benzene and xylenes remains almost constant. The concentration of TMBs also remains at a very low level (1-2%). A change in WHSV changes the conversion, but has no or little effect on the side reactions such as the dealkylation of toluene.

4-5 ALKYLATION OF BENZENE TO LINEAR ALKYL BENZENES (LAB)

These are used in the manufacture of detergents. These detergents are biodegradable. Detergents are made by the sulfonation of LAB. The feed stock for the production of LAB usually consists of linear olefins with 10 - 14 carbon atoms. The catalyst generally used for this reaction is HF.

4-5.1 Experimental

Studies were carried out on the alkylation of benzene with an olefin mixture obtained from a LAB manufacturer. The composition of the olefin mixture (feed) is given below:

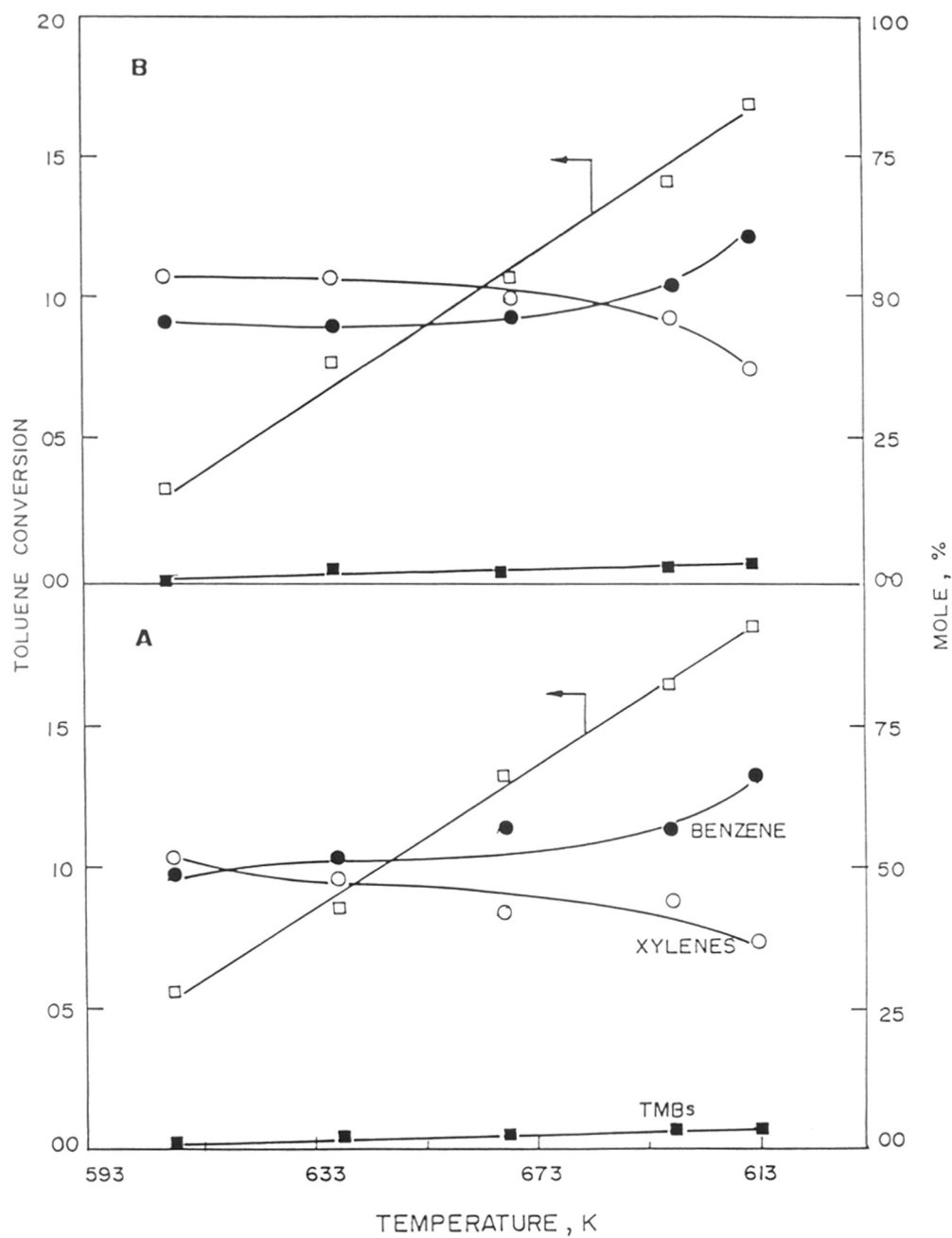


FIG.4.7 : EFFECT OF TEMPERATURE ON THE DISPROPORTIONATION OF TOLUENE OVER H[Al] BETA-28 AND 45 [A AND B RESPECTIVELY].

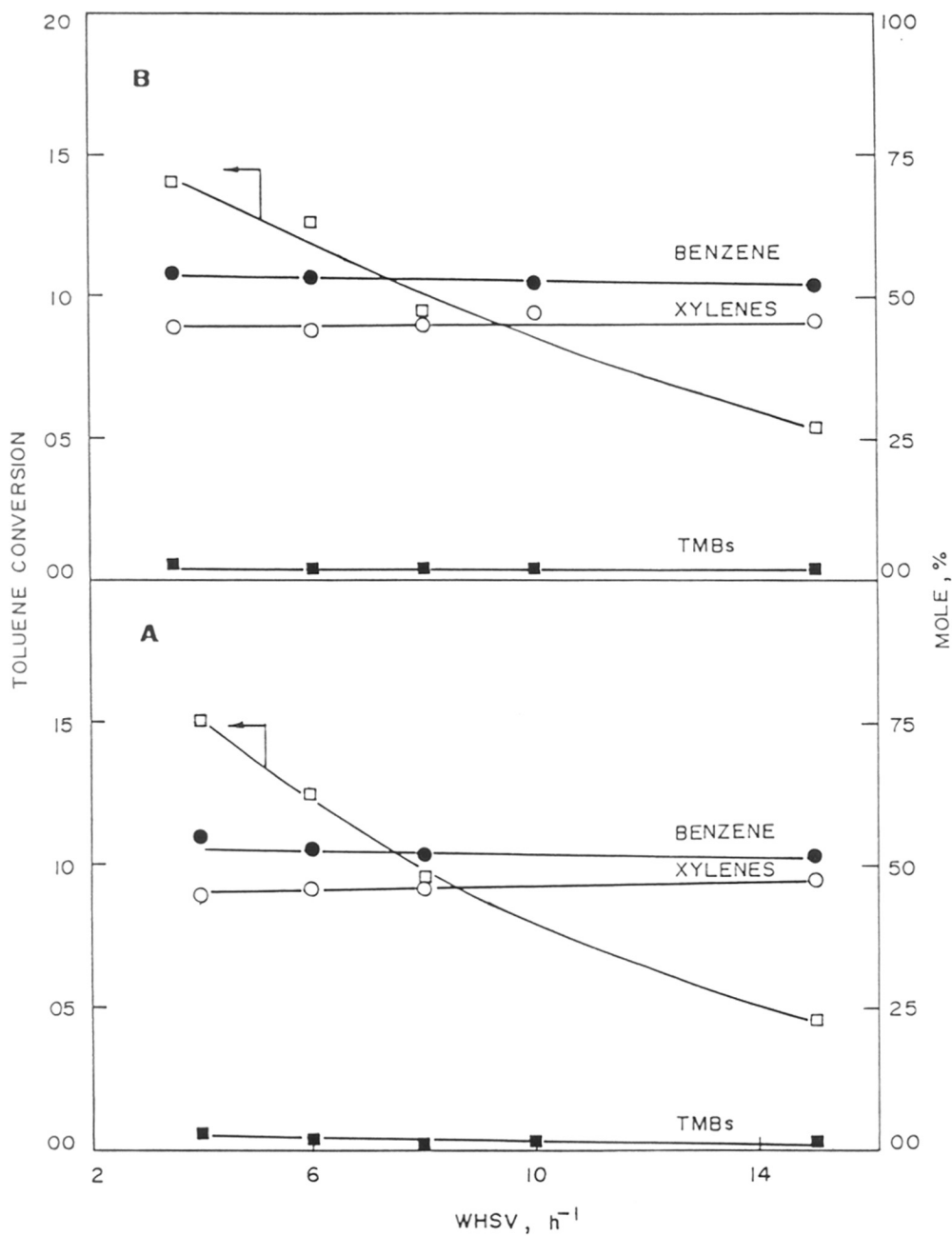


FIG.4.8 : EFFECT OF SPACE VELOCITY (WHSV) ON THE DISPROPORTIONATION OF TOLUENE OVER H[A1] BETA-28 AND 45 [A AND B RESPECTIVELY].

Composition of mixed olefin feed

Composition		Wt %
C ₁₀ OLEF	=	1.4
C ₁₁ OLEF	=	3.9
C ₁₂ OLEF	=	3.3
C ₁₃ OLEF	=	2.6
Rest (Paraffin)	=	88.8

Alkylation of aromatics with α -olefins using zeolites has been described¹⁴⁸. Here monoalkyl benzenes like toluene are alkylated with α -olefins of C₁₀₋₂₀ using large pore zeolite catalyst of SiO₂/Al₂O₃ ranging from 5-30.

In a typical experiment 100 ml of benzene and 20 ml of olefin is taken in the Parr reactor vessel of 300 ml volume. To this was added 5 g of activated H-[Al]-Beta-28 catalyst. The reaction was carried out at 100°C with constant stirring, for 24 hrs.

The reactor was cooled to room temperature, the catalyst was filtered off, the unreacted benzene is removed by distillation. The product was analysed by GC with capillary column (Hewlett Packard 5880). The experiments were repeated with other catalysts, at different temperature and at various reactant compositions.

4-5.2 Results and Discussion

Zeolite Beta has been employed in many hydrocarbon reactions like alkylation of toluene with methanol¹⁴⁹, ethanol and propene, isomerization of meta-Xylene¹⁵⁰, toluene disproportionation¹⁴⁹ etc. In all these reactions, zeolite[Al]-Beta did not show any shape selective property, except in the formation of trimethylbenzenes. The results of the alkylation studies are presented in Table 4.10. At the end of 24 hrs, all the olefin was found to have reacted in all the experiments. Hence, only the product break up (the % of the various phenyl-isomers) is being presented in

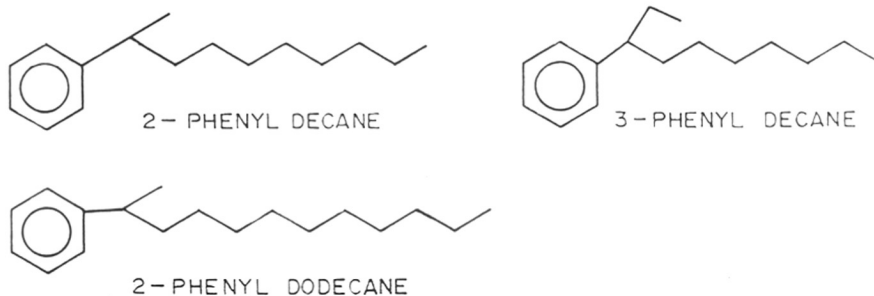
Table - 4.10
Influence of SiO₂/Al₂O₃ ratio on product distribution in alkylation reaction

Ratio of Beta	iφ	Σnφ	C ₁₀							C ₁₁							C ₁₂							C ₁₃							
			2	3	4	5	6	7	2	3	4	5	6	7	2	3	4	5	6	7	2	3	4	5	6	2	3	4	5	6	
R=28	7.9	92.1	8.8	6.0	2.9	2.5	-	-	14.6	9.7	5.1	3.8	1.6	-	11.7	6.9	3.8	3.1	2.5	-	4.1	2.2	1.1	1.0	0.9	28.0	0.42*	0.44*	0.44*	0.44*	0.44*
R=45	7.4	92.6	7.4	4.2	1.9	1.5	-	-	15.1	9.1	5.3	3.2	0.13	-	32.8	0.49*	33.1	0.47*	0.46*	0.46*	0.46*	0.46*	0.46*	0.46*	0.46*	0.46*	0.46*	0.46*	0.46*		
Reliance Sample	4.43	95.57	3.3	3.2	3.3	4.1	-	-	5.8	5.8	6.2	8.1	4.2	-	5.2	5.3	5.5	7.4	7.7	-	3.0	3.0	3.2	4.3	6.8	30.1	0.19*	0.17*	0.17*	0.17*	
			13.9						30.1						31.1						20.3										
			0.23*						0.19*						0.17*						0.14*										

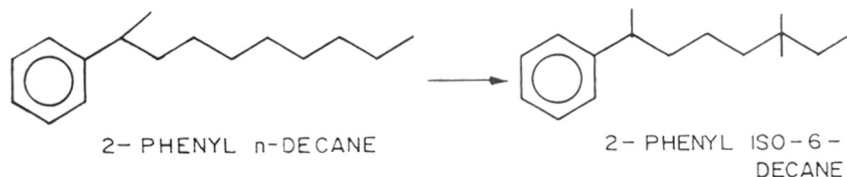
* = 2φ/Σnφ.

Temperature = 373 K ; Benzene : Olefin ratio = 1:1 ; Reaction time = 24 hrs.

the Table. The composition of a commercial LAB sample (supplied by Reliance Industries Ltd., Patalganga, India) which was produced by alkylation using HF is also reported in the table. The total 2-phenyl isomer content of the LAB is also reported. The 2-phenyl (2-φ) isomer is the most valuable component in LAB as it has better emulsibility and detergent properties. It is noticed that the formation of the 2-phenyl isomer is more over zeolite-beta than over HF (44% vs. 17%) at all experimental conditions. This is attributed to the shape selective nature of zeolite-beta. The 2-phenyl isomer is the least bulky of all the isomers. Examining the 2-phenyl content in each C-fraction, it was found that it is nearly constant (~ 40%) suggesting that the isomer distribution is not affected by chain length. The structures of some alkyl benzenes are given below:



When the temperature is changed (373-423 K), there is very little change in the isomer distribution (Table 4.11). The same (~ 42%) 2-phenyl isomer is obtained at all the temperatures. However, the formation of the isomerized products increases with temperature. Iso-products are by-products in which side chain isomerization has taken place (See below). These iso-products are less biodegradable.



The formation of the iso-products could have taken place through isomerization of the n-alkyl products or the n-olefins itself. When the benzene to olefin ratio is increased the

Table - 4.11
 Influence of temperature on alkylation reaction.
 Zeolite Beta R=28, Benzene : olefin = 1:1

Temperature K	iφ	Σnφ	C ₁₀							C ₁₁							C ₁₂							C ₁₃								
			2	3	4	5	6	7	2	3	4	5	6	7	2	3	4	5	6	7	2	3	4	5	6	2	3	4	5	6		
373	5.8	94.2	8.7	5.3	3.5	3.5	-	-	16.2	9.2	4.9	3.5	1.1	-	13.0	6.9	3.7	2.9	2.1	-	4.2	2.4	1.3	1.1	0.8	9.8	0.43*					
			20.9						34.8						28.7																	
			0.42*						0.47*						0.45*																	
398	6.5	93.5	8.6	5.5	3.2	2.3	-	-	15.3	9.0	5.9	3.6	0.9	-	13.2	7.1	4.6	2.9	1.5	-	4.3	2.3	1.6	1.0	0.4	9.7	0.44*					
			19.6						34.7						29.4																	
			0.43*						0.44*						0.45*																	
423	13.7	86.3	7.2	4.5	2.4	2.2	-	-	13.8	8.5	5.0	3.8	1.2	-	11.9	6.7	4.0	3.4	2.2	-	4.0	2.1	1.2	1.1	0.7	9.2	0.43*					
			16.3						32.3						28.3																	
			0.44*						0.43*						0.42*																	

* = 2φ/Σnφ.

product distribution pattern also changes (Table 4.12). At lower concentrations of olefin, the formation of iso-phenyl isomers is lower. No significant influence of silica to alumina ratio of the zeolites over product distribution is observed (Table 4.10).

4-6 CONCLUSIONS

- 1) Isomerization of m-Xylene and isofeed, methylation and disproportionation of toluene reactions on [Al]Beta, ZSM-5, -23, -48, -50, zeolite-Y and mordenite have been studied.
- 2) Disproportionation/isomerization ratio in m-Xylene reaction follows the order **Beta** > ZSM-50 > ZSM-5 > ZSM-48 > ZSM-23 > ZSM-22.
- 3) Zeolite **Beta** does not show shape selectivity in xylene isomers distribution but in trimethylbenzene isomers, it exhibits shape selectivity, suggesting that it has $\sim 7\text{\AA}$ pore opening.
- 4) The m-Xylene conversion can distinguish between 10- and 12- ring pore zeolites (the ratio of 1,3,5-/1,2,4-TMB at zero conversion).
- 5) m-Xylene reaction can rank the medium pore zeolites according to their pore diameter (p-X/o-X ratio).
- 6) It can rank large pore zeolites according to their pore diameter (the ratio of 1,3,5-/1,2,4-TMB and log I/D at zero conversion).
- 7) It can rank the zeolites according to their effective void space (log I/D at zero conversion).
- 8) m-Xylene isomerization on H[Fe]Beta shows the presence of Bronsted acid sites due to bridging hydroxyl groups Si-O-Fe which are weaker than those of [Al]Beta zeolites.

Table - 4.12
 Effect of change in Benzene : Olefin ratio.
 Zeolite [Al]Beta-45 ; Temperature = 373 K

Ratio of feed (by volume)	iφ	Σnφ	C ₁₀						C ₁₁						C ₁₂						C ₁₃					
			2	3	4	5	6	7	2	3	4	5	6	7	2	3	4	5	6	7	2	3	4	5	6	
1 : 1	7.9	92.1	8.8	6.0	2.9	2.5	-	-	14.6	9.7	5.1	3.8	1.6	-	11.7	6.9	3.8	3.1	2.5	-	4.1	2.2	1.1	1.0	0.9	
			20.2						34.8						28.0						9.4					
			0.44*						0.42*						0.42*						0.44*					
1 : 5	2.0	98.0	10.4	6.8	5.0	4.5	-	-	15.9	9.1	6.1	5.0	1.4	-	11.5	6.3	3.8	3.1	1.8	-	3.6	1.9	1.4	0.9	0.8	
			26.7						37.4						26.5						8.6					
			0.40*						0.42*						0.43*						0.44*					

* = $2φ/Σnφ$.

SUMMARY

This thesis is a study of the synthesis, physicochemical characterization and catalytic property of zeolite **beta** and its iron analog.

The influence of various synthesis parameters such as: Reactivity of silica source, template concentration, alkalinity, water content, silica to alumina ratio and temperature were investigated. Different silica sources namely, pyrogenic silica with different particle size, surface area and tetraethyl orthosilicate (TEOS) were utilised. At values of

$$\frac{TEA^+}{SiO_2} = 0.165, \frac{Na^+}{SiO_2} = 0.1, \frac{H_2O}{SiO_2} = 25$$

and a temperature of 423 K good quality crystals of [Al]Beta with varying SiO₂/Al₂O₃ could be synthesised. The difference between the Si/Al ratios in the starting gel and the final product increases with increasing silicon content. A poor yield of crystals was observed in the latter case.

The ferrisilicate analog of zeolite **beta** has also been synthesized using tetraethylorthosilicate, free from Al impurities as the source of silica.

All the samples were characterized by thermal analysis (TG, DTG and DTA), sorption properties, FT-IR, spectroscopy, Temperature Programmed Desorption of NH₃ (TPD of NH₃), solid state MASNMR spectroscopy, Electron Spin Resonance spectroscopy (ESR), Magnetic susceptibility measurements and Mossbauer spectroscopy. On the basis of these studies the following conclusions were drawn:

- * X-ray amorphous nuclei of **beta** zeolite could be detected by thermal analysis, adsorption and IR studies.
- * The pore volume of Na-Beta is about 0.22 ± 0.03 ml/g of zeolite.

- * Mid-IR frequency due to asymmetric stretching vibrations of $-(\text{Si-O-Fe})_n$ units in TEA-[Fe]Beta is shifted to lower wave numbers compared to $-(\text{Si-O-Al})_n$ - units in TEA-[Al]Beta zeolite.
- * The solid state MASNMR ^{29}Si spectrum of TEA-[Fe]Beta is broadened compared to TEA[Al]Beta arising from Si-O-Fe nuclear-electron coupling in the [Fe] analog.
- * Magnetic susceptibility of TEA[Fe]Beta zeolite is 5.8 and .5 B.M., at 94 and 293 K respectively, indicative of Fe^{3+} ions in magnetically dilute environment.
- * The room temperature Mössbauer isomer shift (0.32 nm/s), the absence of hyperfine splitting at 4.2 K, and crystal field splitting into $1 \pm 5/2$, $1 \pm 3/2$, $1 \pm 1/2$ of $6s$ state of Fe^{3+} ion, and internal magnetic field = 46.8T are well within the range for tetrahedral coordination for Fe^{3+} ions by oxide ions.
- * Brönsted acid sites (bridging hydroxyl groups) for [Al] and [Fe]Beta zeolite gave bands at 3605 and 3632 cm^{-1} respectively. Frequency shifts of these vibrations on benzene adsorption was 337 and 310 cm^{-1} respectively showing that [Fe]Beta has weaker acidity compared to [Al]Beta.
- * The thermal stability of surface hydroxyl groups of [Fe]Beta is less than those of [Al]Beta zeolite.

Hydrocarbon reactions like m-Xylene conversion, methylation of toluene, and disproportionation of toluene has been studied over zeolite-H[Al]Beta and H[Fe]Beta. The results obtained over beta zeolite has been compared with that obtained for other large pore zeolites like ZSM-12, mordenite, faujasite and medium pore zeolites like ZSM-5, ZSM-23, ZSM-48.

Three parameters namely, p-Xylene/o-Xylene ratio, isomerization/disproportionation ratio and 1,3,5-/1,2,4-Teimethyl benzene ratio have been used to elucidate the features of the pore system in zeolite beta. The p-Xylene/o-Xylene ratio in m-Xylene conversion reaction over both zeolite H[Al]Beta and H[Fe]Beta was nearly equal to the equilibrium value. This

indicated a lack of constraints for the diffusion of xylene isomers in zeolite **beta**. The isomerization/disproportionation (I/D) ratio (in the reactions of m-Xylene) obtained for zeolite **beta** was in the range found for large pore zeolites like mordenite and ZSM-12. The formation of Trimethylbenzene needs a bulkier transition state. Among the TMB isomers, the formation of 1,2,4-TMB needs the smallest transition state. This factor was utilized to distinguish large pore zeolites from medium pore and small pore zeolites. In this study, the ratio of 1,3,5-/1,2,4-TMB for 10-membered ring zeolites was found to be very low. For **beta** and other large pore zeolites this ratio was always significantly higher even at a very low conversion of m-Xylene.

H-[Fe]**Beta** was less active than the Al-analog, otherwise its shape selectivity in m-Xylene reactions was similar to the Al-analog. Zeolite **beta** exhibited shape selectivity in the alkylation of benzene with long chain linear olefins. The formation of the least bulky 2-phenyl isomer was more over zeolite **beta** than with the conventional catalyst HF. The 2-phenyl isomer content remained constant when the temperature was increased in the range 373-423 K. No significant influence of the $\text{SiO}_2/\text{Al}_2\text{O}_3$ ratio (in the **beta** zeolite) could be observed in this alkylation reaction.

REFERENCES

1. Cronstedt, A., Akad. Handl. Stocholm, **18**, 120 (1756).
2. Breck, D.W., "Molecular Sieve Zeolites", Advan. Chem. Ser. **101**, American Chemical Society, Washington, DC, 1971. Chapter -III p.186-209
3. Breck, D.W., "Molecular Sieve Zeolites", Advan. Chem. Ser. **101**, American Chemical Society, Washington, DC, 1971. Chapter -IV p. 251.
4. McBain, J.W., "The sorption of gases and vapours by solids", Publ. Rutledge and Sons, London, Chapter 5, (1932).
5. Barrer, R.M., Proc. Roy. Soc. (London), **A167**, 393 (1938); Trans. Far. Soc., **40**, 559 (1944).
6. Flanigen, E.M., in "Proceedings of the Fifth International Conference on Zeolites", Rees, L.V.C., (ed.) Heyden and Sons, London (1980).
7. Meier, W.M., Molecular Sieves, Society of Chemical Industry, London, 1968, p.10.
8. Barrer, R.M., "Hydrothermal Chemistry of Zeolites", Academic Press, 1982 p. 8-39.
9. Breck, D.W., "Molecular Sieve Zeolites", Advan. Chem. Ser. **101**, A.C.S., Washington, DC, (1971), p. 45.
10. Barrer, R.M., "Hydrothermal Chemistry of Zeolites", Academic Press, London, 1982, p.251.
11. Davis, M.E., Saldarriaga, C., Montes, C., Garces, J., Crowder, C., Zeolites, 1988, **8** (5), 362-367.
12. Barrer, R.M., "Chemical Nomenclature and Formation of Compositions of Synthetic and Natural Zeolites", Pure and Applied Chem., **51**, 1091 (1979).
13. Sand, L.B., Econ Geol., p.191 (1967).
14. Szostak, R., "Molecular Sieves, Principles of Synthesis and Identification", Van Nostvand Rheinhold, New York, Chapter 2, (1989).

15. Barrer, R.M. and Denny, P.J., *J. Chem. Soc.* (1961) 971.
16. Lok, B.M., Cannan, T.R. and Messina, C.A., *Zeolites* **4**, 289 (1984).
17. Van. Balmoos, R., "Collection of Simulated XRD Powder Patterns for Zeolites", Butterworths, London (1984).
18. Szostak, R., "Molecular Sieves, Principles of Synthesis and Identification", Van Nostvand Rheinhold, New York, Chapter 5, (1989) 283-300.
19. Perego, G., Bellussi, G., Corno, C., Taramasso, M., Buonomo, F. and Esposito, A., in "New Developments in Zeolite Science and Technology", Murakami, Y. et al. (Eds), Elsevier, Amsterdam, p.129 (1986).
20. Ratnasamy, P., Kotasthane, A.N., Shiralkar, V.P., Thangaraj, A., and Ganapathy, S., in "Zeolite Synthesis", ACS Symp. Ser., **398**, 405 (1989).
21. Szostak, R., Thomas, T.L., *J. Catal.* **100**, 555 (1986).
22. Simmons, D.K., Szostak, R. and Agrawal, P.K., *J. Catal.*, **106**, 287 (1987).
23. Pluth, J.J., Smith, J.V., and Bennett, J.M., *Acta Crystallog.*, **C42**, 283 (1986).
24. Charnell, J.F., *J. Cryst. Growth*, **8**, 291 (1971).
25. Rietveld, H.M., *J. Appl. Crystallogr.*, **2**, 65-71 (1969).
26. Flanigen, E.M., Khatami, H., Szymanski, H.A., "Molecular Sieve Zeolites", *Advan. Chem. Seri.*, **101**, ACS, Washington, DC, p.201 (1971).
27. Flanigen, E.M., "Zeolite Chemistry and Catalysis", ACS Monograph, Rabo, J.A. et al. (Eds.), **171**, 111 (1976).
28. Kutz, N., "Heterogeneous Catalysis-11", Sharpiro, B.L. (ed.), p.12 (1984).
29. Topsoe, N., Pendersen, R.K. and Derouane, E.G., *J. Catal.*, **70**, 41 (1981).

30. R. Szostak, "Molecular Sieves, Principles of Synthesis and Identification", Van Nostrand Rheinhold, New York, p.83 (1989).
31. Barrer, R.M., and Breck, D.W., Trans. Faraday Soc., **59**, 2569 (1963).
32. Barrer, R.M., "Zeolites and Clay Minerals as Sorbents and Molecular Sieves", Academic Press, Inc., London.
33. Barrer, R.M. and Gibbson, R.M., Trans. Faraday Soc., **59**, 2569 (1963).
34. Barrer, R.M., Pure and Appl. Chem., **52**, 2143 (1980).
35. Naddenriep, R.J., "Colloid Interface Sci.", **28**, 293 (1968).
36. Miesel, S.L., McCullough, U.J.P., Lechthalev, C.H. and Weisz, P.B., ACS Meeting, Chicago, **I**, 11 (1977).
37. Derouane, E.G., Detremmerie, S., Gabelica, Z. and Blom, N., Appl. Cat. **1**,20, 1981.
38. Barrer, R.M. and Langloy, D.A., J. Chem. Soc., **3804**, 3811, 1817, 1958.
39. Gal, I.G., Tankovie, O., Malcis, S., Raoovanor, P. and Tadorivic, M., Trans Faraday Soc., **67**, 999, 1971.
40. Bremer, H., Morke, W., Schodel, R., Vogt, F., Adv. in Chem. Ser. **121**, 249 (1973).
41. Jacobs, P.A., "Carboniogenic Activity of Zeolites", Chapter II, Elsevier Sci. Publishing Co., Amsterdam, Oxford, New York, **168**, 33 (1977).
42. Ligia Siena de Saldarriga, C., Saldarrage and Davis, M.E., J. Am. Chem. Soc., **109**, 2686 (1987).
43. Tanabe, K., "Solid Acids and Bases", Chap.II, Acad. Press, New York, p.5.
44. Anderson, J.R., Mole, F.K., Rajadhyaksha, R.A. and Sanders, J.V., J. Catal. **58**, 114 (1979).

45. Jacobs, P.A., Uytterhoeven, J.B., Styeys, M., Froment, G. and Weitkamp, G., Proc. 5th Int. Conf. on Zeolites, Naples, Italy, Heyden & Sons, London, 604 (1980).
46. Borade, R.B., Hegde, S.G., Kulkarni, S.B. and Ratnasamy, P., Appl. Catal., **13**, 27 (1984).
47. Sherry, H.S., in "Molecular Sieve Zeolites", Adv. Chem. Ser., **101**, 350 (1971).
48. Rees, L.V.C. and Rao, A., Trans. Fara. Soc., **62**, 2103 (1970).
49. Beck, D.W., "Zeolite Molecular Sieves", Wiley, New-York, Chapter 8 (1974).
50. Eberly, Jr., P.E., in "Zeolite Chemistry and Catalysis", ACS Symp. Ser., **171**, 392 (1976).
51. Derouane, E.G., in "Catalysis by Zeolites", (Ed. B. Imelik et al.), p.5 (1980).
52. Barrer, R.M., Adv. Chem. Ser. **102**, 1 (1971).
53. Flanigen, E.M., Bennett, J.M., Grose, R.W., Cohen, J.P., Patton, R.L., Kirchner, R.M. and Smith, J.V., Nature, **271**, 512, (1978).
54. Grose, R.W. and Flanigen, E.M., U.S. Pat. 4, 061, 724 (1977).
55. Barrer, R.M. and Langley, D.A., J. Chem. Soc., 3804, 3811, 3817 (1958).
56. Breck, D.W., "Zeolite Molecular Sieves", John Wiley and Sons, New-York, 449 (1974).
57. Kuhl, G.H., J. Catal. **29**, 270 (1973).
58. Jacobs, P.A., "Carbonogenic Activity of Zeolites", Chapter II, Elsevier Sci. Publishing Co., Amsterdam, Oxford, New York, **168**, 33 (1977).
59. J.W. Ward, "Zeolite Chemistry and Catalysis", Chapter 2, ed. J.A. Rabo, ACS, Monograph, **171**, 118 (1976).
60. Mortier, W.J., Saur, J., Lercher, J.A. and Noller, H., J. Phys. Chem., **88**, 905 (1984).
61. Hegde, S.G., Kumar, R., Bhat, R.N. and Ratnasamy, P., "Zeolites". **9**, May 231 (1989).

62. Barrer, R.M., in "Hydrothermal Chemistry of Zeolites", (Acad. Press, London) Chapter 6 (1982).
63. Barrer, R.M., in Proc. Sixth Int. Zeol. Conf., Eds. D.H. Olson and Bisio (Butterworths, Surrey, U.K.) p. 870-886 (1984).
64. Tielen, T., Geelen, M. and Jacobs, P.A. in Proc. Int. Symp. Zeolite Catalysis, Eds. P. Fejes and D. Katto (Siofok, Hungary) p.1-18 (1985).
65. Wilsen, S.T., Lok, B.M., Messina, C.A., Cannan, T.R. and Flanigen, E.M., J. Am. Chem. Soc., **104**, 1146-1147 (1982).
66. Lok, B.M., Messina, C.A., Patton, R.L., Gajek, R.T., Cannan, T.R. and Flanigen, E.M., J. Amer. Chem. Soc., **106**, 6092-93 (1984).
67. Taramoso, M., Perego, G. and Notari, B., U.S. Pat. 4,410,501 (1983).
68. Huybrechts, D.R.C., DeBraycker, L. and Jacobs, P.A., Nature, **345**, 6272, p.240-42 and references therein.
69. Davis, M.E., in Report at 1987 Int. Symp. on Innovations in Zeolite Material Science, Nieuwpoort, Belgium (Sept. 1987).Dow Patent application.
70. Davis, M.E., Montes, C., Hathaway, P.E. and Garces, J.M., in Zeolites: Facts, Figures, Futures, Proc. 8th Int. Zeol. Conf., Amsterdam (1989), Ed. P.A. Jacobs et al., Stud. Surf. Sci. and Catal., **49**, Part A, p.199-214.
71. Weisz, P.B. and Frillette, V.J., J. Phy. Chem., **64**, 382 (1960).
72. Weisz, P.B., Frillette, V.J., Maatmean, R.W. and Mowev, E.B., J. Catal., **1**, 307 (1962).
73. Venuto, P.B. and Habib, Jr., E.T., Catal. Rev. Sci. Eng., **18**, 1 (1978).
74. Magee, J.S. and Blazek, J.J., in Ref.8, p.615.

75. Argauer, R.J. and Landolt, G.R., U.S. Pat. 3,702,886 (1972).
76. Vanghan, D.E.W., Chemical Engineering Progress, Feb. 1989, p.31.
77. Csicsery, S.M., Zeolites **4**, 202 (1984).
78. Chen, N.Y., "Industrial applications of shape selective catalysts", (ed. Ward, J.W.), Elsevier Pub., (1987).
79. Derouane, E.G., "Catalysis on the energy scene", Kaliaguine, Mahay, (Eds.), Elsevier, Amsterdam, **1** (1984).
80. Derouane, E.G. and Gabelica, Z., J. Catal. **65**, 486 (1980).
81. Holderich, W. and Gallei, E., Chem. Eng. Tech. **56**, 908 (1984).
82. Dwyer, F.G., "Catalysis of organic reactions" in W.R. Moser (Ed.): Chemical Industries, Vol.5, Marcel Dekker, New York, 1981, p.39.
83. Solinas, V., Monoci, R., Longu, G., Forni, L., Acta Phys. Chem. **31**, 291 (1985).
84. Anderson, R.A., ACS Symp. Ser., **40**, 637 (1977).
85. Ruthven, D.M., "Principles of adsorption and Adsorption processes", John Wiley, NY, (1984).
86. Ritter, R.E. and Magee, J.S., in "ACS Symposium on octane in the Eighties", Miami, September, 1978.
87. Pine, L., Maher, P.J. and Watcher, W.A., J. Catal. **85**, 466 (1984).
88. Anibas, J.A., Corma, A., Fornes, V., and Melo, F.V., J. Catal. **108**, 135 (1987).
89. Corma, A., Fornes, V., Martinez, A., and Orchilles, A.V., in "ACS Symp. Ser. **368** on "Perspectives in Molecular Sieve Science", (W.J. Flank and E. Whyte, Eds.), P.542 (1988).
90. Wadlinger, R.L., Kerr, G.T. and Rosinski, E.J., U.S. Pat. 3,308,069 (1967).

91. Newsam, J.M., Treacy, M.M.J., Koetsier, W.T. and DeGruyter, B.C., *Proc. Roy. Soc., London*, **A420**, 375-405 (1988).
92. Ernst, S., Jacobs, P.A., Martens, J.A. and Weitkamp, J., "Synthesis of zeolite ZSM-12 in the system $(\text{MTEA})_2\text{O}-\text{Na}_2\text{O}-\text{SiO}_2-\text{Al}_2\text{O}_3-\text{H}_2\text{O}$ ", *Zeolites*, **7**, 458-62 (1987).
93. Rollmann, L.D. and Valyocsik, E.W., "Zeolite Molecular Sieves", *Inorg. Synth.*, **22**, 61 (1983).
94. Perez-Pariente, J., Martens, J.A. and Jacobs, P.A., *Zeolites*, **8**, 46-53 (1988).
95. Perez-Pariente, J., Martens, J.A. and Jacobs, P.A., *Appl. Catal.*, **31**, 35-64 (1987).
96. Greg, S.J. and Sing, K.S.W., "Adsorption, surface area and porosity", *Acad. Press, London*, (1967).
97. Dubinin, M.M., *Bull. Acad. Sci., U.S.S.R.*, **23**, 958 (1974).
98. Parker, L.M., Bibby, D.M. and Patterson, J.E., "Zeolites", **4**, 168 (1984).
99. Gabelica, Z., Nagy, B.J., Derouane, E.G. and Gilson, J.P., "Clay Minerals", **19**, 803-824 (1984).
100. Lok, B.K., Cannan, T.R. and Messina, C.A., "Zeolites", **3**, 282-291 (1983).
101. Bond, A.E., Burgers, C.G.V. and Martin, D.E., U.S. Patent No.3793385 (1974) (assigned to BPPLC, U.K.).
102. Olson, D.H., Kokatailo, G.T., Lawton, S.L.L., Meier, W.M., *J. Phys. Chem.* **B5**, 2238-2243 (1981).
103. Martens, J.A., Perez-Pariente, J. and Jacobs, P.A., in *Proc. Int. Symp. Zeolite Catalysis, Siofok, Hungary* (ed. P. Fejes and D. Kallo), *Acta. Phys. Chem.* **31**, 487-495 (1985).
104. Martens, J.A. and Jacobs, P.A., "Zeolites", **6**, 334-348 (1986).

105. Robson, H.E., U.S. Patent No.4560542 (1985) (assigned to Exxon Research and Engineering Company).
106. Kotasthane, A.N., Shiralkar, V.P., Hegde, S.G. and Kulkarni, S.B., "Zeolites", **6**, 253 (1986).
107. Cynthia, T.W. Chu and Clearence, D. Chang, J. Phys. Chem., **89**, 1569-1571 (1985).
108. Lok, B.M., Marcus, B.K., Angellel, "Zeolites", **6**, 185 (1986).
109. Corma, A., Fornes, V., Melo, F. and Perez-Pariente, J. Preprints, ACS Symposium, Div. of Petroleum Chemistry, p.632 (1987).
110. Wolf F., Fuertig, H., Headicke, V., Chem. Tech. (Berlin), **18**, 524 (1966).
111. Szostak, R., Nair, V. and Thomas, L.T., J. Chem. Soc., Faraday Trans. 1, **83**, 487-494 (1987).
112. Woolery, G.L., Alemany, L.B., Dessau, R.M. and Chester, A.W., "Zeolites", **6**, 14 (1986).
113. Rouxhet, P.G. and Samplels, R.E., J. Chem. Soc., Faraday Trans. 1, **70** 2021 (1971).
114. Kustov, L.M., Kazansky, V.B. and Ratnasamy, P., "Zeolites", **7**, 79 (1987).
115. Vedrine, J.C., Auroux, A., Bolis, V., Dejaifve, P., Naccache, C., Wierzchowski, P., Derouane, E.G., Nagy, J.B., Gilson, J., VanHooff, J.H.C., Vanden Berg, J.P. and Wolthuizen, J., J. Catal., **59**, 248 (1979).
116. Meagher, A., Nair, V. and Szostak, R., "Zeolites", **8**, 3 (1988).
117. Garten, R.L., Delgass, W.N. and Boudart, M., J. Catal., **18**, 90 (1970).
118. Plank, C.J., Rosinski, E.J. and Rubin, M.K., U.S. Patent 4,076,842 (1978).
119. Kumar, R. and Ratnasamy, P., J. Catal., **116**, 440 (1989).
120. Ernst, S., Kumar, R. and Weitkamp, J., Catal. Today, **3**, 1 (1988).

121. Valyocsik, E.W., Eur. Patent No.142,317 (1984).
122. Kumar, R. and Ratnasamy, P., J. Catal., **118**, 68 (1989).
123. Kulkarni, S.B., Shiralkar, V.P., Kotasthane, A.N., Borade, R.B. and Ratnasamy, P., "Zeolites", **2**, 313 (1982).
124. Argauer, R.J. and Landolf, G.R., U.S. Pat. 3,702,886 (1972).
125. Rubin, M.K., U.S. Pat. 4,640,829 (1987).
126. Rao, G.N., Kumar, R. and Ratnasamy, P., Appl. Catal., **49**, 307 (1989).
127. Ernst, S., Kokotailo, G.T. and Weitkamp, J., "Zeolites", **7**, 180 (1987).
128. Dewing, J., J. Mol. Catal., **27**, 25 (1984).
129. Mavrodinova, V., Penchev, V., Lohse, U. and Gross, T., "Zeolites", **9**, 203 (1989).
130. Kumar, R., Rao, G.N. and Ratnasamy, P., Appl. Catal., **49**, 307 (1989).
131. Newsam, J.M., Treacy, M.M.J., Koetsier, W.T. and deGruyter, C.B., Proc. Royal Soc. London, **A420**, 375-405 (1988).
132. Meier, W.M. and Olson, D.H., Atlas of Zeolite Structure Types, Structural Commission of Intern. Zeolite Association, (1978).
133. La Pierre, R.B., Rohrman, A.C. Jr., Schlenker, J.L., Wood, J.D., Rubin, M.K. and Rohrbaugh, W.J., "Zeolites", **5**, 346 (1985).
134. Biscoe, N.A., Johnson, D.W., Shanon, M.D., Kokotailo, G.T. and McCusker, L.B., "Zeolites", **8**, 74 (1988).
135. Schlenker, J.L., Rohrbaugh, W.J., Chu, P., Valyocsik, E.W. and Kokotailo, G.T., "Zeolites", **5**, 355 (1985).

136. Rohrman, A.C. Jr., LaPierre, R.B., Schlenker, J.C., Wood, J.D., Valyocski, E.W., Rubin, M.K., Higgins, J.W. and Rohrbaugh, W.J., "Zeolites", **5**, 352 (1985).
137. Martens, J.A., Perez-Pariente, J., Sastre, E., Corma, A. and Jacobs, P.A., *Appl. Catal.*, **45**, 85-101 (1988).
138. Csicsery, S.M., *J. Catal.*, **108**, 433 (1987).
139. Olson, D.H. and Haag, W.O., in "Catalytic Materials: Relationship between Structure and Reactivity", ACS Symp. Ser. No.248, 275 (1984).
140. Kumar, R., Rao, G.N. and Ratnasamy, P., in P.A. Jacobs and R.A. van Santen (Ed.), *Proc. 8th Intern. Zeolite Conf. Stud. Surf. Sci. & Catal.*, **49B**, 1141 (1989), Elsevier, Amsterdam.
141. Babu, G.P., Santra, M., Shiralkar, V.P. and Ratnasamy, P., *J. Catal.*, **100**, 458 (1986).
142. Sivasankar, S., Reddy, K.M., Waghmare, K.J., Harisangam, S.R. and Ratnasamy, P., in *Proc. XI Symp. Iberoamer. Catal.*, **37**, 741 (1988).
143. Rao, B.S., Babu, G.P., Shiralkar, V.P., Kotasthane, A.N. and Ratnasamy, P., in *Proc. 9th Iberoamerican Symp. Catal.*, Lisbon, p.1418 (1984).
144. Benslama, R., Fraissard, J., Albizane, A., Fajula, F. and Figueras, F., "Zeolites", **8**, 196 (1988).
145. Young, L.B., Butter, S.A. and Kaeding, W.W., *J. Catal.*, **76**, 418 (1982).
146. Meshram, N.R., Hedge, S.G., Kulkarni, S.B. and Ratnasamy, P., *Appl. Catal.*, **8**, 359 (1983).
147. Kumar, R. and Ratnasamy, P., *J. Catal.*, **118**, 68 (1989).
148. U.S. Patent 4,731,497 (1988).

149. Ratnasamy, P., Bhat, R.N., Pokhriyal, S.K., Hegde, S.G. and Kumar, R., *J. Catal.*, **119**, 65-70 (1989).
150. Corma, A., Fomes, V., Melo, P. and Perez-Pariente, J., "ACS Symp. Preprints", p.632, Div. Petroleum Chem. (1987).

LIST OF PUBLICATIONS

1. Synthesis of Zeolite **beta** using silica gel as a source of SiO₂.
R.N. Bhat and R. Kumar
J. Chem. Tech. Biotechnol. **48**, 453-466 (1990).
2. Characterization of the acidity of Zeolite **beta** by FT-IR Spectroscopy and TPD of NH₃.
S.G. Hegde, R. Kumar, R.N. Bhat & P. Ratnasamy.
Zeolites, **9**, May 231-237 (1989).
3. Synthesis of Iron-Silicate Analogs of Zeolite **beta**.
R. Kumar, A. Thangaraj, R.N. Bhat & P. Ratnasamy.
Zeolites, **10**, February 85-89 (1990).
4. Reactions of Aromatic Hydrocarbons over Zeolite **beta**.
P. Ratnasamy, R.N. Bhat, S.K. Pokhriyal, S.G. Hegde & R. Kumar.
J. of Catal., **119**, 65-70 (1989).
5. Synthesis of Iron-Silicate Analogs of Zeolite Mordenite.
A.J. Chandwadkar, R.N. Bhat & P. Ratnasamy.
Zeolites, **11**, 42-47 (1991).
6. Meta-Xylene Conversion : An useful Catalytic test Reaction to Characterize the Pore Geometry and Void Space of Zeolites.
R. Kumar, R.N. Bhat & P. Ratnasamy.
Communicated to the "Applied Catalysis".

7. Synthesis, Characterization and Catalytic Properties of Ferrisilicate Analog of Zeolite EU-1.
R. Kumar, A. Thangaraj, R.N. Bhat, M.J. Eapen & S.K. Date.
Communicated to the "J. of Catalysis.

PATENTS

1. An improved process for the separation of Di-hydroxybenzene isomers by using zeolite-Y, (Patent No. NF-4991, Indian).
P.P. Moghe, R.N. Bhat, S.G. Hegde & P. Ratnasamy.
2. An improved process for the separation of Di-hydroxybenzene isomers by using zeolite **beta**, (Patent No. NF-5091, Indian)
P.P. Moghe, R.N. Bhat, S.G. Hegde & P. Ratnasamy.
3. An improved process for the synthesis of p-Acetamol (patent being filed).
P.P. Moghe, R.N. Bhat & S.G. Hegde.
4. Esterification of aliphatic and aromatic acids using zeolites **beta**.
P.P. Moghe, R.N. Bhat, S.G. Hegde & P. Ratnasamy.
(to be Communicated).